REVIEWS OF
MODERN PHYSICS

VOLUME 43, NUMBER 4 OCTOBER 1971

Singularity Structure of the Perturbation Series for the Ground-State Energy of a Many-Fermion System*

GEORGE A. BAKER, JR.
Applied Mathematics Department, Brookhaven National Laboratory, Upton, Long Island, New York

Calculational procedures are developed for the ground-state energy of a many-fermion system. The entire theory is developed from the many-body Schrödinger equation via perturbation theory. The linked cluster expansion is derived by elementary methods. The analytic singularities of the energy function are analyzed, and procedures designed to avoid or overcome them. Results for the calculation of the energy in the presence of a purely repulsive two-body force are reviewed, and the situation is found to be reasonably satisfactory, though good results are restricted to weak potentials when the system is not dilute. Results for an attractive potential surrounding a strongly repulsive core are reviewed, and procedures described for calculations in this case. A sample calculation with an assessment of the probable errors is reviewed.

CONTENTS

* Work supported in part by the U.S. Atomic Energy Commission.

I. INTRODUCTION

The aim of this article is to present a reasonably self-contained account, for the somewhat mathematically inclined physicist, of the specialized topic of the computation of the ground-state energy of a very large system of identical fermions from an assumed two-body interparticle interaction potential. A good general background in quantum mechanics and the mathematical methods of theoretical physics should suffice to read this article, and an effort has been made to avoid the assumption that the reader has a detailed knowledge of other specialized disciplines of theoretical physics.

The problem to which we will address ourselves is quite simply stated. It is, "What is an effective procedure for finding the lowest energy eigenvalue of the system described by the Hamiltonian

$$H=\sum_{i=1}^{N}\frac{\mathbf{p}_i^2}{2M}+\sum_{i<j}^{N}V(|\mathbf{r}_i-\mathbf{r}_j|), \qquad (1.1)$$

when N becomes indefinitely large?" In (1.1), $\mathbf{p}_i$ and $\mathbf{r}_i$ are the momentum and position of the ith particle, $V(x)$ is the interaction potential, and M is the particle mass. We will have in the back of our minds throughout this discussion the problem of "infinite nuclear matter," that is to say a very large system with forces similar to the nucleon–nucleon forces, and will therefore not con-

sider potentials of the full range of generality which occur in nature, nor will we allow more than one species of particles. To do so would necessarily open the lid on the whole Pandora's box of molecules, crystalline solids, etc. There is one significant physical problem which must however be considered. The atomic nucleus and hence infinite nuclear matter have a great many of the properties of a liquid, as is emphasized by the successes of the Bohr liquid-drop model of the nucleus (see, for example, Evans, 1955). In particular, a large system when confined in a box will not uniformly fill the box if the box volume is greater than a certain amount, but will form a bound system and leave the rest of the box relatively unoccupied. Put more accurately, even though according to quantum mechanics every point in the box is equally likely (periodic boundary conditions) to be occupied by any particle, there will be a long-range correlation between the particles, such that in terms of relative coordinates the volume can be divided into two phases. In one phase there is a very high probability of occupation, and in the other a very low probability. This physical effect manifests itself in the mathematics, as we shall see, by the introduction of singularities in the ground-state energy as a function potential strength and density. It is therefore a major goal of any calculational scheme to avoid these singularities.

In addition to the above mentioned physical problem, the calculation is beset by a number of purely mathematical complications, at least some of which arise because of physically understood effects. Before the middle 1950's it was thought that any use of perturbation theory in terms of the potential strength was impossible because the size of successive terms of the perturbation expansion increased as powers of the number of particles. That the energy series should not be a convergent one can be understood in terms of the physical effect of "nuclear collapse." A typical nuclear-type force has a strongly repulsive core and a weakly attractive outer portion. If the sign of the potential is reversed, then there is a strongly attractive core. This type of potential leads (see for example, Blatt and Weisskopf, 1952) to a ground state whose total dimensions are of the same order of magnitude as the radius of the attractive core. In the limit of indefinitely large system size, this collapse will occur no matter how weak the attraction. As we will see later, this extremely dramatic variation of the energy function at zero potential strength is associated with singularities which approach the zero of potential strength in the limit of indefinitely large system size. As the location of the nearest singularity to the origin limits the radius of convergence of the perturbation series, it will follow that the perturbation series has zero radius of convergence for a nuclear-type potential. Brueckner (1955) showed however that the use of perturbation theory was not as hopeless as was previously believed. He showed, and Goldstone (1957) and Hugenholtz (1957) later proved, that in the perturbation expansion of E/N, every term is of order 1 in N. This result greatly stimulated activity in the field as it permitted calculations to be carried out.

A great deal of research has been done on the infinite nuclear matter problem since then in an attempt to improve upon the results of Brueckner and Gammel (1958a). The bulk of this work has aimed at combining as much of the perturbation series as possible into the leading-order term of a new expansion. The construction of this leading-order term usually involves the solution of a nonlinear integral equation. This approach has been extensively reviewed in a series of review articles by Day (1967), Rajaraman and Bethe (1967), and Brandow (1967). Consequently we will not attempt to cover this approach more than by occasional reference. We shall concentrate instead on a parallel approach which has not yet been treated in a review. This parallel approach is concerned with the investigation and exploitation of the analytic structure of the ground-state energy function. There are several problems implicit in that function. For example, the zero radius of convergence of the series remains as a difficulty to be overcome, for it means that the perturbation series is at best asymptotic, and may *or may not even define* the physically correct energy function.

Another problem which occurs, due to the physics, is that of the extremely strong, perhaps infinite, short-range nucleon–nucleon repulsive force. We know physically that the only effect is to exclude the particles from coming closer to each other than a certain minimum distance. To take care of this problem mathematically, Brueckner had the idea of rearranging into a single term all the successive interactions between the same pair of particles, in analogy to Watson's theory of multiple scattering. Inasmuch as the original series is divergent, one is compelled to examine the legitimacy of any rearrangement. When the problem of the "Emery singularities" has been overcome by a slight modification of Brueckner's original K-matrix resummation into an R-matrix resummation, the rearrangement is found to be a valid one. The technical problem of actually producing the terms of the expansion is considerable and is treated at length.

The major conclusions to which we come are briefly these. First, if we consider a system with purely repulsive forces the problem of the liquid drop does not arise. The calculation of the energy of a dilute many-fermion system with arbitrary strength of interaction is well in hand. For weak interactions, so long as order–disorder phenomena of the packing marbles in a box type are avoided, the energy for any density can be computed. Second, if we consider a system with a potential with a repulsive core and an attractive outer portion, the calculational outlook is hopeful. The problem is to locate "saturation density," that is,

where any increase in volume of the system will lead to the appearance of an occupied and an unoccupied phase. We seek the ground-state energy at that density. We believe that through the use of sophisticated series summation techniques applicable to divergent series, the R-matrix expansion at fixed density can be summed to yield accurate values of the ground-state energy at saturation density. A sample calculation (Baker *et al.*, 1970) is described.

II. PRELIMINARIES

A. Rayleigh–Schrödinger Perturbation Theory

The aim of this section is to derive the linked-cluster, perturbation expansion for the ground-state energy of a many-fermion system by elementary methods. The purpose is twofold. It is, first, by avoiding the use of field theoretic methods, to make these results available to a wider group of physicists; and second, to clarify the practical matters of signs and factors of two which will be vital in the subsequent actual evaluation of terms in this expansion.

Our starting point is the time-independent Schrödinger equation for a system of N identical particles interacting by pairwise forces (see for example, Pauling and Wilson, 1935)

$$\sum_{j=1}^{N}\left[-\frac{\hbar^2}{2M}\nabla_j^2\Psi\right]+\left[\sum_{i<j}^{N}v(r_{ij})\right]\Psi=E\Psi, \quad (2.1)$$

where ∇_j^2 is the Laplacian with respect to the coordinates of the jth particle, and r_{ij} is the distance between the ith and the jth particles. Our goal now is to develop a perturbation expansion in powers of the potential strength. We will employ the Rayleigh–Schrödinger perturbation procedure to this end. Let us define

$$H_0=\sum_{j=1}^{N}\left(-\frac{\hbar^2}{2M}\nabla_j^2\right),$$

$$h=\sum_{i<j}^{N}v(r_{ij}). \quad (2.2)$$

Then we wish to find $E(\lambda)$ defined by the eigenvalue equation

$$(H_0+\lambda h)\Psi=E(\lambda)\Psi, \quad (2.3)$$

where we presume that we can solve explicitly

$$H_0\Phi=E(0)\Phi \quad (2.4)$$

for the unperturbed ground-state energy $E(0)$, and wave function Φ. Let us also introduce the wave matrix $\Omega(\lambda)$ such that

$$\Psi=\Omega(\lambda)\Phi \quad (2.5)$$

and expand E and Ω in powers of λ as

$$E(\lambda)=E_0+E_1\lambda+E_2\lambda^2+\cdots,$$
$$\Omega(\lambda)=I+\Omega_1\lambda+\Omega_2\lambda^2+\cdots. \quad (2.6)$$

Upon substituting Eq. (2.6) into Eq. (2.3) and equating coefficients of the same power of λ, we obtain the fundamental Rayleigh–Schrödinger perturbation equations

$$E_n=\langle\Phi\mid h\Omega_{n-1}\mid\Phi\rangle, \quad (2.7)$$

$$\Omega_n=(I-P_0)(E_0-H_0)^{-1}(h\Omega_{n-1}-\sum_{j=1}^{n-1}E_{n-j}\Omega_j), \quad (2.8)$$

where the normalization condition

$$\langle\Phi\mid\Phi\rangle=\langle\Phi\mid\Psi\rangle=1 \quad (2.9)$$

has been used. The projection operator P_0 projects the unperturbed ground state Φ so that $(I-P_0)$ is a state orthogonal to Φ. Prior to the work of Brueckner (1955), it was thought that this expansion was not useful in the many-fermion problem because the successive terms diverged as higher and higher powers of N, the system size. Brueckner recognized that this difficulty does not in fact occur as the terms proportional to N^2, N^3, etc. all cancel, and leave E formally proportional to N only in the limit of a large system. This result was later proven by Goldstone (1957) and Hugenholtz (1957). We will give a different proof here, which we believe makes the practical aspects clearer. It is based only on time-independent perturbation theory and does not require the additional machinery of time-dependent perturbation theory.

B. Basic Diagram Representation of Perturbation Theory

First let us work out explicitly the effect of multiplying Φ by h. To be definite we shall confine our system to a rectangular box of incommensurate sides with volume Γ, and impose periodic boundary conditions. In this way we will avoid any degeneracy between the eigenvalues of the unperturbed system. As we are dealing with fermions, the wave function must be antisymmetric under the interchange of any two coordinates. This condition is conveniently effected by the use of a Slater determinant of single-particle wave functions, due to the properties of determinants. As H_0 is the sum of one-particle operators, we need the solution for the one-particle wave function, subject to our periodic boundary conditions. It is

$$\varphi(\mathbf{r}_j)=\Gamma^{-1/2}\exp(i\mathbf{k}\cdot\mathbf{r}_j), \quad (2.10)$$

where

$$\mathbf{k}=2\pi[(l/L_1)\mathbf{i}+(m/L_2)\mathbf{j}+(n/L_3)\mathbf{k}], \quad (2.11)$$

with L_1, L_2, L_3 the lengths of the three sides of the box, and l, m, n any positive or negative integer, or zero. We will take account of the effects of spin and isotopic spin at a later stage.

The unperturbed wave function will be

$$\Phi=(N!)^{-1/2}\Gamma^{-\frac{1}{2}N}\det\begin{vmatrix}\exp(i\mathbf{k}_1\cdot\mathbf{r}_1) & \exp(i\mathbf{k}_2\cdot\mathbf{r}_1) & \cdots & \exp(i\mathbf{k}_N\cdot\mathbf{r}_1)\\ \exp(i\mathbf{k}_1\cdot\mathbf{r}_2) & \exp(i\mathbf{k}_2\cdot\mathbf{r}_2) & \cdots & \exp(i\mathbf{k}_N\cdot\mathbf{r}_2)\\ \cdot & \cdot & \cdot & \cdot\\ \cdot & \cdot & \cdot & \cdot\\ \cdot & \cdot & \cdot & \cdot\\ \exp(i\mathbf{k}_1\cdot\mathbf{r}_N) & \exp(i\mathbf{k}_2\cdot\mathbf{r}_N) & \cdots & \exp(i\mathbf{k}_N\cdot\mathbf{r}_N)\end{vmatrix}. \tag{2.12}$$

Next we will find it convenient to express the interaction potential in a momentum representation. Thus we define

$$\langle\boldsymbol{\nu}\boldsymbol{\mu}\mid v\mid\boldsymbol{\lambda}\boldsymbol{\eta}\rangle=\Gamma^{-2}\iiiint_{\text{Box}}d^3\mathbf{r}_i\,d^3\mathbf{r}_j\,d^3\mathbf{r}_i'\,d^3\mathbf{r}_j'[\delta(\mathbf{r}_i-\mathbf{r}_i')\delta(\mathbf{r}_j-\mathbf{r}_j')v(\mathbf{r}_{ij})]$$
$$\times\exp(-i\boldsymbol{\nu}\cdot\mathbf{r}_i-i\boldsymbol{\mu}\cdot\mathbf{r}_j+i\boldsymbol{\lambda}\cdot\mathbf{r}_i'+i\boldsymbol{\eta}\cdot\mathbf{r}_j'), \tag{2.13}$$

where we assume that $v(\mathbf{r}_{ij})$ vanishes for $|\mathbf{r}_{ij}|\geq|R|$, where $|R|\leq\frac{1}{2}\min(L_1,L_2,L_3)$. Using the locality of the interaction, and changing to the center of mass and relative coordinates

$$\mathbf{R}=\tfrac{1}{2}(\mathbf{r}_i+\mathbf{r}_j),\qquad \mathbf{r}=\mathbf{r}_i-\mathbf{r}_j, \tag{2.14}$$

Eq. (2.13) at once becomes

$$\langle\boldsymbol{\nu}\boldsymbol{\mu}\mid v\mid\boldsymbol{\lambda}\boldsymbol{\eta}\rangle=\Gamma^{-2}\iint_{\text{Box}}d^3\mathbf{R}\,d^3\mathbf{r}v(\mathbf{r})$$
$$\times\exp[i(\boldsymbol{\lambda}+\boldsymbol{\eta}-\boldsymbol{\nu}-\boldsymbol{\mu})\cdot\mathbf{R}+\tfrac{1}{2}i\mathbf{r}\cdot(\boldsymbol{\lambda}+\boldsymbol{\mu}-\boldsymbol{\nu}-\boldsymbol{\eta})]. \tag{2.15}$$

This integral is most conveniently investigated by using the periodicity of the wave function, remembering that the δ functions in (2.13) are the sort appropriate to periodic boundary conditions; that is to say, a particle near one wall can interact with a particle at the other end of the box just as though it were moved by exactly one box length so as to be near the first particle. Under these circumstances, the integral (2.15) factors giving

$$\langle\boldsymbol{\nu}\boldsymbol{\mu}\mid v\mid\boldsymbol{\lambda}\boldsymbol{\eta}\rangle$$
$$=(2\pi)^3\Gamma^{-1}\delta_{\boldsymbol{\lambda}+\mathbf{n},\boldsymbol{\nu}+\boldsymbol{\mu}}\tilde{v}(\tfrac{1}{2}(\boldsymbol{\lambda}+\boldsymbol{\mu}-\boldsymbol{\nu}-\boldsymbol{\eta})), \tag{2.16}$$

where the δ is a Kronecker delta which is unity when the subscripts are equal and zero otherwise. We get (2.16) because for the $\boldsymbol{\nu}$, $\boldsymbol{\mu}$, $\boldsymbol{\lambda}$, $\boldsymbol{\eta}$ of interest [form (2.11)], $\frac{1}{2}(\boldsymbol{\lambda}+\boldsymbol{\eta}-\boldsymbol{\nu}-\boldsymbol{\mu})$ and $\frac{1}{2}(\boldsymbol{\lambda}+\boldsymbol{\mu}-\boldsymbol{\nu}-\boldsymbol{\eta})$ are necessarily of form (2.11) also, and hence by the orthogonality of the wave functions, (2.16) results. We have used

$$\tilde{v}(k)=(2\pi)^{-3}\int d^3\mathbf{r}v(\mathbf{r})\exp(i\mathbf{k}\cdot\mathbf{r}). \tag{2.17}$$

Form (2.16) shows that, (i) momentum is conserved and (ii) $\langle\boldsymbol{\nu}\boldsymbol{\mu}\mid v\mid\boldsymbol{\lambda}\boldsymbol{\eta}\rangle$ is inversely proportional to the volume. It is to be noted that if we had not used periodic boundary conditions translational invariance would have been destroyed and momentum would not have been conserved in the interaction. We are now in a position, by the completeness of the set of eigenfunctions, to write

$$\delta(\mathbf{r}_i-\mathbf{r}_i')\delta(\mathbf{r}_j-\mathbf{r}_j')v(r_{ij})$$
$$=\Gamma^{-2}\sum_{\boldsymbol{\nu},\boldsymbol{\mu},\boldsymbol{\lambda},\mathbf{n}}\exp(i\boldsymbol{\nu}\cdot\mathbf{r}_i+i\boldsymbol{\mu}\cdot\mathbf{r}_j)\langle\boldsymbol{\nu}\boldsymbol{\mu}\mid v\mid\boldsymbol{\lambda}\boldsymbol{\eta}\rangle$$
$$\times\exp(-i\boldsymbol{\lambda}\cdot\mathbf{r}_i'-i\boldsymbol{\eta}\cdot\mathbf{r}_j'), \tag{2.18}$$

where the sums extend over all the eigenvalues. If we now expand Φ along the ith and jth rows by the Laplace expansion (see, for example, Muir, 1960) in double minors, we obtain

$$\Phi=(N!)^{-1/2}\Gamma^{-\frac{1}{2}N}\sum_{\mathrm{m}\neq\mathrm{n}}\exp(i\mathbf{m}\cdot\mathbf{r}_i'+i\mathbf{n}\cdot\mathbf{r}_j')\Phi_{i,\mathrm{m};j,\mathrm{n}}. \tag{2.19}$$

Thus if we multiply (2.18) times (2.19) and integrate r_i', r_j' over our box, we obtain

$$v(r_{ij})\Phi=(N!)^{-1/2}\Gamma^{-\frac{1}{2}N}\sum_{\mathrm{m}\neq\mathrm{n}}\sum_{\boldsymbol{\nu},\boldsymbol{\mu}}\exp(i\boldsymbol{\nu}\cdot\mathbf{r}_i+i\boldsymbol{\mu}\cdot\mathbf{r}_j)$$
$$\times\langle\boldsymbol{\nu}\boldsymbol{\mu}\mid v\mid\mathbf{m}\mathbf{n}\rangle\Phi_{i,\mathrm{m};j,\mathrm{n}} \tag{2.20}$$

by the orthogonality of the single-particle wave functions. If we now use (2.2) to sum over all pairs of particles, we obtain, by using the Laplace expansion on columns instead of rows,

$$h\Phi=\tfrac{1}{2}(N!)^{-1/2}\Gamma^{-\frac{1}{2}N}\sum_{\mathrm{m}\neq\mathrm{n}}\sum_{\boldsymbol{\nu},\boldsymbol{\mu}}\langle\boldsymbol{\nu}\boldsymbol{\mu}\mid v\mid\mathbf{m},\mathbf{n}\rangle$$
$$\times\Phi(\mathbf{m}\rightarrow\boldsymbol{\nu};\mathbf{n}\rightarrow\boldsymbol{\mu}), \tag{2.21}$$

where by $\Phi(\mathbf{m}\rightarrow\boldsymbol{\nu};\mathbf{n}\rightarrow\boldsymbol{\mu})$ we mean that we have the same Slater determinant as Φ (2.12), except that the column which had momentum $\mathbf{m}$ now has momentum $\boldsymbol{\nu}$ and $\mathbf{n}$, $\boldsymbol{\mu}$. The first summation in (2.21) is over all the momenta in Φ, and the second is over all eigenstates. Of course, the Φ factors vanish if there are two columns the same, so we may as well restrict the summation over

ν and μ to exclude those momenta in $\Phi_{i,m;j,n}$. In order to keep track of more complicated sequences of operations, it has been found advantageous to introduce a pictorial representation. In the first instance we will use diagrams rather similar to those of Goldstone (1957), but will later find those of Hugenholtz (1957) to give a more compact and manageable representation. We will discuss now the ground state; although excited states could also be discussed by the same methods we will not do so here. The lowest N states of the system form the Fermi sea, and we will by convention not picture them so long as they are filled (that is, there is a column for each one in the Slater determinant). The remainder of the states will not be pictured so long as they are empty. We will use a solid line to denote a filled state which is above the Fermi sea, and a dotted line to indicate a hole in the Fermi sea. The action of multiplying by the potential will be called a vertex, and since its effect on the wave function is one of replacement of one momentum state by another, we represent this replacement by a pair of crossed lines. We join these crosses by a wavy line which represents the momentum transfer during the interaction. We have illustrated (2.21) in Fig. 1. The rule in drawing an interaction vertex is that since the occupancy of each state changes, one end of every line which meets at a vertex is blank, according to our convention. There is one exception to this general statement. According to the summations described in (2.21), we can have, for example, $\nu=\mathbf{m}$; that is to say a filled state is involved in the interaction but is left unchanged by it. (In this case we must have also $\mu=\mathbf{n}$ by momentum conservation.) We conventionally represent this case by Fig. 2.

The other operation we must represent in the construction of the Ω_n operators is the multiplication by $(I-P_0)(E_0-H_0)^{-1}$. This operator is diagonal in the representation given by the Slater determinants of (2.21), and is wholly expressible in terms of the momenta of the states which have been emptied, and the new momenta which replace them. In other words, in terms of the line labels in Fig. 1, we find that $(E_0-H_0)^{-1}$ acting on (2.21) contributes a factor of

$$2(\mathbf{m}^2+\mathbf{n}^2-\nu^2-\mu^2)^{-1}/(\hbar^2M). \tag{2.22}$$

In general, acting on any Slater determinant $(E_0-H_0)^{-1}$ gives a factor which comprises the sum (from E_0) of the energies of the states which are emptied, less the sum of the energies of the states which are filled in their place. The factor $(I-P_0)$ is just unity, except for the original Slater determinant, or any permutation of its rows or columns, in which case it is zero. This factor prevents the system from returning to its original state, so that all of the Slater determinants in which the Ω_n may be expanded have at least one state occupied which is outside the Fermi sea.

FIG. 1. Pictorial representation of the action of a vertex on the unperturbed Fermi sea.

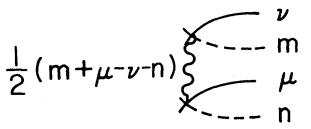

Finally, to describe all the operations necessary to perform the perturbation calculations (2.7) and (2.8), we must consider the inner product of Φ with another Slater determinant. It is well known that two Slater determinants are orthogonal, unless they correspond to the same set of single-particle states. This result can be seen easily as follows. Every term in the expansion of a Slater determinant is proportional to

$$\mathcal{S}=\exp\,(i\sum_{j=1}^{N}\mathbf{K}_{P_j}\cdot\mathbf{r}_j), \tag{2.23}$$

where P_j are a permutation of the j's. By the single-particle state orthogonality, unless there is a term in Φ with the $\mathbf{k}$ dotted into $\mathbf{r}_j$ equal to $\mathbf{K}_{P_j}$ for every j, we have

$$\int\Phi^*\mathcal{S}\prod_{j=0}^{N}d^3\mathbf{r}_j=0, \tag{2.24}$$

but this equality can only hold if the $\{\mathbf{K}\}$ are the same as the $\{\mathbf{k}\}$ except possibly rearranged. Further, if they are the same set then we have

$$\int\Phi^*\Phi\prod_{j=0}^{N}d^3\mathbf{r}_j=1, \tag{2.25}$$

as every one of the $(N!)$ permutations occurs in the expansion of the Slater determinants, and appears with the same sign in both Φ and Φ^*.

The consequence of (2.24) is that the energy perturbation terms can be represented by diagrams which have no lines incident (i.e., they are conventionally represented by blanks) on the left, and no lines leaving on the right. They have, because of the $(I-P_0)$ factor, at least one (and as we shall see, two) filled state and hole lines at each intermediate point. A sample third-order diagram appears in Fig. 3. The formula it represents is (after having been integrated over the coordinate variables)

$$\tfrac{1}{8}\sum_{\mathbf{m},\mathbf{n},\boldsymbol{\nu},\boldsymbol{\mu},\mathbf{n}_1,\boldsymbol{\mu}_1}\frac{\langle\mathbf{n}_1\mathbf{n}\,|\,v\,|\,\boldsymbol{\nu}\boldsymbol{\mu}_1\rangle\langle\mathbf{m}\boldsymbol{\mu}_1\,|\,v\,|\,\boldsymbol{\mu}\mathbf{n}_1\rangle\langle\boldsymbol{\nu}\boldsymbol{\mu}\,|\,v\,|\,\mathbf{m}\mathbf{n}\rangle}{(\hbar^2/2M)^2(\boldsymbol{\nu}^2+\boldsymbol{\mu}_1^2-\mathbf{n}_1^2-\mathbf{n}^2)\,(\boldsymbol{\nu}^2+\boldsymbol{\mu}^2-\mathbf{m}^2-\mathbf{n}^2)} \tag{2.26}$$

FIG. 2. An interaction which leaves the Fermi sea unchanged.

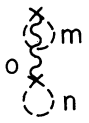

subject to the restrictions:

$\mathbf{m}, \mathbf{n}$	in the Fermi sea, and $\mathbf{m}\neq\mathbf{n}$,	
$\boldsymbol{\mu}, \boldsymbol{\nu}$	not in the Fermi sea, and $\boldsymbol{\mu}\neq\boldsymbol{\nu}$,	
$\mathbf{n}_1$	in the Fermi sea, but $\mathbf{n}_1\neq\mathbf{n}, \mathbf{m}$	
$\boldsymbol{\mu}_1$	not in the Fermi sea, and $\boldsymbol{\mu}_1\neq\boldsymbol{\nu}$,	(2.27)

which come from the fact that a determinant with two rows or columns equal vanishes, and from the sum over the states in the original Slater determinant. The factor of one-eighth comes from three factors of one-half from (2.21). The sign is plus because the columns of Φ underwent an even number of permutations: $(\mathbf{m}, \mathbf{n}, \mathbf{n}_1)\rightarrow(\mathbf{n}, \mathbf{n}_1, \mathbf{m})$. This term arises as part of the first term of

$$E_3=\langle\Phi\mid h\Omega_2\mid\Phi\rangle$$
$$=\langle\Phi\mid h\left(\frac{I-P_0}{E_0-H_0}\right)h\left(\frac{I-P_0}{E_0-H_0}\right)h\mid\Phi\rangle$$
$$-\langle\Phi\mid h\left(\frac{I-P_0}{E_0-H_0}\right)\langle\Phi\mid h\mid\Phi\rangle\left(\frac{I-P_0}{E_0-H_0}\right)h\mid\Phi\rangle. \quad (2.28)$$

Let us next consider the behavior of each term in the Ω_n and E_n as N, the number of particles in the system tends to infinity (N/Γ fixed). From (2.16), $\langle\boldsymbol{\nu}\boldsymbol{\mu}\mid v\mid\boldsymbol{\lambda}\boldsymbol{\eta}\rangle$ is proportional to Γ^{-1} and conserves momentum. When we remember that the states summed over [in (2.26) for example] are eigenstates of the single-particle energy, we can convert, in the limit of $\Gamma\rightarrow\infty$, the momentum sums to integrals

$$\sum_{\mathbf{q}}\rightarrow[\Gamma/(2\pi)^3]\int d^3\mathbf{q} \quad (2.29)$$

as, by (2.11) the level spacing is $(2\pi/L_i)$. As a sample we will analyze (2.26) (Fig. 3). By momentum conservation at the first vertex, there are only three independent momenta created there. At the second vertex there is one more, and at the last vertex none. The momentum conservation there is satisfied automatically. Thus, converting the sums to integrals yields a factor of Γ^4. The three factors of $\langle\mid v\mid\rangle$ yield a factor of Γ^{-3}. The net result is Γ^{+1}. This behavior is what we desire as we seek an energy proportional to the system size. Another example is given in Fig. 4. The second and fourth vertices are displaced downward for clarity. The summation restrictions are:

$\mathbf{m}_1, \mathbf{n}_1$	in the Fermi sea, and $\mathbf{m}_1\neq\mathbf{n}_1$,	
$\boldsymbol{\nu}_1, \boldsymbol{\mu}_1$	not in the Fermi sea, and $\boldsymbol{\mu}_1\neq\boldsymbol{\nu}_1$,	
$\mathbf{m}_2, \mathbf{n}_2$	in the Fermi sea, and $\mathbf{m}_2\neq\mathbf{m}_1, \mathbf{n}_1$, or $\mathbf{n}_2$ $\mathbf{n}_2\neq\mathbf{m}_1$, or $\mathbf{n}_1$,	
$\boldsymbol{\nu}_2, \boldsymbol{\mu}_2$	not in the Fermi sea, and $\boldsymbol{\nu}_2\neq\boldsymbol{\nu}_1$, $\boldsymbol{\mu}_1$, or $\boldsymbol{\mu}_2$ $\boldsymbol{\mu}_2\neq\boldsymbol{\nu}_1$, or $\boldsymbol{\mu}_1$,	
$\mathbf{n}_3$	in the Fermi sea, and $\mathbf{n}_3\neq\mathbf{m}_1, \mathbf{n}_1, \mathbf{m}_2$, or $\mathbf{n}_2$,	
$\boldsymbol{\mu}_3$	not in the Fermi sea, and $\boldsymbol{\mu}_3\neq\boldsymbol{\nu}_1, \boldsymbol{\nu}_2$, or $\boldsymbol{\mu}_2$,	(2.30)

and the term in E_5 it represents is

$$\tfrac{1}{3\,2}\sum_{\substack{\mathbf{m}_1,\mathbf{n}_1,\boldsymbol{\mu}_1,\boldsymbol{\nu}_1\\ \mathbf{m}_2,\mathbf{n}_2,\boldsymbol{\mu}_2,\boldsymbol{\nu}_2\\ \mathbf{n}_3,\boldsymbol{\mu}_3}}\langle\mathbf{m}_1\mathbf{n}_3\mid v\mid\boldsymbol{\nu}_1\boldsymbol{\mu}_3\rangle\langle\mathbf{m}_2\mathbf{n}_2\mid v\mid\boldsymbol{\nu}_2\boldsymbol{\mu}_2\rangle\langle\mathbf{n}_1\boldsymbol{\mu}_3\mid v\mid\boldsymbol{\mu}_1\mathbf{n}_3\rangle\langle\boldsymbol{\nu}_2\boldsymbol{\mu}_2\mid v\mid\mathbf{m}_2\mathbf{n}_2\rangle\langle\boldsymbol{\nu}_1\boldsymbol{\mu}_1\mid v\mid\mathbf{m}_1\mathbf{n}_1\rangle$$
$$\times[(\hbar^2/2M)^4(\boldsymbol{\nu}_1^2+\boldsymbol{\mu}_3^2-\mathbf{m}_1^2-\mathbf{n}_3^2)(\boldsymbol{\nu}_1^2+\boldsymbol{\mu}_3^2+\boldsymbol{\nu}_2^2+\boldsymbol{\mu}_2^2-\mathbf{m}_1^2-\mathbf{n}_3^2-\mathbf{m}_2^2-\mathbf{n}_2^2)$$
$$\times(\boldsymbol{\nu}_1^2+\boldsymbol{\mu}_1^2+\boldsymbol{\nu}_2^2+\boldsymbol{\mu}_2^2-\mathbf{m}_1^2-\mathbf{n}_1^2-\mathbf{m}_2^2-\mathbf{n}_2^2)(\boldsymbol{\nu}_1^2+\boldsymbol{\mu}_1^2-\mathbf{m}_1^2-\mathbf{n}_1^2)]^{-1}. \quad (2.31)$$

There are seven independent momentum sums, and five potential factors. Thus (2.31) is proportional to Γ^2, which if it stood alone would lead to a divergent energy per particle, and render the expansion unusable.

Let us now find the general rule for the Γ dependence for any diagram which arises directly. By arising directly we mean in the first term of (2.28), or more generally from

$$\langle\Phi\mid h\{[(I-P_0)/(E_0-H_0)]h\}^{n-1}\mid\Phi\rangle \quad (2.32)$$

which results from using only the first term on the right in (2.8). Every vertex gives a factor of Γ^{-1} so E_n will contain a factor Γ^{-n}. When momentum conservation is taken into account, every vertex gives addi-

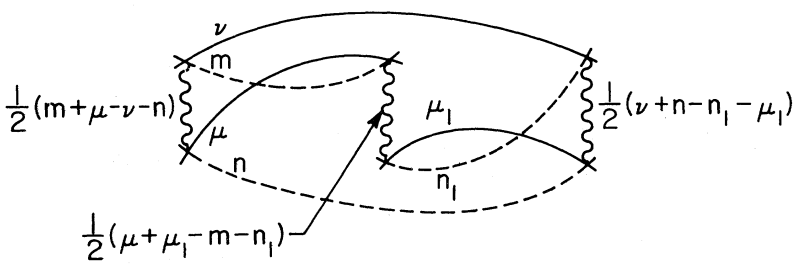

FIG. 3. A sample diagram. This diagram represents Eq. (2.26).

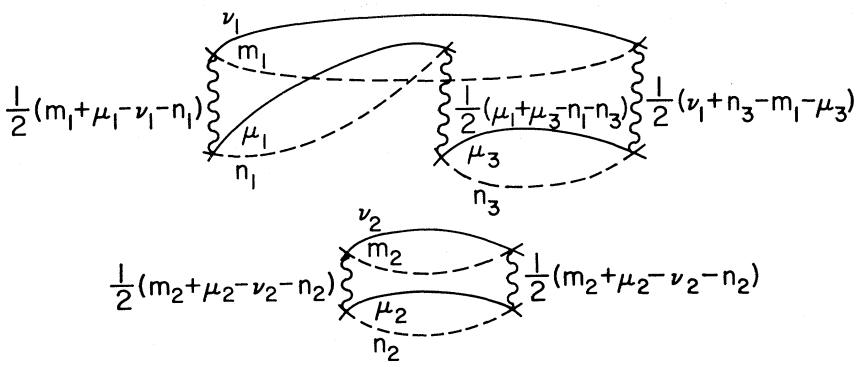

FIG. 4. A sample two-component diagram representing Eq. (2.31).

tional independent momenta (or imposes restrictions) so that the conversion of momentum sums to integrals yields a factor of $\Gamma^{1+(\frac{3}{2}\Delta l)}$, where Δl is the change in the number of lines leaving on the right at that stage in the diagram. There are two exceptions to this rule. The first is shown in Fig. 2 (and its exchange diagram) which contribute a net factor of Γ^1 rather than Γ^0 as would be expected. The second exception is that in which a vertex ends a separate component of the diagram (as do vertices 4 and 5 in Fig. 4). Here the momentum conservation is automatic and we get a factor of Γ^{-1} instead of Γ^{-2}. In each case, the consequence is that we must multiply the results of the above rule by a factor of Γ for each separate component of the diagram. As the net change in the number of lines for a directly arising energy diagram is zero, we find that the dependence on the system size is Γ^s, where s is the number of separate components. We will show that the energy can be reexpressed completely in terms of single component diagrams.

C. Factorization of Separated Component Terms

In order to establish this result, we need a theorem due to Hugenholtz (1957). He actually established a more general result than we prove here. An additional algebraic proof has been given by Franz and Mills (1960). Baker *et al.* (1963) have used this theorem without reference on parts of a single linked diagram, and Bethe *et al.* (1963) have emphasized its value in this regard.

Hugenholtz Factorization Theorem. Consider the perturbation terms represented by a diagram which consists of two given separated components. (Neither of these components need be a linked component.) We will assume that the left (beginning) end of each component has no lines entering it, and that the right most vertex of one component is given to lie to the right of all vertices of the other component. For any single term in the momentum sums represented by the diagram, the sum over all allowed vertex orders (all different diagrams consisting of the two separated components subject to the above restrictions) is equal to the product of the term represented by the first component considered as a diagram in its own right (the energy denominators are as if no other excitation of the Fermi sea were present) times the term represented by the second component considered as a diagram in its own right times $1/(D_1+D_2)$, where D_1 and D_2 are the right most (last) energy denominators of components one and two.

Proof. It will suffice to show, by induction, that the addition of a single vertex to the left end of one component simply multiplies the contribution by the additional propagator (one over the energy denominator) when the sum over all allowed vertex orders is taken. At this stage, no stipulation is made concerning the number of lines entering or leaving either component, and no account is taken of the propagators beyond the right end of either component. The interaction matrix elements do not change with vertex order as they depend only on the incoming and outgoing momenta. We will represent the vertices and the propagators of component α by a_i and $(1/A_i)$ respectively; of component β by b_i and $(1/B_i)$ respectively, with i starting from 1 in both cases. We will add to component β an additional vertex, b_0 with associated propagator $(1/B_0)$. A typical term in the sum over all allowed vertex orders before adding b_0 can be represented as:

$$\begin{aligned} &\text{component } \alpha\text{:} \quad a_1A_1a_2A_2\cdots a_nA_na_{n+1}\cdots \\ &\qquad\qquad\qquad\qquad\qquad\qquad\quad \vdots \\ &\text{component } \beta\text{:} \qquad\qquad\qquad\qquad\quad b_1B_1\cdots. \end{aligned} \tag{2.33}$$

We now add the new vertex on the left of component β, and because of the additivity of the energy denominator in the propagator factors, we obtain for the sum of all vertex orders

$$\{B_0^{-1}\prod_{i=1}^{n}(B_0+A_i)^{-1}+\sum_{j=1}^{n}[\prod_{i=1}^{j}(A_i)^{-1}][\prod_{i=j}^{n}(B_0+A_i)^{-1}]\}R(n,1), \tag{2.34}$$

where $R(n, 1)$ stands for the rest of the term coming the part to the right of vertex a_n and b_1. We may rewrite (2.34) as

$$\{[B_0^{-1}(B_0+A_1)^{-1}+A_1^{-1}(B_0+A_1)^{-1}]\prod_{i=2}^{n}(B_0+A_i)^{-1}+A_1^{-1}\sum_{j=2}^{n}[\prod_{i=2}^{j}(A_i)^{-1}][\prod_{i=j}^{n}(B_0+A_i)^{-1}]\}R(n,1)$$

$$=A_1^{-1}\{B_0^{-1}\prod_{i=2}^{n}(B_0+A_i)^{-1}+\sum_{j=2}^{n}[\prod_{i=2}^{j}(A_i)^{-1}][\prod_{i=j}^{n}(B_0+A_i)^{-1}]\}R(n,1), \quad (2.35)$$

which is $(1/A_1)$ times the same problem with one less term. Repeating this operation until the $\sum$ is exhausted, we are left with

$$B_0^{-1}[\prod_{i=1}^{n}(A_i)^{-1}]R(n,1)=B_0^{-1}R(1,1), \quad (2.36)$$

which is simply $(1/B_0)$ times the summand we had before the addition of vertex b_0. As one can easily verify directly the theorem for α and β consisting of each of the one and two vertex diagrams, we have established the lemma, by induction.

We can illustrate this process by a sample case (see Fig. 5). The sum over all allowed vertex orders for the newly inserted vertex b_0 is, in this case, the three terms (a), (b), and (c). The complete denominator contributions are

$$(a)=A_1^{-1}A_2^{-1}(A_2+B_0)^{-1}(A_2+B_1)^{-1},$$
$$(b)=A_1^{-1}(A_1+B_0)^{-1}(A_2+B_0)^{-1}(A_2+B_1)^{-1},$$
$$(c)=B_0^{-1}(A_1+B_0)^{-1}(A_2+B_0)^{-1}(A_2+B_1)^{-1}.$$

These sum to yield

$$(a)+(b)+(c)=(B_0^{-1}A_1^{-1}A_2^{-1})(A_2+B_1)^{-1}.$$

The term in the first parenthesis is the factored contribution of the two components resulting from the sum of all allowed vertex orders for b_1, the right most vertex. The second factor contains the $(D_1+D_2)^{-1}$ factor mentioned in the theorem. If one of the components had no lines on the right, its right most denominator would of course vanish.

D. Reduction to Single Component Diagrams

We are now in a position to state and prove the fundamental theorem which makes the Rayleigh–Schrödinger perturbation expansion tractable for the many-fermion system.

Linked Cluster Expansion Theorem. The terms in the energy perturbation expansion, E_n, may be represented completely in terms of ground-state to ground-state single-component diagrams. The wave matrix perturbation expansion may be represented completely in terms of diagrams which have no separated component without lines entering or leaving it.

Proof. Referring to the defining Eqs. (2.7) and (2.8), we can immediately establish this theorem for E_1, E_2, and Ω_1 which consist of directly occurring terms only. We will assume that the theorem is true for all $n\leq\theta$, and prove its truth for $\theta+1$. From (2.7), we see that $E_{\theta+1}$ can be derived from h acting on Ω_θ. Since, by hypothesis Ω_n has no separate zero-line to zero line-components, the only way to produce a nonvanishing contribution is to have h of the type illustrated in Fig. 6 which has no lines leaving on the right. It cannot be of the type of Fig. 2 as Ω_n would have had to be a ground-state to ground-state term which is excluded by

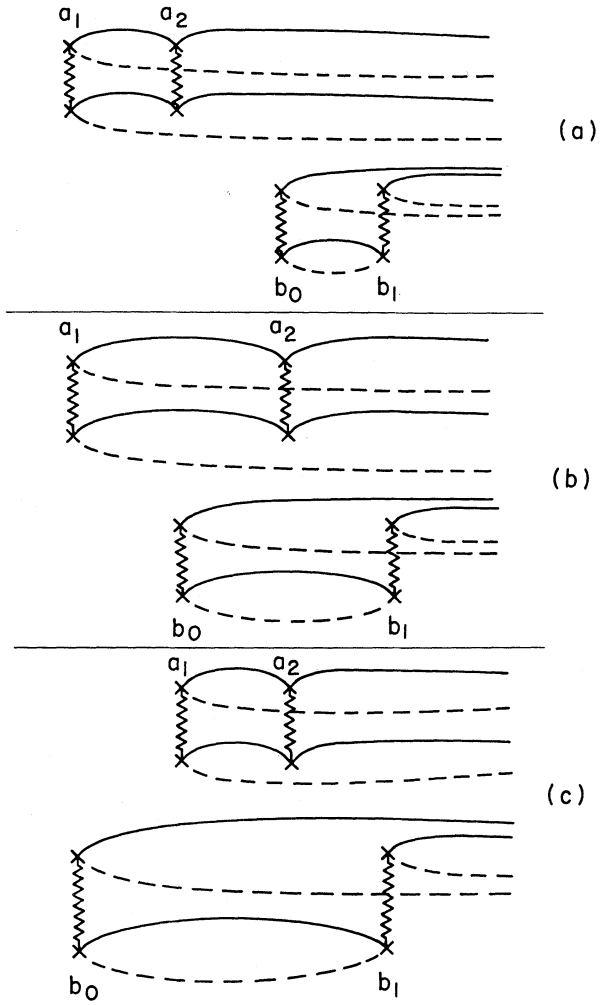

FIG. 5. A sample diagram illustrating the sum over all vertex orders.

FIG. 6. The final vertex of a ground-state to ground-state component of a diagram.

hypothesis. Since a vertex of the type illustrated in Fig. 6 can create at most one ground-state to ground-state component, the theorem is proved for $E_{\theta+1}$. Now consider $\Omega_{\theta+1}$. As there is a left-hand factor of $(I-P_0)$, there are no ground-state to ground-state diagrams in it. Suppose, h contributes a vertex of the type of Fig. 2 or its exchange, Fig. 7. This creates a separate component. The summation restrictions are $\mathbf{m}\neq\mathbf{n}$ and both in the excited Fermi sea. By the excited Fermi sea we mean the set of all the single-particle states comprising the original ground state, except that those states which have been excited to states not in the original Fermi sea are omitted. Let us combine this contribution with the term from the summation in (2.8), $-E_1\Omega_\theta$. These two contributions are the same except that, for the second, the summation restriction is only $\mathbf{m}\neq\mathbf{n}$ and both in the Fermi sea. The difference will be the negative of the term represented by attaching the new vertex to the hole lines on the right in Ω_θ as shown in Fig. 8; although the terms in Fig. 9, which attach a "bubble" to a filled state line can and do occur directly, those in Fig. 8 do not because they involve emptying an already empty state. However, our diagram formalism now includes them, with an extra minus sign, as the residual of the subtraction term in (2.8). The only other way that a separated component of the zero-line to zero-line type can be created is if h represents a vertex of the sort shown in Fig. 6. If it does and creates a separate component, then this component, considered as a diagram in its own right, is, by our construction procedure, a term contributing to E_j, $j=2, \cdots, \theta$. Conversely, any term in such an E_j can arise as such a separated component. All the various vertex orders for the directly occurring separated component will occur and the sum can be performed by means of the Hugenholtz Factorization Theorem. A sample case is shown in Fig. 10 from Ω_3. The only complication comes from the restrictions on the momentum summations. We counter this difficulty by adding in the missing terms to the sum, and taking account of their subtraction by separate diagrams. By the Hugenholtz Factorization Theorem, the vertex order sum is exactly canceled by the subtraction of the corresponding term from the summation in (2.8), which eliminates all the separated zero-line to zero-line

FIG. 7. The exchange diagram of Fig. 2.

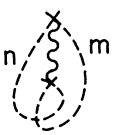

FIG. 8. "Bubble" and its exchange diagram on a hole line. These diagrams arise in the subtraction process.

components in $\Omega_{\theta+1}$, and completes the proof of this theorem. In the case illustrated in Fig. 10, the subtraction term is $(I-P_0)(E_0-H_0)^{-1}E_1\Omega_1$.

We must however give the prescription for drawing the subtraction terms. Suppose the lines (either filled-states or holes) shown in Fig. 11(a) are restricted in the subtraction term to have equal momenta. They can be "pasted" together, as shown in Fig. 11(b). Momentum conservation across the dotted line insures that the momenta on the two new lines is equal. The resulting diagram has no zero-line to zero-line separate component. It has an extra minus sign as it is a subtraction term. This diagram does not occur directly as it has two lines with the same momentum. It is worth noting that when one "pastes" a separated component on and there are two different lines with the same momentum resulting from a previous "pasting" operation, the final result can arise from two different intermediate stages. That is to say A could be pasted to B and then the combination to C, or B to C and then to A. This doubling of the final result can be conveniently accounted for by simply including both pastings of the new component to lines with the same momentum when drawing out all the distinct ground state energy graphs. In Fig. 12, we have shown the topologically distinct (taking account of equivalent lines) "pasted" contributions which occur from the cancellation of Fig. 10. Each one shown is but one of the four occurring "pasted" diagrams of its type.

E. Rules for the Basic Linked Diagram Expansion

By the theorem in the previous section, we need only consider linked (i.e., single-component) diagrams in the expansion of the ground-state energy. We will summarize here the rules drawing the basic diagram expansion, and associating terms in the perturbation series with them. It is to be borne in mind that these refer to a system of N particles in a box of volume Γ

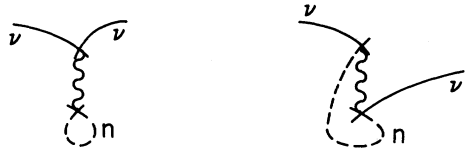

FIG. 9. "Bubble" and its exchange diagram on a filled-state line. These diagrams arise directly.

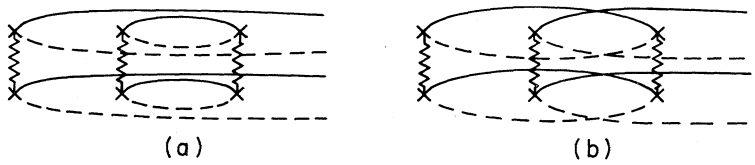

FIG. 10. The two vertex orders for a particular two-component diagram.

subject to periodic boundary conditions and a short-range, but periodic potential interaction.

1. The first order energy is given by

$$\tfrac{1}{2}\sum_{\mathbf{m}\neq\mathbf{n}}[\langle\mathbf{mn}\,|\,v\,|\,\mathbf{mn}\rangle-\langle\mathbf{nm}\,|\,v\,|\,\mathbf{mn}\rangle], \quad (2.37)$$

where $\mathbf{m}$ and $\mathbf{n}$ are in the Fermi sea, and $\langle v\rangle$ comes from (2.16). This term is represented by Figs. 2 and 7.

2. For second, and higher (nth) order, draw all distinct, linked, n vertex diagrams which begin with Fig. 1 and end with Fig. 5. An allowed vertex may be produced by attaching one and only one solid or dotted line to each of the four straight lines in Fig. 13. By convention, the solid lines are attached to the top, and the dotted lines to the bottom, of these straight lines. There are therefore $2^4=16$ such vertex types. In addition, there is the type in which a state is left unchanged. There are eight such vertices, illustrated in Figs. 8 and 9, plus the up–down interchange. Note, however, that the eight vertices represented by Fig. 14, its left-right interchange, and their up–down interchange are excluded, as momentum conservation requires a filled state and a hole to have the same momentum. A state cannot be both occupied and empty at the same time.

3. Label every line with a momentum in such a way that momentum is conserved at every vertex. Sum over all single-particle momentum eigenstates such that the holes lie in the Fermi sea, and the filled states lie outside it.

4. The following terms are to be deleted from the sum: (i) No two lines, situated at least in part one above the other, of the same type may have the same momentum unless cutting both will yield two separate components of the diagram; (ii) No hole line of the same momenta can both enter and leave a single vertex unless cutting both parts of it will yield two separate components of the diagram; (iii) No hole and filled state may have the same momentum.

5. For every vertex include a factor of $\frac{1}{2}\langle\boldsymbol{\nu\mu}\,|\,v\,|\,\mathbf{mn}\rangle$ [see Eq. (2.16)], where the labeling of the lines is as given in Fig. 13.

6. For every propagator (the interval between successive vertices) include a factor of 1/(the sum of the energies of the hole lines minus the sum of the energies of the filled state lines).

7. Multiply by $(-1)^{P+H-C}$, where P is the number of violations of the Pauli principle (a case permitted by an unless of rule 4), H is the number of hole lines, and C is the number of cycles. The cycle count is the number of closed loops in the diagram which can be traced out by following the solid and dotted lines but not the wavy ones. For example, Fig. 3 has $C=1$; Fig. 4 has $C=5$.

Perhaps the only part of these rules not yet commented on is the factor $(-1)^{H-C}$. This factor counts the evenness or oddness of the permutation required to change the final Slater determinant into the original one. It can be seen as follows. We fix our attention on one closed loop or cycle in a basic diagram and start at its left most end. (If there are two, pick either one.) The effect of the vertex action is to replace a Fermi sea state with another momentum from outside the Fermi sea. As we continue (starting out along the filled state line) around the loop, we eventually fill a hole. This filling effects a permutation of the Slater determinant by putting the momentum of the first hole in the position of the second, unless, of course, the hole encountered was the first one, in which case there is no permutation. As we continue about the loop, we generate a cyclic permutation of the hole momenta in the Slater determinants of length equal to the number of holes in the cycle. The number of permutations is one less than the number of holes in the cycle. Thus, for the diagram as a whole the permutation sign factor is $(-1)^{H-C}$.

F. Hugenholtz Contracted Diagrams and Spin Weights

Up until now we have not considered the effects of spin or isotopic spin. First, for spin and isotopic spin independent forces, we need only note that when a potential interaction causes

$$\mathbf{m},\ s_{\mathrm{m}}\rightarrow\boldsymbol{\nu},\ s_{\nu},$$
$$\mathbf{n},\ s_{\mathrm{n}}\rightarrow\boldsymbol{\mu},\ s_{\mu}, \quad (2.38)$$

where the s's are the spin and isotopic spin variables, as

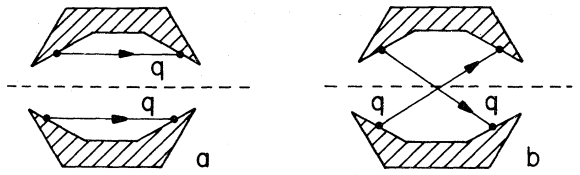

FIG. 11. (a) General separated diagram, with a restriction of the equality of the momentum between a line in each component. (b) The same diagram represented by a connected diagram where equality is insured by momentum conservation.

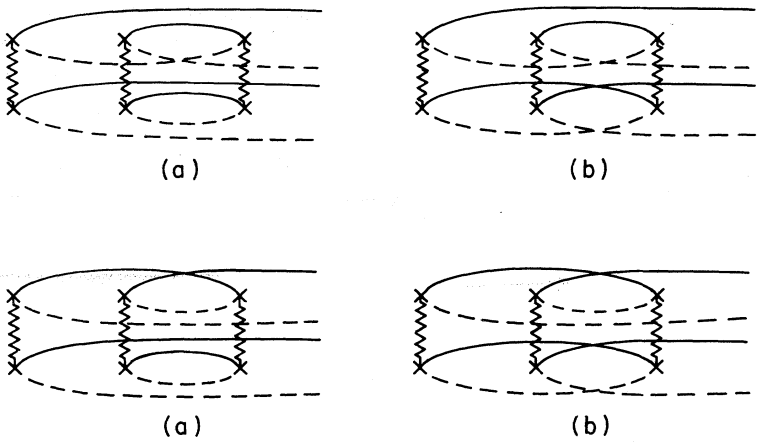

FIG. 12. The inequivalent "pasted" graphs derived from Fig. 10.

pictured in Fig. 13. The spin independences requires $s_m = s_\nu$ and $s_n = s_\mu$. Following the loop structure of the basic diagram, this spin and isotopic spin conservation yields a sum over as many independent spins and isotopic spins as there are cycles in the basic diagram. Hence we have the additional rule, when spin and isotopic spin are present.

8. Multiply the contribution by $(2S+1)^C(2I+1)^C$ to take account of the spin (S) and isotopic spin (I) states in the presence of spin and isotopic spin independent forces.

The trouble with the basic diagrams used so far is that, although they have great clarity standing as they do in one-to-one correspondences with terms in the perturbation expansion, there are too many of them for convenient calculation, and they are not handy for forces which are not spin independent. A more convenient set of diagrams has been introduced by Hugenholtz (1957). Each one corresponds to several basic diagrams. They are obtained from the basic diagrams by shrinking every vertex (Fig. 13) to a dot. Every solid line is replaced by a line with an arrowhead pointing left, and every dotted line by a line with an arrowhead pointing right. The count of cycles is lost in this contraction. The different allowed types of vertices are shown in Fig. 15. With each vertex we have associated a numerical factor which is the number of basic vertices which correspond to that Hugenholtz vertex times two if there are two hole lines entering from the left, times two if there are two filled state lines entering from the left. The product of these factors gives the total number of basic graphs represented by one Hugenholtz graph. This counting rule is equivalent to Hugenholtz's rule of $4^n/2^m$, where n is the order, and m is the number of pairs of equivalent lines (i.e., two lines going in the same direction between the same two vertices). The extra factors of two come because if there are two lines of the same type coming in they can be hooked up in two ways. We only count it for the left side as we think of building the diagram up from left to right, and in this case the symmetry between lines leaving on the right is only a relabeling change of a dummy variable.

As our numerical applications will be concerned with the limit $N\to\infty$, we will now give the rules for the Hugenholtz diagram representation of the ground-state energy of the infinite limit of the many-fermion perturbation series. Except for Rule (4), where terms of order $1/N$ are neglected here, which may be significant when one interchanges the order of summation and letting $N\to\infty$, the transcription is a straightforward summary of what we have said previously. The sums are converted to integrals by (2.29). Also, by (2.29) the number of particles is related to the volume by

$$\Gamma/(2\pi)^3 = 3N/[(2S+1)(2I+1)4\pi k_F{}^3]. \quad (2.39)$$

The rules are, for $N\to\infty$:

(i) The first order energy (represented diagrammatically by Fig. 16) is

$$\lim_{N\to\infty}\left[\frac{E_1 M}{(N\hbar^2)}\right] = \frac{3(2S+1)(2I+1)}{8\pi k_F{}^3}\int_{|\mathbf{m}|\le k_F,|\mathbf{n}|\le k_F} d\mathbf{m}\, d\mathbf{n}$$
$$\times \mathrm{Tr}\{\tilde{v}(0)-\tilde{v}(|\mathbf{m}-\mathbf{n}|)P(\mathbf{m},\mathbf{n})\}/\mathrm{Tr}\{I\}, \quad (2.40)$$

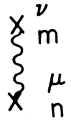

FIG. 13. Conventional representation of a single vertex in a basic diagram.

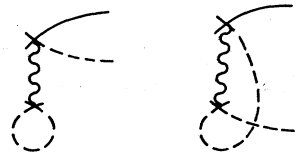

FIG. 14. Disallowed vertices, by momentum conservation and the Pauli principle.

where the trace is taken over the spin and isospin space states corresponding to **m** and **n**. The operator $P(\mathbf{a}, \mathbf{b})$ permutes the spin and isotopic spins variables corresponding to momentum states **a** and **b**.

(ii) For second and higher (nth) order, draw all distinct, linked, n vertex diagrams using the vertices of Fig. 15 which begin with vertex F and end with vertex E.

(iii) Form any basic diagram from the Hugenholtz diagram which has the largest number of cycles possible for that Hugenholtz diagram.

(iv) Label every line in the basic diagram with momentum in such a way that momentum is conserved at every vertex. The labels will be referred to according to the convention of Fig. 13, with a subscript j appended to denote the vertex number. It is to be noted that every line is thus given two names. The relations between them, for example $\nu_2 \equiv m_4$, $\nu_1 \equiv m_5$, $m_1 \equiv \nu_5$, $n_1 \equiv \nu_3$, etc., in Fig. 4, are what distinguish the different diagrams. Integrate the following term over that region where all hole momenta are less than or equal to k_F and all filled state momenta are greater than k_F

$$-3(-1)^{n+P+H-C}(2S+1)^{C-1}(2I+1)^{C-1}/2^m 4\pi k_F{}^3 \times \int d\tau \left[\mathrm{Tr}\left\{\prod_{j=n}^{1}\left[(\tilde{v}(\mathbf{q}_j)I-\tilde{v}(\mathbf{q}_{\mathrm{exch},j})P(\mathbf{m}_j,\mathbf{n}_j)P(\boldsymbol{\mu}_j,\boldsymbol{\nu}_j)\right)P(\mathbf{m}_j,\boldsymbol{\nu}_j)P(\mathbf{n}_j,\boldsymbol{\mu}_j)\right]\right\}\right] \times \left(\mathrm{Tr}\left\{\prod_{j=n}^{1}P(\mathbf{m}_j,\boldsymbol{\nu}_j)P(\mathbf{n}_j,\boldsymbol{\mu}_j)\right\}\prod_{j=1}^{n-1}D_j\right)^{-1}, \quad (2.41)$$

where n is the number of vertices, P the number of violations of the Pauli principle, H the number of hole lines, C the maximum number of cycles, S the spin, I the isotopic spin, m the number of pairs of equivalent lines, k_F the Fermi momentum, $\tilde{v}$ is defined by (2.17), $\mathbf{q}_j$ is the momentum transfer at vertex j, $\mathbf{q}_{\mathrm{exch},j}$ is the exchanged momentum, and D_j is the energy of the filled state lines minus that for the hole lines for the section of the diagram between the jth and the $(j+1)$st vertex. The trace is to be taken over the H independent spins and isotopic spins associated with the H holes. It is to be noted that Rule (4) (iii) for basic diagrams is an automatic consequence here and that those Hugenholtz diagrams which can be separated by cutting a single hole and a single filled state line vanish on that account.

(v) An exception to form (2.41) occurs for "bubble" vertices (type J). The permutation operator multiplying $\tilde{v}(q_{\mathrm{exch},j})$ is only $P(\mathbf{m}_j, \mathbf{n}_j)$ as $P(\mathbf{m}_j, \mathbf{n}_j) = P(\boldsymbol{\mu}_j, \boldsymbol{\nu}_j)$ for this type of vertex, so that what for moving vertices AI is a single line, for vertex J is moving a pair of lines.

We note that we like to treat as a group all those diagrams which have bubble insertions at the same vertex position in given Hugenholtz graph. This procedure cancels certain divergences which would otherwise occur and will be discussed later. We represent this sum by a "flag" as shown in Fig. 15.

III. THE SINGULARITY AT THE ORIGIN

In the previous chapter we established that the energy per particle was formally of order unity in every order of the perturbation expansion and did not diverge as the system size (fixed density) increased indefinitely. In this chapter we will examine the convergence and summability properties of the resultant limiting series. The material of this chapter is based primarily on the work of Baker (1963, 1970).

We first establish, for a system interacting by means of a soft repulsive square-well potential that the radius of convergence for the ground-state energy of the N-body system (at fixed density) tends to zero as N tends to infinity at least as fast as $N^{-\gamma}$, where γ is any positive number less than $\frac{1}{3}$. This result implies that the perturbation series is, at best, an asymptotic one. We consider the complete perturbation series for

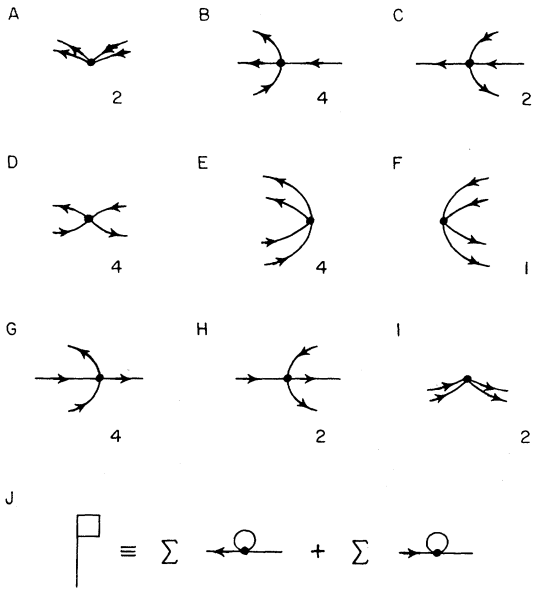

FIG. 15. Hugenholtz vertices with statistical weight factors.

more general potentials which may include attractive as well as repulsive forces, and bound every order. We find that it diverges no faster than a geometrical series times $(n!)$, where n is the order of the term. We consider the problem of assigning a meaning to the sum of the series and show that, provided the density is low enough (small compared to the jamming density for hard spheres), it may be summed, even though divergent, to the $\lim_{N\to\infty} E_N(V)$, where $E_N(V)$ is the energy per particle for a potential of real, positive strength V in the N-body problem.

Finally we show that certain rearrangements, though not all, of the potential perturbation series, highly important from the practical point of view, also define the same physically correct function.

A. Singularities in the Two-Body, Square-Well Force Problem

In order to investigate the many-body problem with a square-well interaction, we shall first investigate the problem of a particle in a spherical box with a square-well potential of strength V near the origin. The potential is

$$\begin{aligned} &V, && 0<r<a,\\ &0, && a<r<a+b,\\ &+\infty, && a+b<r. \end{aligned} \tag{3.1}$$

By solving Schrödinger's equation (see, for example, Schiff, 1949) we may easily establish that the energy of the lowest state, as a function of the potential strength, is given by the solution of

$$\tanh\left[\left(\frac{2m}{\hbar^2}(V-E)\right)^{1/2}a\right]\Big/\left[\left(\frac{2m}{\hbar^2}(V-E)\right)^{1/2}a\right]$$
$$=-\frac{b}{a}\tan\left[\left(\frac{2m}{\hbar^2}E\right)^{1/2}b\right]\Big/\left[\left(\frac{2m}{\hbar^2}E\right)^{1/2}b\right]. \tag{3.2}$$

When $V=0$, it follows readily from the trigonometric identity $\tan\alpha+\tan(\pi-\alpha)=0$ that the ground-state energy is

$$E(0)=(\hbar^2/2m)[\pi^2/(a+b)^2]. \tag{3.3}$$

As $V\to\infty$, the left-hand side of (3.2) tends to zero, the wave function is compressed into the region $a<r<a+b$, and the energy tends to

$$\lim_{V\to+\infty} E(V)=(\hbar^2/2m)(\pi^2/b^2). \tag{3.4}$$

In fact, if $|(V-E)^{1/2}a|$ is large and we are not near the poles of the left-hand side of (3.2), then we see, by approximating the right-hand side of (3.2) for $\tan(x)$ near $x=\pi$ by $(x-\pi)$, that $E(V)$ is approximately given by (3.4) for all V in the neighborhood of infinity, except near V real and negative. This statement is true when we start V toward infinity along the positive real axis.

When $V\to-\infty$, the right-hand side of (3.2) tends to zero, the wave function falls into the region $0<r<a$, and the energy tends to

$$\lim_{V\to-\infty}[E(V)-V]=(\hbar^2/2m)(\pi^2/a^2). \tag{3.5}$$

Again approximating $\tanh(x)$ near $x=i\pi$ by $(x-i\pi)$, we find (3.5) valid for large V not near V real and positive.

The difference of these two results for, say, V large and imaginary implies the existence of at least one complex conjugate pair of branch points. We may locate them as follows: It is well known that the branch points of $E(V)$ occur where $(dV/dE)=0$ (see, for instance, Kober, 1957). If we define

$$\begin{aligned} z^{1/2}&=[(2m/\hbar^2)(V-E)]^{1/2}a,\\ t^{1/2}&=[(2m/\hbar^2)E]^{1/2}b, \end{aligned} \tag{3.6}$$

then the equation for the critical points of $E(V)$ becomes

$$\left[\frac{t^{3/2}\cos^2(t^{1/2})}{2t^{1/2}-\sin(2t^{1/2})}\right]\left[\frac{2z^{1/2}-\sinh(2z^{1/2})}{z^{3/2}\cosh^2(z^{1/2})}\right]=\left(\frac{b}{a}\right)^3, \tag{3.7}$$

subject to (3.2). If $(b/a)\gg1$, then the solution is approximately given by

$$2t^{1/2}-\sin(2t^{1/2})=0, \qquad \cosh(z^{1/2})=0, \tag{3.8}$$

as

$$[\cos^2(t^{1/2})]/[\cosh^2(z^{1/2})]\propto(b/a)^2, \quad (b/a)\gg1. \tag{3.9}$$

Hence, in this limit we have the branch points at (Kober, 1957) approximately

$$V=\hbar^2/2ma^2[-\tfrac{1}{4}\pi^2+(a/b)^2(12.1372\pm10.3789i)]. \tag{3.10}$$

For the case $a=b$, $E(V)$ satisfies, by symmetry, the relation

$$E(V)-E(-V)=V, \tag{3.11}$$

and hence we expect the branch point to be on the imaginary axis. For V pure imaginary, (3.11) implies $t=-z^*$, and (3.7) reduces to

$$\mathrm{Re}\{[2z^{1/2}-\sinh(2z^{1/2})]/[z^{3/2}\cosh^2(z^{1/2})]\}=0. \tag{3.12}$$

We compute that the branch points are at the points

$$\begin{aligned} z&=-6.3\pm4.6i,\\ V&=(\hbar^2/2ma^2)(\pm9.2i). \end{aligned} \tag{3.13}$$

As b continues to decrease until $b/a\ll1$, we find reciprocally to (3.8) above, that the branch points

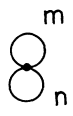

FIG. 16. Hugenholtz representation of Figs. 2 and 6 (first-order energy).

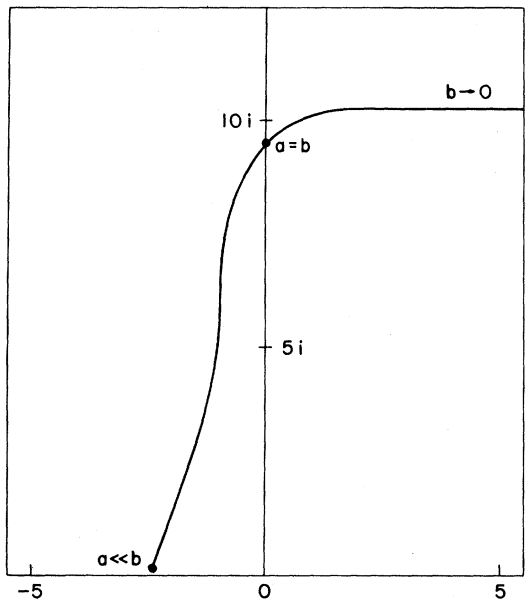

FIG. 17. Trajectory of the branch point in the ground-state energy for one particle in a box.

occur for

$$2z^{1/2}-\sinh\,(2z^{1/2})=0,$$

$$\cos\,(t^{1/2})=0, \qquad (3.14)$$

which implies that, approximately

$$z=-12.1372\pm 10.3789i, \qquad t=(\tfrac{1}{2}\pi)^2,$$

$$V=(\hbar^2/2ma^2)$$

$$\times[-12.1372\pm 10.3789i+(\tfrac{1}{2}\pi)^2(a/b)^2], \qquad (3.15)$$

so that the branch points recede to plus infinity along a path parallel to the positive real axis. The trajectory of this branch point is shown in Fig. 17 as a function of b.

Katz (1962) has illuminated the nature of these branch points. They result from the degeneracy of the ground state and the first excited state. If we cut the complex plane from these points to infinity, we have by (3.4) and (3.5) a single-valued function of V with no other branch points. However, if we join the two branch points by a cut (encircling both of them can easily be shown to leave the function unchanged), we find some of the additional branch points discussed by Katz where the ground state is degenerate with the second, third, ··· excited states.

For the higher excited states (angular momentum=0), the analysis is similar. For instance, for the case $b/a\gg 1$, we need the nth root for t in (3.8) for the nth excited state instead of the first root which we used for the first state. Hence, (3.10) becomes, approximately,

$$V_n\approx(h^2/2ma^2)\,[-(j+\tfrac{1}{2})^2\pi^2+(a/b)^2((n-j)^2\pi^2$$
$$-\tfrac{1}{4}\{\ln[4\pi(n-j)]\}^2\pm i(n-j)\pi\ln[4\pi(n-j)])]$$
$$j=0,\,1,\,\cdots,\,n-1, \qquad (3.16)$$

as long as the correction to $-(j+\frac{1}{2})^2\pi^2$ is small. There are now n pairs of branch points for the nth state. We previously found one pair for the ground state, or first state.

B. Singularities in the Many-Body, Square Well Force Problem

We now consider for simplicity the many-fermion (spinless here) system interacting with a simple square-well potential.

We shall show that there is at least one (pair) of branch points which tends to the origin of the V plane as N tends to infinity by traversing two paths in the complex plane to a certain point. The paths we take will never pass further from the origin than a distance which tends to zero as N tends to infinity. They will yield two different values of $E(V)$ for the same V, hence imply the existence of at least one branch point. The occurrence of a branch point stops the convergence of the Taylor series at that point. Let us consider a system defined by the Hamiltonian

$$H=\sum_{i=1}^{N}\frac{p_i^2}{2m}+\sum_{i<j}^{N}v(|\,r_i-r_j\,|), \qquad (3.17)$$

which is enclosed in a large box of volume Γ, such that $\rho=N/\Gamma$. The function $v(r)$ is taken to be a square well of range a and strength V.

Let us follow the energy as a function of V as V becomes progressively more attractive. We study the case of Fermi–Dirac statistics. The result here is well known.[1] The system collapses rapidly to a size of order a. The kinetic energy of the highest state ($n\propto N^{1/3}$) is proportional[1] to $N^{2/3}$. However, the potential energy of each particle is approximately NV as each particle feels the attraction of every other particle. Thus, for the collapsed state, we have for each particle a problem equivalent to one particle in a box with a square-well potential of strength $\mathcal{V}=NV$. The parameter b is related to the total volume Ω, and hence is proportional to $(N/\rho)^{1/3}$. It becomes very large as N goes to infinity. If we go to an attractive potential of strength V proportional to $N^{-[1/(3+\epsilon)]}$, then (for N very large) the potential energy per particle (proportional to $N^{(2+\epsilon)/(3+\epsilon)}$) will dominate the kinetic energy. Also, we will be to the left of all the branch points in the complex $\mathcal{V}$ plane for the first $n=N^{1/3}$ states. The analysis equivalent to that given above for angular momentum states different from zero is similar; for $b/a\gg 1$ the branch

[1] See, for example, Blatt and Weisskopf (1962), Chap. 3, Sec. 4.

points will close on the axis at the various appropriate binding energies. Returning to zero angular momentum, if we now approximate the tanh (x) in Eq. (2.2) by $x-n_{\max}\pi i$ for x near $n_{\max}\pi i$, we may continue on $\mathfrak{V}$ around the arc of a circle to the positive real axis, as long as we are careful to avoid points for which

$$\cos(t^{1/2})=0 \quad \text{or} \quad 2t^{1/2}-\sin(2t^{1/2})=0, \qquad (3.18)$$

which can easily be done. At this point, the collapsed state has been continued to the positive real axis and, in terms of the energy per particle, is of the order of $N^{(2+\epsilon)/(3+\epsilon)}$. As the potential energy per particle is still NV, the wave function must still be concentrated in a sphere of size a. However, if we continue from the origin straight out the positive real axis, then we know, physically, that as V tends to infinity we obtain the hard-core Fermi gas. The energy per particle is bounded for all V, $0\leq V<\infty$, at least for densities which are small compared to closest packing of hard spheres. Thus, we conclude that we must have encircled at least one branch point. As our above argument is valid for any $\epsilon>0$, $E(V)$ must have a radius of convergence of not more than the order of $N^{-1/3}$. Hence, in the limit as N tends to infinity, the radius of convergence of $E(V)$ for the potential we are considering tends to zero. As we showed formally in the previous chapter that each term in the expansion $E(V)/N$ is finite, we conclude that the expansion is a divergent one.

Our information on the direction in which the closest singularities approach the origin and, hence, the angle in which the series is asymptotic, is less definite. However, if we assume that the angular distribution of the correct many-body branch points is somewhat like those for the collapsed state problem, even though for $\mathfrak{V}$ of the order of -1 we are nowhere near the collapsed state, we get a physically fairly reasonable result. Looking, for low density, at the closest state of widest angle, we have $(n\propto N^{1/3}, j=0)$ from (3.16),

$$\mathfrak{V}_n\approx(\hbar^2/2ma^2)\times[-\tfrac{1}{4}\pi^2+Aa^2\rho^{2/3}\pm iB\ln N/N^{1/3}], \qquad (3.19)$$

where A is a constant independent of N. From (3.19) it is evident that, for ρ small compared to the density for the closest packing of hard spheres, the branch points for $V=\mathfrak{V}/N$ approach the axis from the negative real direction. If the second and third terms of (3.19) are not small compared to the first, then (3.19) is not valid, and no conclusions can be drawn from it. Hence, at least for ρ small enough, we find that $E(V)/N$ is asymptotic in the cut plane

$$-\pi<\arg V<\pi. \qquad (3.20)$$

This does not, of course, necessarily mean $E(V)$ is analytic in the cut plane.

The case of Bose–Einstein statistics is similar to the above. However, in the collapsed state all particles occupy the lowest state so that we find the radius of convergence to be only of order $V=N^{-1}$. This result may be true for Fermi–Dirac statistics as well, but we have proved only the less restrictive $V=N^{-1/3}$ instead.

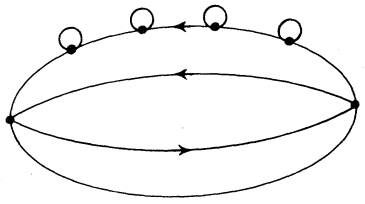

FIG. 18. A divergent bubble diagram.

We wish to point out that an argument similar to the above has been advanced previously for the case of quantum electrodynamics by Dyson (1952). He was able to show by considering e^2 negative that a phenomenon similar to the collapsed state occurs where electrons and positrons gather into separate regions of space and form a state of energy arbitrarily lower than that of the vacuum.

C. The Rate of Divergence

In this section we shall enumerate the terms contributing to the nth order of perturbation theory and bound each term for Fermi–Dirac spinless particles. We shall then estimate the rate of divergence of the perturbation series. It could diverge more slowly than our estimates, due to cancellation between terms, but as we have shown in the previous section, it cannot converge. In order to enumerate all the terms it is convenient to use the Hugenholtz diagram representation explained in the previous chapter.

The potential function $\bar{v}(k)$ introduced in (2.17) is, for a square-well potential

$$\bar{v}(k)=V[\sin(ak)-ak\cos(ak)]/(2\pi^2k^3). \qquad (3.21)$$

This precise form is not used in the following analysis but only some general aspects of it; namely, that it is bounded and goes to zero as k^{-2} as $k\to\infty$.

In order to enumerate all the basic diagrams in the nth order, we use the counting rule of Fig. 15. Vertex J is defined as the sum of bubbles on all occupied lines plus bubbles on all hole lines. If this is not done, diagrams such as shown in Fig. 18 diverge when taken separately, but when the sum over diagrams with bubbles in all possible positions is taken, this divergence is canceled. We will discuss this point further below.

Let us introduce a counting function $Q(n, N)$ which is equal to the number of basic diagrams of order n with N external occupied state lines (and hole lines) on the right and none on the left. The number of terms in the nth-order expansion of the energy will be related to $Q(n, 0)$. If we include vertex F, we will include some disconnected diagrams. If we omit vertex F, we will omit some connected ones. As we shall see, however, it

TABLE I. Enumeration of diagrams.

n	1	2	3	4	5	6
F	2	4	84	4324	335 348	34 775 108
G	2	4	84	4900	454 004	60 987 716
H	0.5	0.25	1.31	16.9	328	8491

is a matter of indifference to the rate of divergence whether vertex F is included (except for the first vertex) or not. We may now write recursion relations for the function Q. The subscript denotes the nature of the last vertex.

$$Q_A(n+1,N)=2\binom{N}{2}Q(n,N),$$

$$Q_B(n+1,N)=4\binom{N+1}{2}\binom{N+1}{1}Q(n,N+1),$$

$$Q_C(n+1,N)=2\binom{N-1}{1}Q(n,N-1),$$

$$Q_D(n+1,N)=4\binom{N}{1}\binom{N}{1}Q(n,N),$$

$$Q_E(n+1,N)=4\binom{N+2}{2}\binom{N+2}{2}Q(n,N+2),$$

$$Q_F(n+1,N)=\max[1,Q(n,N-2)],$$

$$Q_G(n+1,N)=4\binom{N+1}{1}\binom{N+1}{2}Q(n,N+1),$$

$$Q_H(n+1,N)=2\binom{N-1}{1}Q(n,N-1),$$

$$Q_I(n+1,N)=2\binom{N}{2}Q(n,N),$$

$$Q_J(n+1,N)=(1-\delta_{N,0})Q(n,N), \tag{3.22}$$

where

$$\binom{a}{b}$$

are the standard binomial coefficients, which, of course, equal the number of ways of taking a things, b at a time. Summing the terms in (3.22) we obtain the relation

$$\begin{aligned}Q(n+1,N)=&[(1-\delta_{N-2,0})Q(n,N-2)\\&+4(N-1)Q(n,N-1)+(6N^2-2N+1-\delta_{N,0})Q(n,N)\\&+4(N+1)^2NQ(n,N+1)\\&+(N+2)^2(N+1)^2Q(n,N+2)],\quad n>1,\\Q(1,N)=&0,\quad N\neq 2,\quad Q(1,2)=1.\end{aligned}\tag{3.23}$$

The Kronecker delta $\delta_{N-2,0}$ arises from the exclusion of disconnected diagrams caused by not allowing vertex F to follow a state with zero lines on the right. If we drop the $Q(n, N-2)$ term, we eliminate vertex F altogether (except for the first vertex). We illustrate in Table I the number of basic diagrams and a lower bound to the number of Hugenholtz diagrams. This bound is obtained by noting that no more than 4^n basic diagrams may correspond to one Hugenholtz diagram. Row F is the number of basic diagrams with no external lines that have only one (the first except in first order) F vertex. This number is less than or equal to the total number of connected diagrams. Row G is the number of basic diagrams with no external lines which never return to the ground state. This number is greater than or equal to the total number of connected diagrams. Row H is a lower bound to the number of Hugenholtz diagrams. It is Row F over 4^n. In the first four orders it varies from about $\frac{1}{4}$ to $\frac{1}{2}$ the actual number. In order to estimate the number of diagrams for large n, we use the fact that there are the same number of lines entering on the left as leaving on the right; for instance, if N is changed by $+1$ at one vertex in the diagram, it must be lowered at some subsequent vertex. In Table II we give several possible types of raising and lowering combinations, together with their weight factors and the root mean factor per vertex. The weight factor assumes N lines of each type entering from the left. The root mean weight factors are approximate. In the type designation in Table II, the plus sign is used to lump all contributions of the designated types of vertex together and $\cdots$ indicates other parts of the diagram that may intervene before the indicated level reduction occurs. We can see from Table II that the most heavily weighted paths in (n, N) space will be the ones in which the largest values of N are reached. If type V combinations are used, a value of $N=n$ can be reached and, hence, we get

$$\text{weight } (FFF\cdots EEE)\simeq 4^n(n/2!)^4. \tag{3.24}$$

Similarly, using types II, III, or IV we get again (3.24). Except for III and IV, the 4^n becomes $(4.5)^n$. The total number of allowed paths in (n, N) space is less than one-half the number of random walks in one dimension which return to the origin in n steps, where steps of length 0, 1, and 2 are allowed. This is easily computed (see, for instance, Montroll, 1960) as

$$\begin{aligned}\tfrac{1}{2}P(0,n)&=(4\pi)^{-1}\int_0^{2\pi}(e^{-2ik}+e^{-ik}+1+e^{+ik}+e^{2ik})^n\,dk\\&=(4\pi)^{-1}\int_0^{2\pi}\left[\frac{\sin(\frac{5}{2}k)}{\sin(\frac{1}{2}k)}\right]^n dk,\end{aligned}\tag{3.25}$$

which, by the method of steepest descents (see, for example, Jeffreys and Jeffreys, 1950) is, for large n, approximately $5^n(16\pi n)^{-1/2}$. Thus, the total number of diagrams can increase no faster than

$$(23)^n[(n/2)!]^4\approx(1.5)^n(2n!). \tag{3.26}$$

TABLE II. Path weights.

	Type	Total weight factor	Root mean weight factor per vertex
I.	$A+D+I$	$6N^2-2N+1-\delta_{N,0}$	$6(N-\frac{1}{6})^2$
II.	$C+H\cdots B+G$	$16N^2(N+1)^2$	$4(N+\frac{1}{2})^2$
III.	$C+H\cdots C+H\cdots E$	$16N(N+1)^3(N+2)^2$	$2.5(N+7/6)^2$
IV.	$F\cdots B+G\cdots B+G$	$16(N+2)^2(N+1)^3N$	$2.5(N+7/6)^2$
V.	$F\cdots E$	$(N+2)^2(N+1)^2$	$(N+\frac{3}{2})^2$

On the other hand, using only the most heavily weighted path with type II contributions only, we have at least as many as given by (3.24). Hence, the number of diagrams is asymptotically something like $AB^n(2n!)$. According to the data in Table I, $A\approx 0.12$, $B\approx 1.0$.

After the diagrams have been enumerated, the next step is to bound each individual diagram. There are basically two possible types of divergences which the diagrams could possess. The first would be a singularity for a finite value of the internal momenta, and the second would be a divergence for an infinite value of the internal momenta. We will examine now the first type of situation. For the many-body perturbation theory diagrams, the action of the exclusion principle always prevents any divergence from a finite internal momentum plane. We will illustrate this situation for a case in which there is apparently an arbitrarily strong singularity. The diagram is given in Fig. 19. The contribution to E/N of the direct (no exchanges) term is

$$\frac{(-1)^{n-1}}{(2\pi)^{3n}}\left(\frac{3}{4\pi k_F{}^3}\right)\int d^3q\prod_{i=1}^{n}(d^3m_i)\times[v(q)]^n/\prod_{i=2}^{n}\left[\mathbf{q}\cdot(\mathbf{q}+\mathbf{m}_i-\mathbf{m}_1)\frac{k^2}{m}\right],$$
$$|\mathbf{m}_1-\mathbf{q}|>k_F,\qquad |\mathbf{m}_i+\mathbf{q}|>k_F,\qquad 1<i\leq n,$$
$$|\mathbf{m}_i|\leq k_F,\qquad 1\leq i\leq n,\quad (3.27)$$

where we are treating the case without spin or isotopic spin, and k_F is the magnitude of the wave vector at the top of the Fermi sea. Apparently (3.27) diverges as q^{2-n} as $|q|$ goes to zero. However, following Hugenholtz (1957), if we neglect quadratic terms in q, we may convert (3.27) into

$$3\left(-\frac{m}{\hbar^2}\right)^{n-1}(2\pi)^{-2n}k_F{}^{n-2}\int_0^\infty dqq^3[v(q)]^n\times\int_0^1\cdots\int_0^1\mu_1\,d\mu_1\prod_{i=2}^{n}\frac{\mu_i\,d\mu_i}{(\mu_1+\mu_1)},\quad (3.28)$$

where the μ_i are cosines of the angles between m_i and q (except that $\mu_1=-\cos$). We see from (3.28) that the integrand actually vanishes at $q=0$ instead of becoming singular. The problem of a vanishing denominator ($\mu_1=\mu_i=0$) does not cause any difficulty for, doing the integrals over μ_i, $i=2,\cdots,n$, we obtain

$$3\left(-\frac{m}{\hbar^2}\right)^{n-1}(2\pi)^{-2n}k_F{}^{n-2}\int_0^\infty dqq^3[v(q)]^n\times\int_0^1\mu_1\,d\mu_1[1-\mu_1\ln(1+\mu_1)+\mu_1\ln\mu_1]^n.\quad (3.29)$$

Since the nth root of the integrand for μ_1 is bounded, the entire term increases only geometrically as n goes to infinity.

As mentioned earlier, Fig. 18 may by itself diverge. We will now consider the bubble diagrams in more detail. First, the contribution of a bubble on a hole line has the opposite sign from that of a bubble on a filled-state line. This change of sign follows because such contributions arise from the subtraction terms in the Rayleigh–Schrödinger perturbation theory, as we saw in the previous chapter. The effect of a bubble on a filled-state line or momentum k is to insert a vertex contribution of

$$2\int d^3m[\tilde{v}(0)-\tilde{v}(\mathbf{k}+\mathbf{m})],\qquad |m|<k_F\quad (3.30)$$

and raise the power of the denominator by unity. On a hole line, there is the same contribution as (3.30) except that the overall sign is now minus, and k now stands for the momentum of the unoccupied state. Hence, summing over bubbles on all lines, we obtain

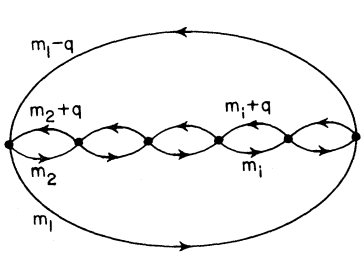

FIG. 19. A successive hole, filled-state interaction diagram.

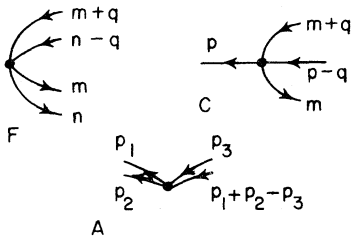

FIG. 20. Labeled "free" momentum-originating vertices.

for the contribution of a J vertex a factor in the integrand of

$$2\int_{|m|<k_J} d^3m \times \sum_{i=1}^{j}[\tilde{v}(\mathbf{k}_i+\mathbf{m})-\tilde{v}(\mathbf{m}_i+\mathbf{m})]/\sum_{i=1}^{j}(\mathbf{k}_i^2-\mathbf{m}_i^2), \quad (3.31)$$

where j is the number of holes or filled-state lines present, $\mathbf{k}_i$ the filled-state momenta, and $\mathbf{m}_i$ the hole momenta. The $\tilde{v}(0)$ terms have canceled as the number of holes must equal the number of filled-state lines in this type of diagram. If $\tilde{v}$ depends on the exchange momentum transfer, as well as on the momentum transfer, then the $\tilde{v}(0)$ terms will not cancel but they will not adversely affect the following analysis. Since $\tilde{v}$ depends only on the magnitude of its argument, it follows easily that the integrals of v appearing in (3.31) depend only on $|\mathbf{k}_i|$ and $|\mathbf{m}_i|$. Furthermore, since $\mathbf{k}_i^2>k_F^2\geq\mathbf{m}_i^2$, the denominator may vanish only when all the momenta lie in the Fermi surface. But, for that case the numerator also clearly vanishes. Hence, the contribution of a summed bubble vertex is bounded by a quantity related to the first derivative of the integral of $\tilde{v}$ appearing in (3.31). If the bubble diagrams are not summed, singularities may arise (Tolmachev, 1961).

We have seen, from analyzing the different types of apparent singularities that may occur for finite internal momenta, that they do not contribute any additional divergence to the perturbation series.

In order to study the possible divergence of a diagram at infinite values of the internal momenta, we will consider each type of vertex which is allowed by the Pauli exclusion principle to originate a momentum which may be infinite. These vertices are A, C, and F. First, if we label vertex F as shown in Fig. 20, then the vertex contributes $\tilde{v}(q)$, and the denominator following it has a nonnegative part plus $2\mathbf{q}\cdot(\mathbf{q}+\mathbf{m}-\mathbf{n})$. As $\tilde{v}(q)$ goes to zero as q^{-2}, and we are doing only three-dimensional integrals, this remark suffices to show that the integral over the "free" momenta q originated at F vertices must converge at infinity at least as dq/q^2. If we label a C vertex as shown in Fig. 15, then the vertex again contributes a factor of $\tilde{v}(q)$. If we consider only the new line $m+q$ and hole m, then the next denominator is something nonnegative plus $q^2+2\mathbf{m}\cdot\mathbf{q}$. Again the integral over q converges at infinity at least as dq/q^2. The analysis of A is slightly more complex: Pick any hole $\mathbf{m}$, then we may write

$$\mathbf{p}_1=\mathbf{m}+\mathbf{q}_1, \qquad \mathbf{p}_3=\mathbf{m}+\mathbf{q}_3. \quad (3.32)$$

In this notation $\mathbf{q}_3$ will be the "free" momentum created at this vertex. The vertex will contribute a factor $\tilde{v}(\mathbf{q}_3-\mathbf{q}_1)$, and the next denominator to the right will be something nonnegative plus $q_3^2+2\mathbf{q}_3\cdot\mathbf{m}$. As we have shown above, the exclusion principle keeps this quantity from vanishing in an unfortunate manner for $\mathbf{q}_3$ and $\mathbf{m}$ finite, so we may replace the q_3^2 in the volume element divided by it with a constant for the purpose of bounding the integral over q_3. Our task is thus reduced to bounding

$$\max_{q_1}\int_0^\infty dq_3\, d\Omega_3\,|\,\tilde{v}(\mathbf{q}_3-\mathbf{q}_1)\,|, \quad (3.33)$$

where Ω_3 is the solid angle for $\mathbf{q}_3$. A bound for (3.33) follows easily when we note that

$$|\,\tilde{v}(x)\,|\leq A/(1+Bx^2) \quad (3.34)$$

for a square well, or any other potential which decays at least this fast at infinity.

It now follows easily that, since there are no divergences on any of the integrations and there are at most $n+1$ internal three-dimensional momenta in a diagram of nth order, any nth-order basic diagram contributes at most

$$M_1(M_2)^n, \quad (3.35)$$

where M_1 and M_2 are determinable constants. To show this we may break a general diagram of the form

$$\int v_1(1/D_1)v_2\cdots v_{n-1}(1/D_{n-1})v_n\,d\tau \quad (3.36)$$

down into a number of factors depending on (essentially) single variables only, in the general manner indicated above. Then each single integration may be bounded. We get something like

$$\max(|\,v_n\,|)\prod_{i=1}^{n-1}[\int|\,v_i(1/D_i^*)\,|]\iint d\mathbf{m}\,d\mathbf{n}, \quad (3.37)$$

where m and n are the two holes which occur in every diagram. Hence, we have shown so far that the perturbation series diverges at worst as

$$M_3(2n)!(M_4)^n. \quad (3.38)$$

We shall now show that (3.38) can be greatly improved upon. Although the argument is not rigorous, we believe that it makes the result quite plausible. It is based on the observation that when many excited states are filled, the denominators are, on the average, much larger than when very few excited states are present. If the range of the various internal momenta is determined by the convergence properties of the potentials or the exclusion principle alone, and not by the energy denominators which depend on N, then we may think of each hole, filled-state, line pair as contributing an average excitation energy. When there

are N of these pairs, the denominator will be, on the average, N times as large.

We must now determine when the ranges are so restricted. Clearly, the energy range of every hole momentum is completely restricted by the Pauli exclusion principle. It therefore remains to check the free momenta. We can do this by the familiar procedure of counting powers at infinity of each free momentum q. To facilitate this power counting, we may compute from (3.21)

$$\int_{-1}^{+1} \tilde{v}(|\,\mathbf{q}_1-\mathbf{q}_2\,|)\,dx_{12}=\frac{4\pi Va}{q_1q_2}\times[j_0(a(q_1+q_2))-j_0(a(q_1-q_2))], \quad (3.39)$$

where x_{12} is the cosine of the angle between $\mathbf{q}_1$ and $\mathbf{q}_2$. As the quantity in square brackets in (3.39) is bounded for all q_1 and q_2 by 2, we see that a vertex operator involving two free momenta may simply be divided equally between them, i.e., one inverse power for each one. This property is a general one possessed by most of the potentials with which we shall be concerned and not just by the square well. Its origin is that the coefficient of x_{12} in $|\,\mathbf{q}_1-\mathbf{q}_2\,|$ is $(-2q_1q_2)$.

Referring to the above analysis of the free momentum-creating vertices A, C, and F, we see (also let $p_2=r-q_1$, with r possibly free for vertex A) that they contribute factors of A, q^{-1}; C, q^{-2}; and F, q^{-2}. A similar analysis of the vertices which may terminate a free momentum shows that they contribute factors of A, q^{-1}; B, q^{-1}; and E, q^{-2}, where q is the one free momentum which can be annihilated at the vertex. To be sure of not overlapping in our counting, we will consider only the originating and the terminating vertex for each free momentum. If we consider all nine types of pairs of vertices, we find that all but AA and AB have at least 3 inverse powers of q, and hence determine the range of their respective free momentum. The other two pairs have only a factor of q^{-2} and so the range of q is possibly controlled by the energy denominators. By considering the integral (Gröbner and Hofreiter, 1958, No. 131.7.)

$$\int_0^\infty \frac{dx}{(A+x^2)^n}=(\pi)^{1/2}\frac{\Gamma(n-\frac{1}{2})}{[2\Gamma(n)A^{n-1/2}]}, \quad (3.40)$$

we see that the approximate effect of an integration determined by the energy denominator is to multiply the magnitude of the result by $(A)^{1/2}$. When there are several denominators involved, the integration will affect the multiplication by $(\hat{A})^{1/2}$, where $\hat{A}$ is some kind of a mean A. If an A vertex occurs when there are N excited states, then we expect that the "free" momentum created will be annihilated on the average when there are of the order of N excited states present also. We also compute roughly the probability (fraction of diagrams) of the pairs AA, AB, and AE occurring. These are the only pairs which contain A as the first member. The number of such pairs is

$$AA=\binom{2}{2}=1,$$

$$AB=\binom{2}{2}\binom{N}{1}=N,$$

$$AE=\binom{2}{2}\binom{N}{2}=\tfrac{1}{2}N(N-1), \quad (3.41)$$

and their relative probability will be

$$AA=1/[\tfrac{1}{2}N(N+1)+1],$$

$$AB=N/[\tfrac{1}{2}N(N+1)+1],$$

$$AE=\tfrac{1}{2}N(N-1)/[\tfrac{1}{2}N(N+1)+1]. \quad (3.42)$$

For vertex AE, the contribution will be $1/N$ at each denominator times the number of diagrams. For AA and AB, we must take only $1/(\hat{N})^{1/2}$ for the first denominator to the right of the first A vertex. Thus, averaging over the possible final vertices, we get a factor of

$$[\tfrac{1}{2}(N-1)+(N+1)/(\hat{N})^{1/2}]/[\tfrac{1}{2}N(N+1)+1] \quad (3.43)$$

for the first denominator to the right of A. This factor, however, tends to $1/N$ as N tends to infinity. The algebraic identity given by Hugenholtz (1957)

$$\sum_{\text{permutation}} \xi_1^{-1}(\xi_1+\xi_2)^{-1}\cdots(\xi_1+\xi_2+\cdots+\xi_n)^{-1}=(\xi_1\xi_2\cdots\xi_n)^{-1} \quad (3.44)$$

is also suggestive in this regard as there are exactly $n!$ permutations. Hence, we may divide the weight factors given in (3.22) by N, and multiply by some constant Λ in order to calculate the total contributions. When we calculate the contribution in this way, an analysis similar to that in (3.23) to (3.26) and Table II shows us that the nth order in perturbation theory diverges no faster than

$$\Gamma n!(\tilde{\Lambda})^n, \quad (3.45)$$

where $\tilde{\Lambda}$ is a multiple of Λ.

The so-called ladder insertions (several successive A vertices) form a special case. Integration over each free momentum (in the simple ladder diagram) in the region near the Fermi surface contributes a factor proportional to $\ln(\frac{1}{2}\,|\,\mathbf{m}+\mathbf{n}\,|+k_F-\frac{1}{2}\,|\,\mathbf{m}-\mathbf{n}\,|)$. For r successive such factors, the final integration over the hole momenta $\mathbf{m}$ and $\mathbf{n}$ gives a result proportional to $n!$. However, there are only 2^r of these terms, so they contribute terms at most of order $r!$. When a ladder insertion occurs with m hole lines present, its contribution is cut to the order of $(r!)/m^{r+1}$ $(r\gg m)$ as can be seen from the integral

$$\int_0\cdots\int_0 \prod^m dx_i \ln^r(\sum^m x_i).$$

The rest of an nth-order diagram will contribute like a diagram of order $n-r$, or as we have seen $(n-r)!$. Summing over all partitions, we get $\sum r!(n-r)!$, which is again of order $n!$. Thus, although the ladder diagrams contribute more than their proportional amount, they will not increase the rate of divergence of the series as a whole.

Summing out the ladder insertions with a K matrix, will not render the whole series convergent, as can be seen by counting up the remaining contributions.

We believe that, although for certain potentials (such as S-state interaction only, which does not lead to a collapsed state and, hence, yields a convergent series) cancellation between terms may occur so as to decrease the rate of divergence, there is no better general bound than (3.45). The derivation of (3.45) did not depend strongly on the properties of the potential, but only on $|v(q)|$ being bounded and going to zero like q^{-2} as q went to infinity.

D. The Summability of the Perturbation Series

In the previous sections we have found that the formal perturbation series of Sec. II is at best asymptotic for the usual type of potentials. Since it does not therefore converge for any interaction strength however small, it is a very real problem to assign a meaning to this series and to determine whether it indeed represents the true physical function.

The notion [articulated by Heavyside as quoted by Hardy (1956)] is still widely held that for a series to have a finite value it must be convergent. A divergent series would of course have an infinite value. Solutions of physical problems must always be in finite terms, or convergent series, otherwise nonsense results. Still, as we shall see, divergent series need not necessarily be given up as hopeless. Consider, for example, the series studied by Euler

$$f(x)=1-1!x+2!x^2-3!x^3+\cdots.$$

Plainly the successive terms of this series diverge eventually for $x\neq 0$, no matter how small x is. However, the integral

$$\varphi(x)=\int_0^\infty \frac{e^{-t}}{1+xt}\,dt$$

has the same expansion as $f(x)$ in powers of x at $x=0^+$. Furthermore, we can write

$$\varphi(x)=\sum_{j=0}^{N} j!(-x)^j-\int_0^\infty \frac{(-xt)^{N+1}e^{-t}\,dt}{1+xt}.$$

If $\mathrm{Re}\,(x)>0$, then we have $|1+xt|\geq 1$, so that the remainder integral is bounded by $(N+1)!x^{N+1}$ in magnitude. If $\mathrm{Re}\,(x)<0$ and $\phi=\arg x$, then we have $|1+xt|\geq|\sin\phi|$, so that the remainder integral is bounded by $|\mathrm{cosec}\,(\phi)|\,(N+1)!x^{N+1}$. Hence, in any angular wedge, we have $-\phi\leq\arg(x)\leq\phi$, $\phi<\pi$. The remainder function

$$R_N(x)=\varphi(x)-\sum_{j=0}^{N} j!(-x)^j$$

is bounded, uniformly in N and x by a constant multiple of the first term neglected. This property is a stronger property than the usual definition of an asymptotic series. Any function $g(x)$ is said to be asymptotic in an angular wedge $|\arg x|\leq\psi$ to the formal power series $f(x)$ if

$$\lim_{x\to 0^+}\{[g(x)-\sum_{j=0}^{N} j!(-x)^j]/x^N\}=0$$

for all N. The difference here is that the uniformity is missing. That this difference is a real one can be seen by the example

$$h(x)=\varphi(x)+\exp(-x^{-1/2}).$$

This example is asymptotic ($\psi<\pi$) in the above described usual sense as all the derivatives of $\exp(-x)^{-1/2}$ along rays $|\arg x|\leq\psi<\pi$ vanish as $x\to 0$. Nevertheless, $h(x)$ does not satisfy the bounding property possessed by $R_N(x)$, as $x^{-N}\exp(-x^{-1/2})$ has a maximum of $(2N/e)^{2N}$ at $x=(2N)^{-2}$ which is asymptotically much larger than $N!$, and approaches arbitrarily close to the origin.

If we are willing to restrict our attention to the class of functions with well behaved remainders, then a precise answer can be given to the problem of uniqueness of a function defined by a formal power series. According to Hardy (1956), Carleman has proved that a necessary and sufficient condition for

$$|g(z)|\leq\alpha_n{}^n|z|^n,\quad(|z|\leq r_0<\infty),\quad|\arg z|\leq\tfrac{1}{2}\pi \qquad (3.46)$$

to imply $g(z)=0$, is that $\sum\alpha_n{}^{-1}$ diverge (for suitably regular α). Rephrased, this means that if the remainders satisfy (3.46), then there can be at most one function asymptotic in the sense (3.46) to a given formal power series. If the many-body perturbation series is asymptotic in the angular sector $|\arg V|\leq\frac{1}{2}\pi$ [in the sense of (3.46)], then this theorem means, since $(n!)^{1/n}\propto n$ implies $\sum\alpha_n{}^{-1}$ diverges, that there is at most one function which is regular for real positive V and asymptotically equal to the perturbation series. That the desired solution, for a soft, repulsive square-well potential, is regular, follows directly from our analysis in Sec. III.B, and from perturbation theory which shows the existence of a bounded derivative for positive real potentials. We feel for potentials in which there is a strong but finite central repulsion, so that no collapsed state is possible, that for very weak potentials ($V\approx 0$) the behavior should be essentially that of the central repulsions. That case was analyzed in detail in Sec. III.B and the location of the singularities nearest the origin estimated. It was found that they approached the origin from the direction of the negative real axis. Their origin

physically is the well known collapse phenomenon (for V negative) in an attractive short range potential well. Then we feel that it is physically reasonable to suppose that, at least for very weak potentials, the ground-state energy is asymptotic in the closed right-half plane. Let me mention, however, that the type of singularities found in super-conductivity

$$Ae^{-B/V} \tag{3.47}$$

are excluded here as they do not satisfy (3.46) for V pure imaginary. We have argued in a previous paper (Baker and Kahane, 1969) that for the usual sort of potential with a central repulsion plus short range attraction, superconductivity should not be a problem. We also remark that the nearest singularity of course sets a limit on the radius of convergence so that while $V=0$ is a regular point for a system of finite size N, the radius of convergence tends to zero as N tends to infinity.

We will now prove, based on our analysis of the location of the singularities of the energy function for finite N, and other known properties, that the perturbation series defines the physically correct function. The method of proof is to establish an analytic continuation method which is valid for finite N, and to show that it is so, uniformly, for all finite N. We then take the limit as N goes to infinity, and demonstrate that this analytic continuation defines the physically correct function from the "infinite nuclear matter" power series.

Let the energy per particle in the N-fermion problem with pair interaction $V\varphi(r)$ be

$$E_N(V) = \sum_{n=0}^{\infty} {}_N e_n V^n \tag{3.48}$$

This series has a nonzero radius of convergence as mentioned above, and by analytic continuation defines $E_N(V)$ everywhere in the complex V plane, except at singular points or on branch cuts. This analytic continuation is conveniently given by Mittag-Leffler's method (Hardy, 1956). We define

$$E_N(V,\delta) = \sum_{n=0}^{\infty} \frac{{}_N e_n V^n}{\Gamma(\delta n+1)} \tag{3.49}$$

For every $\delta>0$, $E_N(V,\delta)$ is an entire function of V as $E_N(V)$ is analytic at $V=0$. Also, Hardy (1956), has shown, Theorem 135, that

$$\lim_{\delta\to 0} E_N(V,\delta) = E_N(V) \tag{3.50}$$

uniformly, in any closed and bounded region in the Mittag-Leffler star of $E_N(V)$. The Mittag-Leffler star is defined by cutting the complex V plane from every singularity to infinity along rays. As we have pointed out above, $E_N(V)$ is regular for positive real V (at least V small), and hence the positive real axis in the neighborhood of $V=0$ is interior to the Mittag-Leffler star for all N. The meaning we wish to assign

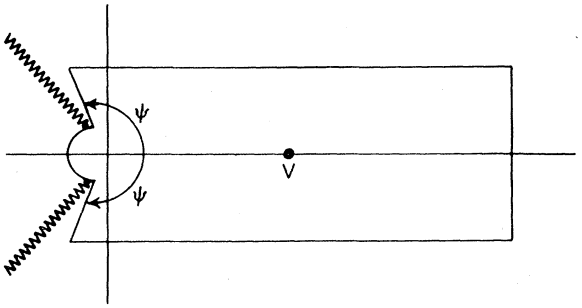

FIG. 21. N-dependent integration contour.

to the sum of the perturbation series for infinitely many fermions is

$$\lim_{N\to\infty} E_N(V) = \lim_{N\to\infty}\lim_{\delta\to 0} E_N(V,\delta). \tag{3.51}$$

We would like to interchange the order of limits in (3.51) to $\lim_{\delta\to 0}\lim_{N\to\infty}$. For this interchange to be correct, it is sufficient to show that $\lim_{N\to\infty}$ is uniform for δ small enough. To this end, let us introduce the Mittag-Leffler function

$$\varphi_\delta(z) = \sum_{n=0}^{\infty} \frac{z^n}{\Gamma(1+\delta n)} \xrightarrow[|z|\to\infty]{} (1-z)^{-1},$$
$$\tfrac{1}{2}\pi\delta \le |\arg z| \le \pi. \tag{3.52}$$

For V less than the radius of convergence we have, by Cauchy's Theorem, for regular functions of a complex variable,

$$E_N(V,\delta) = (2\pi i)^{-1}\oint \varphi_\delta(V/u) E_N(u)\,(du/u), \tag{3.53}$$

where the contour is a circle about the origin inside the circle of convergence. Again, using Cauchy's Theorem, we may deform the contour as shown in Fig. 21, provided we cross no singular points of $E_N(u)$. If we now restrict $\pi\delta<2\psi$, then as for $\psi\le|\arg(V/u)|\le\pi$, we have

$$u^{-1}\varphi_\delta(V/u)\to(u-V)^{-1} \tag{3.54}$$

as V/u tends to infinity, $\varphi_\delta(V/u)$ is bounded on the contour of Fig. 21. We may now shrink the circular arc part of the contour to the origin. As $E_N(u)$ is bounded, and the length of the arc goes to zero, the contribution from this part of the contour goes to zero. Hence we can replace the contour of Fig. 21 by that of Fig. 22 which is now independent of N. However, $E_N(u)$ tends to a finite limit at every point on this contour and does so uniformly. Hence, for all $\pi\delta<2\psi$, taking the limit of (3.53), we have that $E_N(V,\delta)$ tends uniformly to

$$E(V,\delta) = (2\pi i)^{-1}\oint \varphi_\delta(V/u) E(u) u^{-1}\,du. \tag{3.55}$$

By the properties of $\varphi_\delta(x)$, we deduce that

$$E(V) = \lim_{\delta\to 0} E(V,\delta) = \lim_{\delta\to 0}\lim_{N\to\infty} E_N(V,\delta). \tag{3.56}$$

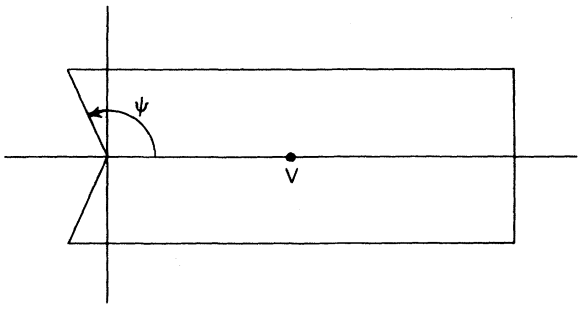

FIG. 22. N-independent integration contour.

That is to say, we may obtain $E(V)$ correctly from the V series by first taking the limit as system size increases indefinitely, and then summing the series. The limiting function necessarily has the asymptotic expansion

$$E(V)=\sum_{n=0}^{\infty} e_n V^n,$$

where

$$e_n=\lim_{N\to\infty} {}_N e_n$$

by our construction, and the usual theorems on the limits of a sequence of analytic functions and limits of the sequence of its derivatives. We can see roughly how the Carleman restriction comes into play by noting that we can get $E(V, \delta)$ by simple series summation only when $\delta>1$, and we can only prove analyticity in δ for $0<\delta<2\psi/\pi$. Thus, if $2\psi/\pi>1$ we can establish $E(V, \delta)$ over a range of δ and analytically continue it uniquely to $\delta=0$, whereas if $2\psi/\pi<1$, we cannot make contact and sum in this manner. In the latter case, Carleman's Theorem assures us that indeed there is not a unique analytic continuation, but in the former case, which obtains for the problem at hand, we do have a unique analytic continuation and a well defined sum for the energy series.

Consequently, we conclude that if the potential is such that the function $E(V)$ is asymptotic in the sense of (3.46) in the closed right-half plane and our estimated bound (3.45) for the perturbation series holds, then that series defines a unique function and it is the physically correct one [in the sense of (3.51)].

E. Rearrangements of the Perturbation Series

We have by now established the existence of a perturbation series for the energy per particle in the ground state of a many-fermion system interacting by forces which include a strong, short-range repulsion. This series is divergent, but nevertheless is summable to a unique answer which is the physically correct one. In this section, we show that under certain conditions the series can be rearranged and still yield the correct answer. The results in this section are based on Baker (1970). To see that this procedure needs consideration, consider the following example of a purely mathematical nature:

$$1+2x^2+2x^4+2x^6+2x^8+\cdots \tag{3.57}$$

which can be summed for small x as

$$(1+x^2)/(1-x^2); \tag{3.58}$$

however, by rearranging (3.57) as

$$1+\frac{1}{2}\left(\frac{2x}{1+x^2}\right)^2+\frac{1}{2}\cdot\frac{3}{4}\left(\frac{2x}{1+x^2}\right)^4 + \frac{1\cdot3\cdot5}{2\cdot4\cdot6}\left(\frac{2x}{1+x^2}\right)^6+\cdots, \tag{3.59}$$

we obtain a series which is now also convergent for large x. Summing up directly, we get for large x

$$(x^2+1)/(x^2-1). \tag{3.60}$$

As (3.58) is a meromorphic function, it represents the unique analytic continuation of the series (3.57) throughout the whole complex plane. The result (3.60), seemingly valid for large x, is the negative of (3.58) and thus incorrect. Nevertheless (3.59) gives the correct sum for small x. This example illustrates that some care is necessary in the rearrangement of a series.

We will now rearrange, formally, the series (3.48) as

$$\mathcal{E}_N(V)=\sum_{n=0}^{\infty} {}_N a_n\Big[V^n\sum_{j=0}^{\infty} {}_N b_{n,j}V^j\Big]. \tag{3.61}$$

We require

$${}_N e_m=\sum_{n=0}^{m} ({}_N a_n)({}_N b_{n,m-n}) \tag{3.62}$$

in order that this be a formal rearrangement of the energy. In order to facilitate our development, we will introduce the auxiliary function

$$\mathcal{E}_N(V,\lambda)=\sum_{n=0}^{\infty} {}_N a_n\lambda^n V^n\Big(\sum_{j=0}^{\infty} {}_N b_{n,j}V^j\Big). \tag{3.63}$$

We will assume that the rearrangement has preserved the bounds for the original series in the sense that

$$\sum_{n=0}^{m} |\,({}_N a_n)({}_N b_{n,m-n})\,|\le A(BN^\gamma)^m \quad\text{and}\quad \Gamma'(\Lambda')^m m!, \tag{3.64}$$

the second bound holding uniformly in N. Under this assumption, there exists a circle $|\,V\,|\le\rho(N)$, for which the double series converges uniformly and absolutely, provided $|\,\lambda\,|\le R>1$. It follows, then, by standard arguments that for V in this circle

$$\mathcal{E}_N(V,1)=E_N(V). \tag{3.65}$$

We now wish to extend $\mathcal{E}_N(V,\lambda)$ by analytic continuation to a wider domain. This may be done, again

by the Mittag–Leffler method. To this end we introduce

$$\mathcal{E}_N(V,\lambda,\delta,\eta)=\sum_{n=0}^{\infty}\frac{{}_Na_n\lambda^nV^n}{\Gamma(\eta n+1)}\times\left(\sum_{j=0}^{\infty}\frac{{}_Nb_{n,j}V^j}{\Gamma[(j+n)\delta+1]}\right). \quad (3.66)$$

The analytic continuation is then given by

$$\mathcal{E}_N(V,\lambda)=\lim_{\delta\to 0}\lim_{\eta\to 0}\mathcal{E}_N(V,\lambda,\delta,\eta) \quad (3.67)$$

throughout the Mittag–Leffler star. If there exists a path, interior to the Mittag–Leffler star, connecting $(V=0,\ \lambda=1)$ with $(V=\tilde{V},\ \lambda=1)$ for all N, then by analytic continuation from (3.65), we have (3.65) also valid for $(V=\tilde{V},\lambda=1)$. Now as this path is a closed and bounded set, and as, from our discussion of the V series, $E_N(V)$ tends to a finite limit at every point of such a path, it does so uniformly in N; thus we conclude that under these assumptions

$$E(V)=\mathcal{E}(V,1)=\sum_{n=0}^{\infty}a_n(V^n\sum_{j=0}^{\infty}b_{n,j}V^j). \quad (3.68)$$

We have established that this series is summable to the correct value provided the rearrangement satisfies (3.64) and there exists a path in the Mittag–Leffler star joining $(V=0,\ \lambda=1)$ and the point of interest. The imposition of the second part of (3.64) is necessary to insure that the limiting analytic continuation be unique.

We remark that when (3.68) is known to be summable, and the terms in square brackets are at least asymptotic in an angular wedge $0\leq|\arg V|\leq\psi\geq\frac{1}{2}\pi$ in the sense of (3.46), then Carleman's Theorem assures us that it sums to the correct result in any connected region of summability. To see this, we need only note that a finite number of terms from the n and j sums in (3.68) will suffice to give any finite order coefficient. These restrictions on the square bracket quantities are certainly valid for resummation of the ladder diagrams into a K matrix when the potential is purely repulsive. This result follows as the series is closely related to a series of Stieltjes (Baker *et al.*, 1963). The R-matrix procedure (Baker and Kahane, 1969), also satisfies those restrictions for $R(V)$ is convergent when V is bounded and of finite range; and for usual potentials $R(V)$ is nonsingular in the neighborhood of the positive real V axis.

It is worth noting that the example at the beginning of this section violates one of our conditions. To see that this is so, rewrite (3.59) as

$$1+\frac{1}{2}\left(\frac{2x}{1+x^2}\right)^2\lambda+\frac{1}{2}\cdot\frac{3}{4}\left(\frac{2x}{1+x^2}\right)^4\lambda^2+\cdots=\left[1-\left(\frac{2x}{1+x^2}\right)^2\lambda\right]^{-1/2}. \quad (3.69)$$

Now, it is not possible to pass from small x to large x without crossing the unit circle in the complex x plane, by the Jordan curve theorem. For x on the unit circle, we find that

$$1\leq[2x/(1+x^2)]^2\leq\infty \quad (3.70)$$

so that points on the unit circle in the x plane lie on the branch cut introduced by the Mittag–Leffler summation of the λ series when $\lambda=1$. Hence there is no path within the Mittag–Leffler star which connects large and small values of x, and thus no necessity for the sum of (3.59) to be the same function in the two regions.

As pointed out in Baker (1970), some methods now in use cannot be justified by these procedures, and for independent reasons may not be employed with full confidence.

FIG. 23. Ladder diagrams.

IV. THE REPULSIVE FORCE PROBLEM

In the preceding two sections we have established a formal series expansion for the ground-state energy and found that although it is divergent, it can still be used to define the physical solution to the many-fermion problem. In this chapter we consider the problem in which the forces are purely repulsive. Here, there can be no bound states or condensation phenomena to complicate the problem. Physical intuition is very effective, based on elementary considerations alone, in analyzing which perturbation terms will contribute significantly, at least in the important low-density limit. In the case in which attractions are also present, there are additional complications and we will discuss these in the next chapter.

A. The K-Matrix Rearrangement

In order to make the perturbation series useful, in a practicable problem, some sort of rearrangement was considered desirable by most workers. The reason was that in the nuclear problem there is a very strong repulsive potential core and even if the series were convergent (which it is not) a great many terms would be required to deal with such a large force. The same problem arises in two-body scattering. There we recognize that even though the potential is very large (even infinite), the effect is finite. It simply excludes the wave function from the region of the repulsive core. Brueckner had the idea of rearranging into a single term all of the so-called ladder diagrams in the energy (see Fig. 23), in analogy to Watson's theory of multiple scattering. Also, by the same procedures, two or more successive vertex A interactions (Fig. 15) between the same pair of lines would be reduced to a single term. For example, vertex D would combine as illustrated in Fig. 24.

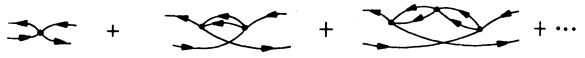

FIG. 24. The ladder sum starting with vertex D.

In order to evaluate this sum, we must first write down a typical term. From (2.41), we see that the first step is to evaluate the Tr { } over spin and isotopic spins. In Fig. 25 we have illustrated a typical basic diagram. From the figure we see clearly that there are two cycles. Any odd number of exchanges leads to one cycle, and any even number undoes the exchange and leads back to two cycles. For example, an interchange at vertex 2 and vertex 3 leads, except for the momentum labels, to an identical figure. The momentum labels can also be made identical by replacing the integration variable $\mathbf{q}_2$ by $\mathbf{n}-\mathbf{m}-\mathbf{q}_2$. Likewise, any term can be reexpressed as one involving 0 or 1 exchanges on the last vertex, accordingly as the number of exchanges is even or odd. Hence, using $\nu=(2S+1)(2I+1)$, (2.41) for a ladder diagram reduces to

$$\frac{-3(-1)^{n\nu}}{8\pi k_F{}^3}\int d\tau\,\frac{[\prod_{j=1}^{n-1}\tilde{v}(|\mathbf{k}_{j-1}-\mathbf{k}_j|)][\tilde{v}(|\mathbf{k}_0-\mathbf{k}_{n-1}|)-\tilde{v}(|\mathbf{k}_0+\mathbf{k}_{n-1}|)/\nu]}{\prod_{j=1}^{n-1}(k_j{}^2-k_0{}^2)}, \tag{4.1}$$

where the region of integration is that allowed by the Pauli exclusion principle. The denominators have been reexpressed through the identity

$$(\tfrac{1}{2}\mathbf{p}+\mathbf{k}_j)^2+(\tfrac{1}{2}\mathbf{p}-\mathbf{k}_j)^2-(\tfrac{1}{2}\mathbf{p}+\mathbf{k}_0)^2-(\tfrac{1}{2}\mathbf{p}-\mathbf{k}_0{}^2)=2(k_j{}^2-k_0{}^2) \tag{4.2}$$

which uses momentum conservation to eliminate the dependence on the total momentum of the hole lines, which equals that for the filled-state lines. If we think of the integration over the various $\mathbf{k}_j$ as again discrete sums, then the terms (4.1) in the ladder sequence are successive terms in a matrix geometric progression, and can be generated by iteration of the integral equation

$$K(\mathbf{k}',\mathbf{k}'';p,k_0)=\tilde{v}(|\mathbf{k}'-\mathbf{k}''|)-\int_{|\mathbf{k}'''+\frac{1}{2}\mathbf{p}|>k_F;\,|\mathbf{k}'''-\frac{1}{2}\mathbf{p}|>k_F}d\mathbf{k}'''\,\frac{\tilde{v}(|\mathbf{k}'-\mathbf{k}'''|)K(\mathbf{k}''',\mathbf{k}'';p,k_0)}{(k''')^2-k_0{}^2}, \tag{4.3}$$

where

$$\lim_{N\to\infty}[E_L m/(N\hbar^2)]=(3/8\pi k_F{}^3)\int_{|\mathbf{k}_0+\frac{1}{2}\mathbf{p}|\le k_F;\,|\mathbf{k}_0-\frac{1}{2}\mathbf{p}|\le k_F}d\mathbf{p}\,d\mathbf{k}_0[\nu K(\mathbf{k}_0,\mathbf{k}_0;p,k_0)-K(\mathbf{k}_0,-\mathbf{k}_0;p,k_0)]. \tag{4.4}$$

The p dependence of K enters through the Pauli exclusion principle, and the k_0 dependence through the energy denominator. The replacement at the other vertices is easily seen to be given by the solution of the same equation, [Eq. (4.3)] except that the denominator in (4.3) now depends on the total excitation of the Fermi sea. As the rules for the potential perturbation series call for the sum over all linked-cluster diagrams (Sec. II.E), there will occur a diagram corresponding, for example, to every term in the infinite sequence illustrated in Fig. 24 every time a vertex D occurs. Hence we can, as Brueckner showed, rearrange the potential perturbation expansion in powers of the K matrix using the same rules as in Sec. II.E, except:

(i) replace the $\tilde{v}$ with K-matrix elements (this replacement sums exactly all the second-order terms, so that no K diagram of two vertices is required.)

(ii) there shall not be two successive A vertices between the same pair of equivalent lines.

By transforming (4.3) to a coordinate space representation (we will give an approximate version below) we can show that for $v(r)$ repulsive, all the necessary criteria of Sec. III are met so that this K-matrix rearrangement of the perturbation series defines the same ground-state energy. It is to be noted that the K of v series is divergent, as is also the E of K series.

Brueckner has gone one step further and summed an additional class of diagrams into the K matrix. Suppose on every line in the graph we include the series of insertions shown in Fig. 26, as well as any number of these insertions on the same line. The insertion of one

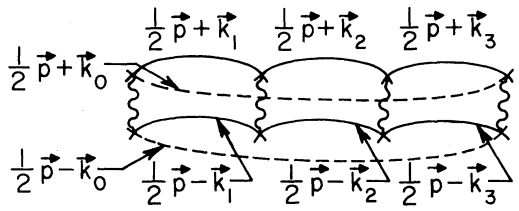

FIG. 25. Fourth-order basic ladder diagram.

of these sequences of terms is, as there is the same denominator before and after each of these terms by momentum conservation, given by $D^{-1}\bar{K}D^{-1}$, where K is an average over the hole momentum m in Fig. 26. All of these terms, of course, occur in the series. In addition, we may have any number of such sequences of insertions on every line. This yields

$$D^{-1}-D^{-1}\bar{K}D^{-1}+D^{-1}\bar{K}D^{-1}\bar{K}D^{-1} -D^{-1}\bar{K}D^{-1}\bar{K}D^{-1}\bar{K}D^{-1}+\cdots, \quad (4.5a)$$

which can be formally summed to yield

$$(D+\bar{K})^{-1}. \quad (4.5b)$$

As Brueckner points out, this sum can be thought of as a self-energy correction. When the insertions are allowed on the lines that define the K matrices, a self-consistent, *nonlinear* integral equation results for the K matrix. It is unproven whether this additional rearrangement of the energy series still leads to the same energy function as the original series, but we are inclined to the view that it does so, at least for repulsive potentials. However as we shall see later, the numerical approximations necessary to make this additional rearrangement a computationally practical one are sufficiently inadequate as to make its use seem to us to be presently inadvisable.

We now describe, following Brueckner and Masterson (1962), the approximations and procedures which are used in K-matrix calculations. In order to carry out calculations, it is usual to eliminate the dependence of the K matrices on the total momentum by making the following approximations. An energy denominator D

$$D=E(\tfrac{1}{2}\mathbf{p}+\mathbf{k}')+E(\tfrac{1}{2}\mathbf{p}-\mathbf{k}') -E(\tfrac{1}{2}\mathbf{p}+\mathbf{k})-E(\tfrac{1}{2}\mathbf{p}-\mathbf{k}), \quad (4.6)$$

where $\mathbf{p}$ is the total momentum, $\mathbf{k}$ is the relative momentum in the initial state, and $\mathbf{k}'$ the relative momentum in the intermediate state (an integration variable in the K-matrix equations), is set equal to

$$D=2[E(k')-E(k)]. \quad (4.7)$$

This is correct if the E's are approximately quadratic functions of their argument. The Pauli principle requires that the integration over $\mathbf{k}'$ be restricted to a region R such that

$$|\tfrac{1}{2}\mathbf{p}+\mathbf{k}'|>k_F \quad \text{and} \quad |\tfrac{1}{2}\mathbf{p}-\mathbf{k}'|>k_F \quad \text{in} \quad R. \quad (4.8)$$

This is approximated by replacing

$$\int_R dk' \rightarrow \int dk' F(p,k'), \quad (4.9)$$

where

$$\begin{aligned} F(p,k')&=0, && (k'^2+\tfrac{1}{4}p^2)^{1/2}<k_F \\ &=1, && k'-\tfrac{1}{2}p>k_F \\ &=\frac{k'^2+\frac{1}{4}p^2-k_F^2}{k'p}, && \text{otherwise.} \end{aligned} \quad (4.10)$$

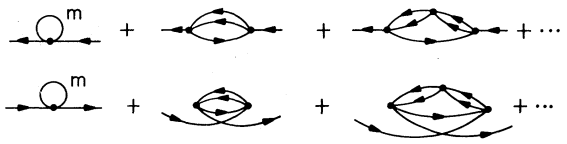

FIG. 26. The ladder sum starting with vertex J.

To eliminate $\mathbf{p}$ completely, an average value $\bar{p}$ is used in place of p:

$$\begin{aligned} \tfrac{1}{4}\bar{p}^2&=\tfrac{3}{5}k_F^2\left(1-\frac{k}{k_F}\right) \\ &\times\left[\left(1+\frac{1}{2}\frac{k}{k_F}+\frac{1}{6}\frac{k^2}{k_F^2}\right)\Big/\left(1+\frac{1}{2}\frac{k}{k_F}\right)\right] && k<k_F \\ &=0 && k>k_F. \end{aligned} \quad (4.11)$$

The effect of these two approximations, usually called angular averaging and center-of-mass averaging has been studied extensively. Baker *et al.* (1963) find them to be "adequate".

Irwin (1963) has investigated the angular averaging, and Köhler (1969) the center-of-mass averaging, separately, and found them to be good approximations.

The off-energy shell effects have to be approximated also [the K matrices and single-particle energies depend on the excitation of the Fermi sea as we pointed out above; we have already suppressed this fact in writing (4.6)]. By transforming into coordinate space and making a partial wave expansion, we obtain the following set of equations. The Green's function is

$$G_{kl}(r,r')=\int_0^\infty k''^2\,dk'' \times\frac{j_l(k''r)j_l(k''r')}{2[E(k'')-\Delta(k)]}F(\bar{p},k'',k), \quad (4.12)$$

where j is a radial Bessel function, l is the angular momentum, and

$$\begin{aligned} \Delta(k)&=E(k) && k<k_F \\ &=E(k_F)-f[E(k_F)-E(0)] && k\geq k_F, \end{aligned} \quad (4.13)$$

where f is chosen arbitrarily. It is in the definition of $\Delta(k)$ that approximations to off-energy shell effects manifest themselves. Continuing with the equations, we have that the wave function u satisfies the integral equation

$$u_{kl}(r)=j_l(kr) -\frac{2}{\pi}\int_0^\infty G_{kl}(r,r')V(r')u_{kl}(r')r'^2\,dr', \quad (4.14)$$

where V is the potential. The K matrices are given by

$$K_l(k)=\frac{2}{\pi}\int_0^\infty j_l(kr)V(r)u_{kl}(r)r^2\,dr, \quad (4.15)$$

and the single-particle energies by

$$E(m)=\tfrac{1}{2}m^2+4\left[\int_0^{(k_F-m)/2}2k^2\,dkI+\int_{(k_F-m)/2}^{(k_F+m)/2}\left(1-\frac{m^2+4k^2-k_F^2}{4km}\right)k^2\,dkI\right]$$
$$m<k_F$$
$$=\tfrac{1}{2}m^2+4\left[\int_{(m-k_F)/2}^{(m+k_F)/2}\left(1-\frac{m^2+4k^2-k_F^2}{4km}\right)k^2\,dkI\right]$$
$$m\geq k_F, \quad (4.16)$$

where

$$I=\sum_l(2l+1)\begin{pmatrix}\nu-1, & l \text{ even}\\ \nu+1, & l \text{ odd}\end{pmatrix}K_l(k). \quad (4.17)$$

Finally, the average binding energy per particle is

$$E_b=\frac{3}{2k_F^3}\int_0^{k_F}[E(m)-\tfrac{1}{2}m^2]m^2\,dm. \quad (4.18)$$

The factors in (4.16) arise as follows; the expected equation is

$$E(m)=\tfrac{1}{2}m^2+[\nu/(2\pi)^3]\times\int d\mathbf{n}[(\mathbf{mn}\mid K\mid\mathbf{mn})-1/\nu K_{\text{exchange}}]. \quad (4.19)$$

Instead of $\mathbf{n}$, the variable $\mathbf{k}=\frac{1}{2}(\mathbf{m}-\mathbf{n})$ has been used, and the requirement $n<k_F$, and an integration over the angles of $\mathbf{k}$, result in the factors.

The single-particle energy [Eq. (4.16)], is then substituted back into (4.7), the Green's functions are recomputed, and new single-particle energies obtained. This process is continued until self-consistent single-particle energies are obtained. This iterative solution is necessary because of the nonlinearity of the equations. The computational techniques are adequately discussed in the original papers and we will not deal with them in this article. There have been a number of other effective procedures developed to deal with special cases of the K-matrix problem. In particular we mention the schemes of Köhler and McCarthy (Köhler, 1969 and references therein), and Kallio and Day (1969). These procedures appear to be useful when there is a strong attraction and only the hole state, but not the particle state energy is made self-consistent. Otherwise the resultant integral equation has a singular kernel (Köhler and McCarthy) or the iteration scheme fails to converge with adequate speed (Kallio and Day). A method due to Haftel and Tabakin (1970), which appeared too late for integration into this review article, involves a solution by matrix inversion in momentum space and may be a very efficient numerical procedure.

These procedures were, of course, developed with the intention that they should be applicable to problems in which both attractive and repulsive forces are present, but we will discuss that in a later section. Later in this section we will investigate their utility in the repulsive force problem.

A characterization of those potentials, for which the inclusion of self-consistent energies in the denominator of the Green's functions is a valid rearrangement of the series, is not known. It is known that a self consistent solution to these equations can fail to exist even for the simple, repulsive square-well potential at higher density (Baker *et al.*, 1963), as well as in the liquid He^3 problem (Brueckner and Gammel, 1958b). Whether this defect is removed by a more exact treatment (Gammel and Nuttall, 1965) of the off-energy shell effects [the approximation made in (4.13)] is unknown.

B. Low-Density Rearrangements

Further rearrangements of the K-matrix series were found by many workers to be desirable. In the first place, the numerical calculations involved are quite complex and require a high speed computer to get through them. In the second place (see, for example, Bethe, 1965), the K-matrix series is not automatically a low-density series.

Undoubtedly, the most ideal method yet proposed for this problem, in principle at least, is that developed by Bethe and his co-workers. However, as it has been thoroughly reviewed by Day (1967), Rajaraman and Bethe (1967), and Brandow (1967), we will only touch briefly on the physical ideas. Through the introduction of the reference spectrum method (Bethe *et al.*, 1963) a number of the qualitative features of the higher order diagrams were studied. In particular, one can see roughly from (2.41) that for each new hole momentum introduced there is a factor of k_F^3 (which is proportional to the density, ρ) multiplying the contribution. It can happen however that the new denominator will contribute a factor of k_F^{-2} if the bulk of the contributions to the integral come when the momenta in it are of the order of the Fermi momentum. Also, self-energy-type insertions lead to singularities, due to raising the same denominator to higher powers; however, the inclusion of the corresponding insertions on the other type of line (hole or filled-state) cancels this singularity, as we explained in the previous chapter. Thus Bethe and his co-workers have been led to the "hole-line" approximation where the diagrams of the K-matrix expansion are grouped by the number of independent hole-line momenta. It can then be shown that the results of the n hole-line approximation can be expressed in terms of the n-body scattering operator (in the presence of a Fermi sea). The difficulties of this approach lie in the calculation of the 2-, 3-, ··· body scattering operators. Various approximate treatments have been proposed as described in the above-mentioned review article. Day (1969) has also considered four-body terms. A persistent problem with this approach is the treatment of the intermediate state energy denomi-

nators. The goal has been to treat them in such a way as to improve convergence. We note that the Brandow (1966) choice which includes the self-energies on the hole-lines but not the filled-state lines is not useful here. [One virtue of this choice is that a variant of the Hugenholtz Factorization Theorem, Sec. II.C shows that hole-line self-energy corrections are on the energy shell; the other virtue is that for net attractive potentials $E(k'')-\Delta(k)$ in Eq. (4.12) is always large.] The reason is that Eq. (4.12) must necessarily have a vanishing denominator for a repulsive potential as $E(k_F)-\Delta(k_F)<0$. Thus the effect is simply that there is a branch cut along the positive real V axis. This choice has also been criticized as either wrong or deceptive for the case of nuclear-type potentials (Baker, 1970).

Although Bethe and his collaborators aimed to apply their theory to potentials with both attractive and repulsive parts, their arguments are relevant, *a fortiori*, to the repulsive potential problem.

A different tack was pioneered by Huang, Yang, and Lee [Huang and Yang (1957); Lee and Yang (1957)]. They introduced two methods: The method of pseudopotentials, and the method of binary collisions. They applied these procedures specifically to the hard sphere gas (both Bose and Fermi statistics were considered). The results were an expansion in (k_Fa), where a is the hard core radius, or more generally the scattering length. They obtained the first two terms. Further terms involve other two-body scattering parameters, and aspects of the potential which are not given by two-body scattering parameters. Efimov and Amusia (1964; Efimov, 1965) and independently Baker (1965a) have carried this expansion further. It is valid for any strength potential and low density. For weaker potentials, the range in density is greater. It is calculationally simpler to use than the previously discussed series rearrangements, and although not so good in principle, it is quite adequate for certain problems. We will discuss this expansion in detail in Sec. IV.E and attempt to access its accuracy.

C. The Potential Perturbation Series Expansion Through Fourth Order

In order to provide a standard of comparison and evaluation for the various proposed approximations, Baker *et al.*, (1963) calculated through fourth order the complete potential perturbation series for the simple repulsive square-well potential. There is one first-order diagram, one second-, four third-, and 46 fourth-order diagrams. Of the 46, fourth-order diagrams, there are

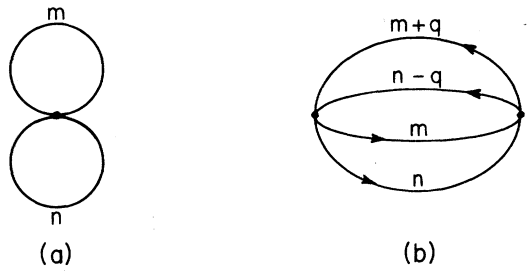

FIG. 27. First- (B1), and second-order (B2) perturbation theory diagrams.

only 28 distinct nonzero diagrams. First, the momentum transform of a square well of strength 1 and width c is, by (2.17)

$$\tilde{v}(q)=(1/2\pi^2q^3)[\sin(qc)-qc\cos(qc)]. \quad (4.20)$$

We will obtain the terms in the expansion as

$$\Delta EMc^2/(N\hbar^2)=A_1(VMc^2/\hbar^2)+A_2(VMc^2/\hbar^2)^2 +A_3(VMc^2/\hbar^2)^3+\cdots \quad (4.21)$$

for a potential of strength V. Referring to (2.40), we obtain the contribution A_1, which comes solely from Fig. 27a. It is

$$3/(4\pi k_F^3)\int_{|\mathbf{m}|\le k_F,\ |\mathbf{n}|\le k_F} d\mathbf{m}\,d\mathbf{n}[\tilde{v}(0)-\tfrac{1}{2}\tilde{v}(|\mathbf{m}-\mathbf{n}|)]. \quad (4.22)$$

This integral can be done analytically in terms of the sine integral Si (x): The result is

$$[(k_Fc)^3/9\pi]\{2-(72/x^6)[x^3\,\mathrm{Si}\,(x)-4-3x^2 +(4+x^2)\cos(x)+4x\sin(x)]\}, \quad (4.23)$$

where x is $2k_Fc$.

The contribution A_2 comes solely from Fig. 27b. It is, by (2.41),

$$\frac{-3}{4\pi k_F^3c^2}\int d\mathbf{m}\,d\mathbf{n}\,d\mathbf{q}\,\frac{\tilde{v}(q)[\tilde{v}(q)-\tfrac{1}{2}\tilde{v}(|\mathbf{n}-\mathbf{m}-\mathbf{q}|)]}{q^2+\mathbf{q}\cdot(\mathbf{m}-\mathbf{n})}, \quad (4.24)$$

where the integration is carried over all values allowed by the Pauli exclusion principle; that is, all hole-line momenta are in the Fermi sea, and all filled-state line momenta are outside the Fermi sea:

$$|\mathbf{m}|\le k_F,\quad |\mathbf{n}|\le k_F,\quad |\mathbf{m}+\mathbf{q}|>k_F,\quad |\mathbf{n}-\mathbf{q}|>k_F$$

As a further sample of the perturbation series terms, we write out the third-order terms which correspond to Fig. 28. The various contributions are:

Figure 28a:

$$B3=3/(4\pi k_F^3c^4)\int\frac{d\mathbf{m}\,d\mathbf{n}\,d\mathbf{q}\,d\mathbf{q}_1v(q)v(|\mathbf{q}-\mathbf{q}_1|)[v(q_1)-\tfrac{1}{2}v(|\mathbf{m}-\mathbf{n}+\mathbf{q}_1|)]}{[q^2+\mathbf{q}\cdot(\mathbf{m}-\mathbf{n})][q_1^2+\mathbf{q}_1\cdot(\mathbf{m}-\mathbf{n})]}, \quad (4.25)$$

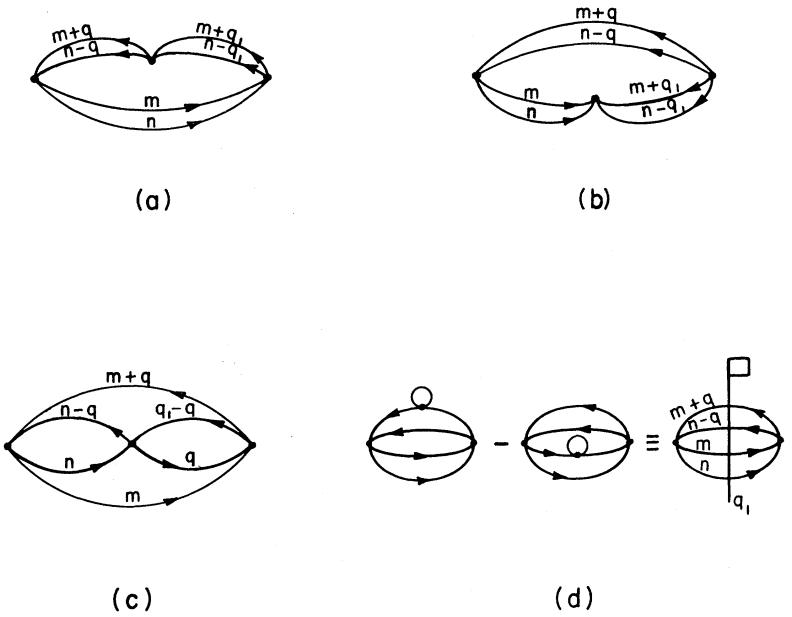

FIG. 28. Third-order perturbation theory diagrams: (a) B3, (b) H3, (c) R3, (d) F3.

Figure 28b:

$$H3=3/(4\pi k_F{}^3c^4)\int \frac{d\mathbf{m}\,d\mathbf{n}\,d\mathbf{q}\,d\mathbf{q}_1 v(q)v(q_1)[v(|\,\mathbf{q}-\mathbf{q}_1\,|)-\frac{1}{2}v(|\,\mathbf{q}+\mathbf{q}_1+\mathbf{m}-\mathbf{n}\,|)]}{[q^2+\mathbf{q}\cdot(\mathbf{m}-\mathbf{n})][q^2-q_1{}^2+(\mathbf{q}-\mathbf{q}_1)\cdot(\mathbf{m}-\mathbf{n})]}, \tag{4.26}$$

Figure 28c:

$$R3=3/(\pi k_F{}^3c^4)$$
$$\times\int \frac{d\mathbf{m}\,d\mathbf{n}\,d\mathbf{q}\,d\mathbf{q}_1\{[v(q)-\frac{1}{2}v(|\,\mathbf{m}+\mathbf{q}-\mathbf{q}_1\,|)][v(q)-\frac{1}{2}v(|\,\mathbf{n}-\mathbf{q}_1\,|)][v(q)-\frac{1}{2}v(|\,\mathbf{n}-\mathbf{m}-\mathbf{q}\,|)]-\frac{3}{8}v(|\,\mathbf{n}-\mathbf{m}-\mathbf{q}\,|)v(|\,\mathbf{m}+\mathbf{q}-\mathbf{q}_1\,|)v(|\,\mathbf{n}-\mathbf{q}_1\,|)\}}{[q^2+\mathbf{q}\cdot(\mathbf{m}-\mathbf{n})][q^2+\mathbf{q}\cdot(\mathbf{m}-\mathbf{q}_1)]}, \tag{4.27}$$

Figure 28d:

$$F3=-3/(2\pi k_F{}^3c^4)\int \frac{d\mathbf{m}\,d\mathbf{n}\,d\mathbf{q}\,d\mathbf{q}_1 v(q)[v(q)-\frac{1}{2}v(|\,\mathbf{n}-\mathbf{m}-\mathbf{q}\,|)]}{[q^2+\mathbf{q}\cdot(\mathbf{m}-\mathbf{n})]^2}[v(|\,\mathbf{q}+\mathbf{m}+\mathbf{q}_1\,|)-v(|\,\mathbf{m}+\mathbf{q}_1\,|)]. \tag{4.28}$$

The fourth-order contributions are illustrated in Figs. 29–34. We will not give the equations derivable from them here, but refer to Baker *et al.* (1963) for those. They are broken into classes of similar integrand structure. We will however note the following errors in that paper. Crichton and Anderson (1967) have pointed out that (2.15) of Baker *et al.* (1963) is wrong for IIA.5–6, but the formula given there for IIA.1–4 also holds for diagrams IIA.5–6. In addition we note that Eq. (2.13) of Baker *et al.* (1963) is misprinted and the factor 2^{11} should have been 2^{12} as was actually used in the computation. Further in Table II, the argument x_2 for Diagram II.9 should have been $|\,\mathbf{q}+\mathbf{q}_1\,|$ instead of $|\,\mathbf{q}-\mathbf{q}_1\,|$. This error has caused the tabulated results there and in Baker *et al.* (1964) to be slightly wrong for II.9.

The integrals were evaluated by Monte-Carlo procedures and the number of repetitions varied from 2×10^5 to 2.8×10^6. The error estimates are based on the Monte-Carlo estimates of the variance. Details are contained in the original paper. The values for II.9, IIA.2 (=IIA.4), IIA.5, and IIA.6 have been corrected in this report with the assistance of M. F. Hind. In the code for IIA.2, one of the Pauli restrictions was wrongly programmed in the original work. This error also persisted to the work of Baker *et al.* (1964). We give the fourth-order results in Table III. The diagrams which are, in principle, included in Brueckner K-matrix approximation through fourth order, are B1, B2, B3, F3, I.1, III.1, III.7+8, IV.1, IV.2, and IV.3.

We mention that III.3–6, 11, 12 vanish automatically because we cannot have a hole and a filled state with the same momentum.

The two hole-line approximation is identical with the

Brueckner approximation. The diagrams, including the self-energy corrections, which contribute to the three hole-line approximation of the "Cornell group" (see Sec. IV.B) are H3, R3 (completing third order), I.2, I.3+4, I.5, II.1, II.2, II.5, II.6, II.7, II.12, II-A.1, IV.4, IV.5, IV.6, and IV.7.

Careful attention to Table III yields the following observation, which is not unexpected on general grounds. The Brueckner approximation forms a quite adequate approximation to the first four orders of the potential energy expansion to the ground-state energy at the lowest densities. [Nuclear saturation density (Day, 1967) is $k_F c = 0.544$, for reference.] The three hole-line approximation works substantially better and is accurate to higher density. The leading corrections to the ladder approximation ($B1+B2+B3+$ I.1$+\cdots$) are the ring ($R3$) diagram and the hole–hole interaction diagram ($H3$) and those derived from them by ladder-type insertions, rather than the self-energy-type insertions. At low to moderate densities, the inclusion of those self-energy insertions which have four independent hole momenta (IV.1, IV.4, IV.5, IV.6, and IV.7) do not improve the accuracy of the three hole-line approximation. It is just as well that there is no advantage to their inclusion because, as Baker *et al.* (1963) have shown, the numerical approximations used to solve the self-consistent energy problem fail in the lowest order (III.1 and III.7+8) in which they enter even to give the correct sign of the correction.

If we rearrange the K-matrix rearrangement with no self-energy corrections, which we refer to as the ladder rearrangement, according to the number of independent hole-line momenta, then we observe that an effective

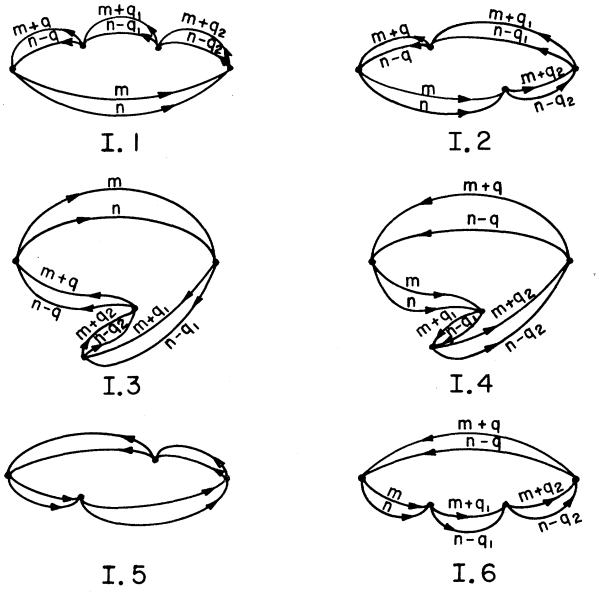

FIG. 29. Class I, fourth-order perturbation theory diagrams.

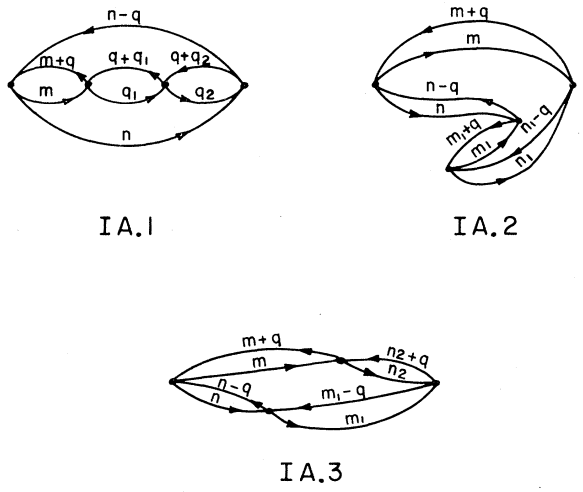

FIG. 30. Class IA, fourth-order perturbation theory diagrams.

procedure is obtained for treating the ground-state energy of the low-density, repulsive potential many-fermion system. This rearrangement can be shown to satisfy conditions (3.64). As we remarked above (Sec. B) the n hole-line approximation can be expressed in terms of the m-body scattering operators ($m \leq n$). Since these are analytic Re $(V) \geq 0$, near $V=0$, for purely repulsive forces, we conclude that this rearrangement is valid. The problem is, of course, that the three-body and higher operators are difficult to compute accurately, as are those higher-order contributions which depend only on integrals over products of two-body operators.

In order to investigate the effect on the many-fermion energy of different potentials which are equivalent for the two-body scattering problem, and thus to study whether that information is sufficient to pin down the many-fermion energy, Baker *et al.* (1964) have repeated the calculation of the first four orders of the potential perturbation series, as well as the ladder and Brueckner approximations for a nonsingular, but velocity-dependent force, which exactly simulates a hard core potential for two-body scattering. The force used is defined as follows: Let $\mu(r)$ be greater than or equal to one, and $\mu(\infty)=1$. Then, if Λ is Legendre's operator with eigenvalues $l(l+1)$,

$$v = -\left([\mu(r)-1]\nabla^2 + \nabla\mu\cdot\nabla + \tfrac{1}{4}\nabla^2\mu + \{\mu r^{-2} - [\rho(r)+a]^{-2}\}\Lambda - \tfrac{1}{2}\mu'[\mu'/(8\mu) - r^{-1}]\right) \quad (4.29)$$

exactly simulates (Baker, 1962) a hard core of radius

$$a = \int_0^\infty \{1-[\mu(r)]^{-1/2}\}\, dr, \quad (4.30)$$

where

$$\rho(r) = \int_0^r [\mu(r)]^{-1/2}\, dr. \quad (4.31)$$

This force does not, of course, exactly simulate a hard

TABLE III. Monte Carlo calculations.

	$k_{FC}=0.25$		$k_{FC}=0.50$		$k_{FC}=0.75$	
Diagram	Value	Deviation	Value	Deviation	Value	Deviation
B1[a]	5.567499×10^{-4}	...	4.551588×10^{-3}	...	1.589397×10^{-2}	...
B2[a]	-1.960×10^{-4}	1.2×10^{-6}	-1.346×10^{-3}	2.4×10^{-6}	-3.827×10^{-3}	4.6×10^{-6}
B3[a]	7.003×10^{-5}	5.7×10^{-7}	4.146×10^{-4}	1.7×10^{-6}	9.742×10^{-4}	3.1×10^{-6}
H3[b]	1.75×10^{-7}	1.6×10^{-9}	4.45×10^{-6}	4.3×10^{-8}	2.57×10^{-5}	2.0×10^{-7}
R3[b]	-8.60×10^{-7}	6.8×10^{-9}	-2.14×10^{-5}	1.6×10^{-7}	-1.175×10^{-4}	6.4×10^{-7}
F3[a]	3.95×10^{-8}	2.3×10^{-10}	2.10×10^{-6}	5.0×10^{-8}	1.89×10^{-5}	2.5×10^{-7}
Σ3	6.939×10^{-5}	5.7×10^{-7}	4.00×10^{-4}	1.7×10^{-6}	9.013×10^{-4}	3.2×10^{-6}
ΣB3	7.007×10^{-5}	5.7×10^{-7}	4.167×10^{-4}	1.7×10^{-6}	9.931×10^{-4}	3.1×10^{-6}
I.1[a]	-2.506×10^{-5}	1.9×10^{-7}	-1.288×10^{-4}	4.4×10^{-7}	-2.571×10^{-4}	1.1×10^{-6}
I.2[b]	-6.30×10^{-8}	6.1×10^{-10}	-1.36×10^{-6}	5.0×10^{-8}	-6.82×10^{-6}	1.5×10^{-7}
I.3+4[b]	-6.22×10^{-8}	6.0×10^{-10}	-1.41×10^{-6}	4.5×10^{-8}	-7.10×10^{-6}	9.4×10^{-8}
I.5[c,b]	-6.30×10^{-8}	6.1×10^{-10}	-1.36×10^{-6}	5.0×10^{-8}	-6.82×10^{-6}	1.5×10^{-7}
I.6	-9.93×10^{-10}	1.8×10^{-11}	-5.58×10^{-8}	9.5×10^{-10}	-5.16×10^{-7}	8.6×10^{-9}
I-A.1	-1.01×10^{-8}	2.9×10^{-10}	-5.36×10^{-7}	1.6×10^{-8}	-4.68×10^{-6}	1.4×10^{-7}
I-A.2	-4.65×10^{-9}	1.8×10^{-10}	-2.40×10^{-7}	8.4×10^{-9}	-2.00×10^{-6}	6.0×10^{-8}
I-A.3	-9.39×10^{-9}	1.5×10^{-10}	-4.94×10^{-7}	7.2×10^{-9}	-4.24×10^{-6}	5.8×10^{-8}
II.1[b]	3.07×10^{-7}	3.1×10^{-9}	6.71×10^{-6}	1.0×10^{-7}	3.15×10^{-5}	2.2×10^{-7}
II.2[c,b]	3.07×10^{-7}	3.1×10^{-9}	6.71×10^{-6}	1.0×10^{-7}	3.15×10^{-5}	2.2×10^{-7}
II.3	2.45×10^{-9}	4.3×10^{-11}	1.38×10^{-7}	2.1×10^{-9}	1.26×10^{-6}	1.7×10^{-8}
II.4[c]	2.45×10^{-9}	4.3×10^{-11}	1.38×10^{-7}	2.1×10^{-9}	1.26×10^{-6}	1.7×10^{-8}
II.5[b]	9.00×10^{-8}	4.5×10^{-10}	2.72×10^{-6}	1.0×10^{-7}	1.39×10^{-5}	1.9×10^{-7}
II.6[b]	2.28×10^{-7}	1.5×10^{-9}	4.22×10^{-6}	9.5×10^{-8}	1.86×10^{-5}	2.9×10^{-7}
II.7[b]	-2.77×10^{-9}	2.3×10^{-11}	-1.46×10^{-7}	1.2×10^{-9}	-1.20×10^{-6}	1.0×10^{-8}
II.8	-4.66×10^{-9}	1.7×10^{-10}	-1.96×10^{-7}	3.7×10^{-9}	-1.34×10^{-6}	1.8×10^{-8}
II.9	1.36×10^{-9}	2.6×10^{-11}	7.44×10^{-8}	1.3×10^{-9}	6.52×10^{-7}	1.1×10^{-8}
II.10	5.04×10^{-10}	1.3×10^{-11}	2.92×10^{-8}	7.2×10^{-10}	2.80×10^{-7}	7.0×10^{-9}
II.11[c]	-4.66×10^{-9}	1.7×10^{-10}	-1.96×10^{-7}	3.7×10^{-9}	-1.34×10^{-6}	1.8×10^{-8}
II.12[c,b]	-2.77×10^{-9}	2.3×10^{-11}	-1.46×10^{-7}	1.2×10^{-9}	-1.20×10^{-6}	1.0×10^{-8}
II-A.1[b]	-9.12×10^{-8}	4.6×10^{-10}	-2.80×10^{-6}	3.7×10^{-8}	-1.68×10^{-5}	1.7×10^{-7}
II-A.2	2.96×10^{-9}	4.5×10^{-11}	1.70×10^{-7}	2.3×10^{-9}	1.63×10^{-6}	1.5×10^{-8}
II-A.3	-6.88×10^{-10}	1.0×10^{-11}	-4.26×10^{-8}	6.2×10^{-10}	-4.57×10^{-7}	6.7×10^{-9}
II-A.4[c]	2.96×10^{-9}	4.5×10^{-11}	1.70×10^{-7}	2.3×10^{-9}	1.63×10^{-6}	1.5×10^{-8}
II-A.5	4.92×10^{-9}	4.4×10^{-11}	2.62×10^{-7}	2.0×10^{-9}	2.28×10^{-6}	2.1×10^{-8}
II-A.6	4.59×10^{-9}	6.6×10^{-11}	2.43×10^{-7}	3.2×10^{-9}	2.08×10^{-6}	2.8×10^{-8}
III.1[a]	-3.01×10^{-7}	2.1×10^{-9}	-6.13×10^{-6}	9.7×10^{-8}	-3.01×10^{-5}	2.8×10^{-7}
III.2	-4.59×10^{-9}	5.9×10^{-11}	-2.54×10^{-7}	3.0×10^{-9}	-2.31×10^{-6}	2.7×10^{-8}
III.7+8[a]	3.66×10^{-7}	1.6×10^{-9}	8.28×10^{-6}	1.2×10^{-7}	4.21×10^{-5}	3.0×10^{-7}
III.9+10	6.86×10^{-9}	2.0×10^{-10}	3.67×10^{-7}	9.3×10^{-9}	3.15×10^{-6}	6.5×10^{-8}
IV.1[a]	-6.2×10^{-12}	1.0×10^{-12}	-3.46×10^{-9}	3.3×10^{-10}	-9.75×10^{-8}	3.8×10^{-9}
IV.2[a]	-1.35×10^{-8}	4.9×10^{-10}	-6.79×10^{-7}	4.5×10^{-8}	-4.62×10^{-6}	1.4×10^{-7}
IV.3[c,a]	-1.35×10^{-8}	4.9×10^{-10}	-6.79×10^{-7}	4.5×10^{-8}	-4.62×10^{-6}	1.4×10^{-7}
IV.4[b]	1.83×10^{-10}	9.8×10^{-12}	3.60×10^{-8}	1.2×10^{-9}	6.15×10^{-7}	1.0×10^{-8}
IV.5[c,b]	1.83×10^{-10}	9.8×10^{-12}	3.60×10^{-8}	1.2×10^{-9}	6.15×10^{-7}	1.0×10^{-8}
IV.6[b]	3.90×10^{-11}	3.2×10^{-12}	7.70×10^{-9}	3.6×10^{-10}	1.40×10^{-7}	3.9×10^{-9}
IV.7[c,b]	3.90×10^{-11}	3.2×10^{-12}	7.70×10^{-9}	3.6×10^{-10}	1.40×10^{-7}	3.9×10^{-9}
Σ4	-2.438×10^{-5}	1.9×10^{-7}	-1.149×10^{-4}	5.5×10^{-7}	-1.991×10^{-4}	1.4×10^{-6}
ΣB4	-2.509×10^{-5}	1.9×10^{-7}	-1.280×10^{-4}	4.8×10^{-7}	-2.544×10^{-4}	1.2×10^{-6}
Σ3HL4	-2.437×10^{-5}	1.9×10^{-7}	-1.148×10^{-4}	5.0×10^{-7}	-1.974×10^{-4}	1.3×10^{-6}

TABLE III (*Continued*)

Diagram	$k_FC=1.0$		$k_FC=1.5$	
	Value	Deviation	Value	Deviation
B1[a]	3.936174×10^{-2}	...	1.475170×10^{-1}	...
B2[a]	-7.495×10^{-3}	1.9×10^{-5}	-1.715×10^{-2}	4.8×10^{-5}
B3[a]	1.538×10^{-3}	5.0×10^{-6}	2.190×10^{-3}	1.1×10^{-5}
H3[b]	7.87×10^{-5}	5.6×10^{-7}	2.81×10^{-4}	2.2×10^{-6}
R3[b]	-3.30×10^{-4}	1.7×10^{-6}	-7.98×10^{-4}	7.7×10^{-6}
F3[a]	8.08×10^{-5}	8.3×10^{-7}	5.05×10^{-4}	4.6×10^{-6}
Σ3	1.368×10^{-3}	5.3×10^{-6}	2.178×10^{-3}	1.4×10^{-5}
ΣB3	1.619×10^{-3}	5.1×10^{-6}	2.695×10^{-3}	1.2×10^{-5}
I.1[a]	-3.347×10^{-4}	2.1×10^{-6}	-3.01×10^{-4}	4.7×10^{-6}
I.2[b]	-1.75×10^{-5}	3.4×10^{-7}	-3.93×10^{-5}	6.6×10^{-7}
I.3+4	-1.85×10^{-5}	3.4×10^{-7}	-4.51×10^{-5}	6.8×10^{-7}
I.5[c,b]	-1.75×10^{-5}	3.4×10^{-7}	-3.93×10^{-5}	6.6×10^{-7}
I.6	-2.19×10^{-6}	3.7×10^{-8}	-1.16×10^{-5}	2.3×10^{-7}
I-A.1	-1.89×10^{-5}	5.4×10^{-7}	-1.01×10^{-4}	1.0×10^{-6}
I-A.2	-7.82×10^{-6}	2.2×10^{-7}	-4.56×10^{-4}	8.8×10^{-7}
I-A.3	-1.67×10^{-5}	2.4×10^{-7}	-8.50×10^{-5}	8.4×10^{-7}
II.1[b]	7.40×10^{-5}	4.8×10^{-7}	1.20×10^{-4}	1.2×10^{-6}
II.2[c,b]	7.40×10^{-5}	4.8×10^{-7}	1.20×10^{-4}	1.2×10^{-6}
II.3	5.23×10^{-6}	7.0×10^{-8}	2.39×10^{-5}	3.3×10^{-7}
II.4[c]	5.23×10^{-6}	7.0×10^{-8}	2.39×10^{-5}	3.3×10^{-7}
II.5[b]	3.42×10^{-5}	3.9×10^{-7}	4.76×10^{-5}	9.5×10^{-7}
II.6[b]	4.18×10^{-5}	5.4×10^{-7}	5.85×10^{-5}	1.4×10^{-6}
II.7[b]	-4.23×10^{-6}	2.9×10^{-8}	-1.06×10^{-5}	2.1×10^{-7}
II.8	-4.00×10^{-6}	6.6×10^{-8}	-6.23×10^{-5}	3.9×10^{-7}
II.9	2.54×10^{-6}	4.6×10^{-8}	9.68×10^{-6}	2.7×10^{-7}
II.10	1.22×10^{-6}	3.2×10^{-8}	6.38×10^{-6}	1.7×10^{-7}
II.11[c]	-4.00×10^{-6}	6.6×10^{-8}	-6.32×10^{-6}	3.9×10^{-7}
II.12[c,b]	-4.23×10^{-6}	2.9×10^{-8}	-1.06×10^{-5}	2.1×10^{-7}
II-A.1[b]	-5.21×10^{-5}	5.4×10^{-7}	-2.17×10^{-4}	9.8×10^{-7}
II-A.2	7.34×10^{-6}	9.9×10^{-8}	4.98×10^{-5}	8.0×10^{-7}
II-A.3	-2.35×10^{-6}	3.6×10^{-8}	-2.03×10^{-5}	2.8×10^{-7}
II-A.4[c]	7.34×10^{-6}	9.9×10^{-8}	4.98×10^{-5}	8.0×10^{-7}
II-A.5	9.18×10^{-6}	8.1×10^{-8}	4.86×10^{-5}	8.2×10^{-7}
II-A.6	8.13×10^{-6}	1.3×10^{-7}	3.89×10^{-5}	1.1×10^{-6}
III.1[a]	-8.32×10^{-5}	5.3×10^{-7}	-2.78×10^{-4}	1.8×10^{-6}
III.2	-9.81×10^{-6}	1.3×10^{-7}	-5.69×10^{-5}	8.0×10^{-7}
III.7+8[a]	1.155×10^{-4}	6.7×10^{-7}	3.68×10^{-4}	2.9×10^{-6}
III.9+10	1.24×10^{-5}	1.6×10^{-7}	6.53×10^{-5}	6.4×10^{-7}
IV.1[a]	-9.08×10^{-7}	2.2×10^{-8}	-1.55×10^{-5}	1.7×10^{-7}
IV.2[a]	-1.65×10^{-5}	3.7×10^{-7}	-6.42×10^{-5}	8.9×10^{-7}
IV.3[c,a]	-1.65×10^{-5}	3.7×10^{-7}	-6.42×10^{-5}	8.9×10^{-7}
IV.4[b]	3.74×10^{-6}	4.7×10^{-8}	2.47×10^{-5}	3.4×10^{-7}
IV.5[c,b]	3.74×10^{-6}	4.7×10^{-8}	2.47×10^{-5}	3.4×10^{-7}
IV.6[b]	9.42×10^{-7}	2.4×10^{-8}	9.36×10^{-6}	1.9×10^{-7}
IV.7[c,b]	9.42×10^{-7}	2.4×10^{-8}	9.36×10^{-6}	1.9×10^{-7}
Σ4	-2.24×10^{-4}	2.9×10^{-6}	-3.20×10^{-4}	8.2×10^{-6}
ΣB4	-3.363×10^{-4}	2.4×10^{-6}	-3.55×10^{-4}	6.1×10^{-6}
Σ3HL4	-1.98×10^{-4}	2.5×10^{-6}	-3.02×10^{-4}	6.5×10^{-6}

TABLE III. (*Continued*)

Diagram	$k_{FC}=2.0$ Value	$k_{FC}=2.0$ Deviation	$k_{FC}=3.0$ Value	$k_{FC}=3.0$ Deviation
B1[a]	3.901006×10^{-1}	...	1.574696×10^{0}	...
B2[a]	-2.868×10^{-2}	5.9×10^{-5}	-5.367×10^{-2}	3.3×10^{-4}
B3[a]	2.44×10^{-3}	2.0×10^{-5}	2.73×10^{-3}	1.2×10^{-4}
H3[b]	4.99×10^{-4}	5.7×10^{-6}	8.21×10^{-4}	2.1×10^{-5}
R3[b]	-2.61×10^{-4}	1.3×10^{-5}	$+4.75\times10^{-3}$	2.0×10^{-4}
F3[a]	1.51×10^{-3}	1.5×10^{-5}	4.45×10^{-3}	6.6×10^{-5}
Σ3	4.19×10^{-3}	2.9×10^{-5}	1.275×10^{-2}	2.4×10^{-4}
ΣB3	3.95×10^{-3}	2.5×10^{-5}	7.18×10^{-3}	1.4×10^{-4}
I.1[a]	-2.25×10^{-4}	9.4×10^{-6}	-1.09×10^{-4}	2.8×10^{-5}
I.2[b]	-4.13×10^{-5}	1.4×10^{-6}	-3.54×10^{-5}	4.6×10^{-6}
I.3+4	-4.69×10^{-5}	1.3×10^{-6}	-2.71×10^{-5}	4.0×10^{-6}
I.5[c,b]	-4.13×10^{-5}	1.4×10^{-6}	-3.54×10^{-6}	4.6×10^{-6}
I.6	-2.39×10^{-5}	7.0×10^{-7}	-2.82×10^{-5}	2.0×10^{-6}
I-A.1	-2.80×10^{-4}	5.2×10^{-6}	-1.35×10^{-3}	8.4×10^{-5}
I-A.2	-1.77×10^{-4}	2.6×10^{-6}	-1.06×10^{-3}	5.6×10^{-5}
I-A.3	-2.32×10^{-4}	3.2×10^{-6}	-1.30×10^{-3}	1.2×10^{-4}
II.1[b]	1.98×10^{-5}	3.9×10^{-6}	-2.46×10^{-4}	3.2×10^{-5}
II.2[c,b]	1.98×10^{-5}	3.9×10^{-6}	-2.46×10^{-4}	3.2×10^{-5}
II.3	2.86×10^{-5}	1.4×10^{-6}	-1.00×10^{-4}	1.3×10^{-5}
II.4[c]	2.86×10^{-5}	1.4×10^{-6}	-1.00×10^{-4}	1.3×10^{-5}
II.5[b]	-3.51×10^{-5}	2.7×10^{-6}	-2.39×10^{-4}	3.3×10^{-5}
II.6[b]	-1.67×10^{-5}	4.0×10^{-6}	-2.36×10^{-4}	4.2×10^{-5}
II.7[b]	$+1.05\times10^{-5}$	1.1×10^{-6}	1.36×10^{-4}	1.1×10^{-5}
II.8	$+1.92\times10^{-5}$	1.8×10^{-6}	1.38×10^{-4}	1.2×10^{-5}
II.9	5.1×10^{-6}	1.0×10^{-6}	-9.50×10^{-5}	7.9×10^{-6}
II.10	8.46×10^{-6}	7.4×10^{-7}	-3.51×10^{-5}	6.7×10^{-6}
II.11[c]	$+1.92\times10^{-5}$	1.8×10^{-6}	1.38×10^{-5}	1.2×10^{-5}
II.12[c,b]	$+1.05\times10^{-5}$	1.1×10^{-6}	1.36×10^{-4}	1.1×10^{-5}
II-A.1[b]	-5.28×10^{-4}	3.6×10^{-6}	-1.228×10^{-3}	5.3×10^{-5}
II-A.2	1.61×10^{-4}	3.5×10^{-6}	5.79×10^{-4}	2.6×10^{-6}
II-A.3	-7.87×10^{-5}	1.5×10^{-6}	-3.76×10^{-4}	1.5×10^{-5}
II-A.4[c]	1.61×10^{-4}	3.5×10^{-6}	5.79×10^{-4}	2.6×10^{-6}
II-A.5	1.25×10^{-4}	3.1×10^{-6}	3.48×10^{-4}	1.8×10^{-5}
II-A.6	9.00×10^{-5}	4.2×10^{-6}	2.85×10^{-4}	2.3×10^{-5}
III.1[a]	-5.75×10^{-4}	5.7×10^{-6}	-1.248×10^{-3}	6.5×10^{-5}
III.2	-1.71×10^{-4}	3.7×10^{-6}	-5.92×10^{-4}	3.1×10^{-5}
III.7+8[a]	7.36×10^{-4}	1.0×10^{-5}	1.568×10^{-3}	6.5×10^{-5}
III.9+10	1.80×10^{-4}	2.4×10^{-6}	6.71×10^{-4}	3.3×10^{-5}
IV.1[a]	-8.43×10^{-5}	8.8×10^{-7}	-3.90×10^{-4}	7.7×10^{-6}
IV.2[a]	-1.32×10^{-4}	2.6×10^{-6}	-2.67×10^{-4}	4.6×10^{-5}
IV.3[c,a]	-1.32×10^{-4}	2.6×10^{-6}	-2.67×10^{-4}	4.6×10^{-5}
IV.4[b]	1.21×10^{-5}	1.8×10^{-6}	-4.86×10^{-4}	3.3×10^{-5}
IV.5[c,b]	1.21×10^{-5}	1.8×10^{-6}	-4.86×10^{-4}	3.3×10^{-5}
IV.6[b]	3.12×10^{-5}	8.4×10^{-7}	8.95×10^{-5}	5.5×10^{-6}
IV.7[c,b]	3.12×10^{-5}	8.4×10^{-7}	8.95×10^{-5}	5.5×10^{-6}
Σ4	-1.111×10^{-3}	2.8×10^{-5}	-5.83×10^{-3}	2.6×10^{-4}
ΣB4	-4.12×10^{-4}	1.6×10^{-5}	-7.13×10^{-4}	1.3×10^{-4}
Σ3HL4	-9.74×10^{-4}	1.9×10^{-5}	-3.53×10^{-3}	1.8×10^{-4}

[a] Included in the Brueckner approximation.
[b] Included in the three hole-line approximation.
[c] Identical with a previous diagram (but must be added to find the total fourth-order coefficient).

core in the many-body problem except in the limit of zero density where only binary collisions are important.

They selected, for convenience in these calculations,

$$\mu(r)=1+se^{-r/\beta}$$
$$s=(2e^{0.5}-1)^2-1=4.2782422, \quad (4.32)$$

which implies $a=\beta$.

The structure of the importance of various diagrams was found to be qualitatively the same as in Table III. However, for moderate and higher density, the velocity-dependent force is less repulsive than the hard core force, as can be seen in ladder approximation in Fig. 35. That the ratio drops can be understood qualitatively from the observation that the energy for the hard core

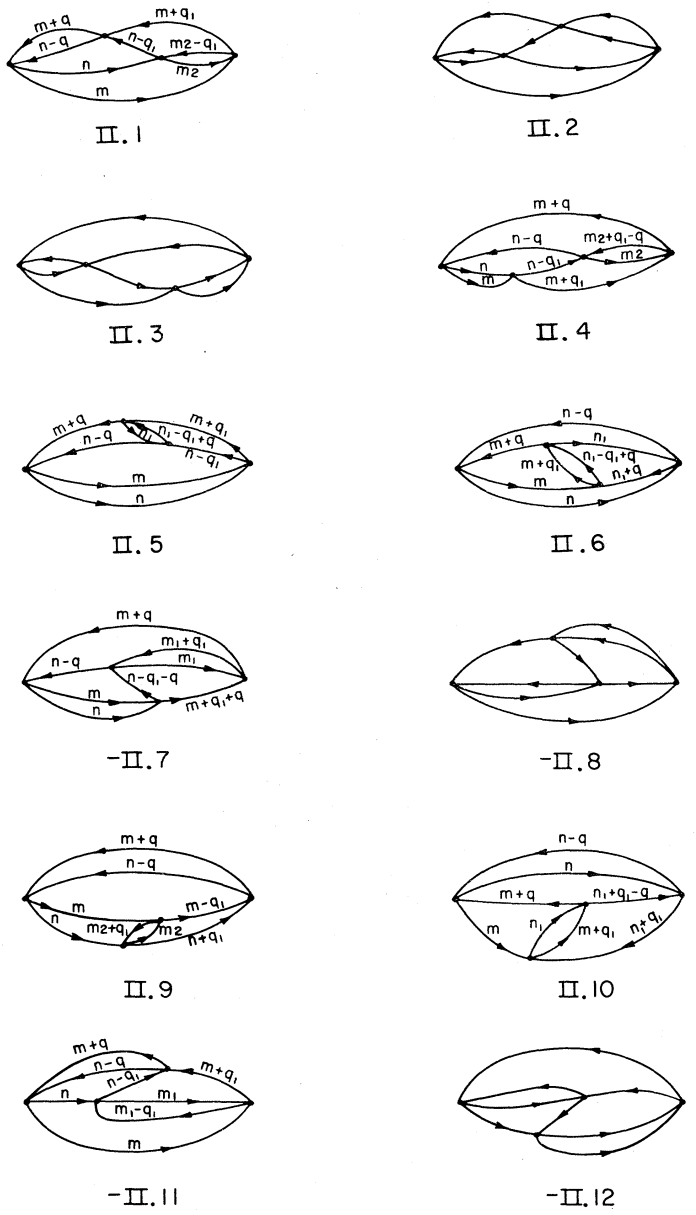

FIG. 31. Class II, fourth-order perturbation theory diagrams.

system goes to infinity at some jamming density, while for the velocity-dependent force the energy does not. Thus, even in ladder approximation, we would expect that the hard core force would seem stronger.

D. The Fermi Momentum Expansion

In order to provide a computationally simpler formalism, we will expand the series rearrangement discussed in the previous section in powers in k_F in the manner mentioned in Sec. IV.B. We will follow the work of Baker (1965a). Unfortunately that paper was marred by several errors as pointed out by Amusia and Efimov (1968). We will use a formalism similar to theirs as it is more compact and easily manipulated.

Our procedure for obtaining the expansion of the ground-state energy of a many-fermion system in terms of the Fermi momentum is to select, from the perturbation expansion in the potential, all those terms which can contribute through the desired order in k_F, and sum them to all orders in the potential strength. The basis of our selection procedure is the observation that the creation of an independent hole momentum at a potential vertex implies that the contribution of the diagram must vanish at least as one higher power of k_F in the limit as k_F goes to zero. The reason for this result is that the volume in momentum space is proportional to k_F^3; however, there is one more denominator which may reduce the volume factor by k_F^2 leaving a net

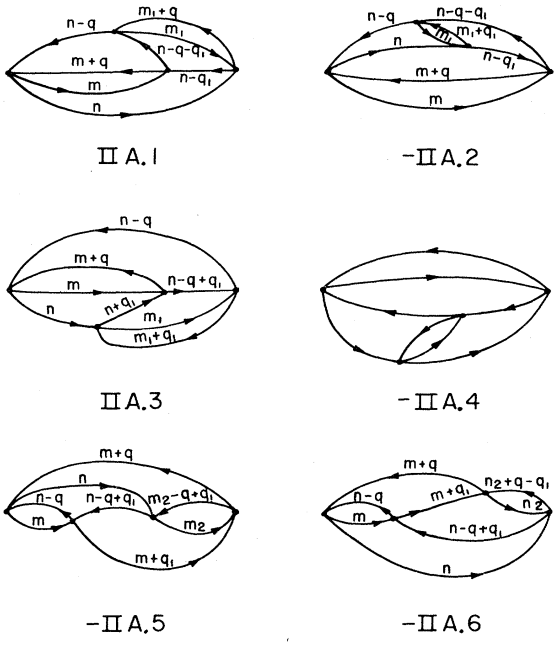

FIG. 32. Class IIA, fourth-order perturbation theory diagrams.

result of $k_F{}^1$. The only vertex which neither creates nor destroys a hole is the particle–particle scattering vertex illustrated in Fig. 15.

Since the leading terms in the energy are of the order $k_F{}^3$, it follows that if we agree to replace every vertex by the sum of all ladder insertions as discussed in Sec. IV.A, we may obtain the $(2+n)$th order in k_F by considering the nth in potential strength to find the basic graphs.

By examination of the catalog of graphs given in the previous section, we may classify the basic graphs for the first six orders in k_F as follows: Those proportional to $k_F{}^3$ are elaborations of B1. Those proportional to $k_F{}^5$ are elaborations of R3 and H3. Those proportional to $k_F{}^6$ are elaborations of F3, I.6, I-A.1, I-A.2, I-A.3, II.3=II.4, II.5, II.7=II.12, II.8=II.11, II.9, II.10, II-A.1, II-A.2=II-A.4, II-A.3, II-A.5, II-A.6, III.2, and III.9+10. The other diagrams in that catalog are either included as part of the elaboration of the above, or (IV.4–7) are of higher order in k_F. These sequences must be expanded in k_F to give the Fermi momentum expansion. For instance, the ladder diagrams, B1, B2, B3, I.1,··· all vanish as $k_F{}^3$ as k_F goes to zero; however, they also contribute terms like $k_F{}^4$, $k_F{}^5$, $k_F{}^6$, etc. Starting with the elaborations of F3 terms proportional to $k_F{}^6 \ln k_F$ are obtained.

The first step in our expansion procedure is to obtain an expansion of the sum of the ladder energy diagrams. This sum may be easily evaluated [Eq. (4.4)] in terms of the K matrix defined by Eq. (4.3). We may rewrite (4.3) using matrix notation as

$$\mathbf{K}=\mathbf{v}-\mathbf{vGK}, \tag{4.33}$$

where $\mathbf{G}$ has the diagonal matrix elements

$$F(\mathbf{p}, \mathbf{k}''')/[(k''')^2-k_0{}^2]$$

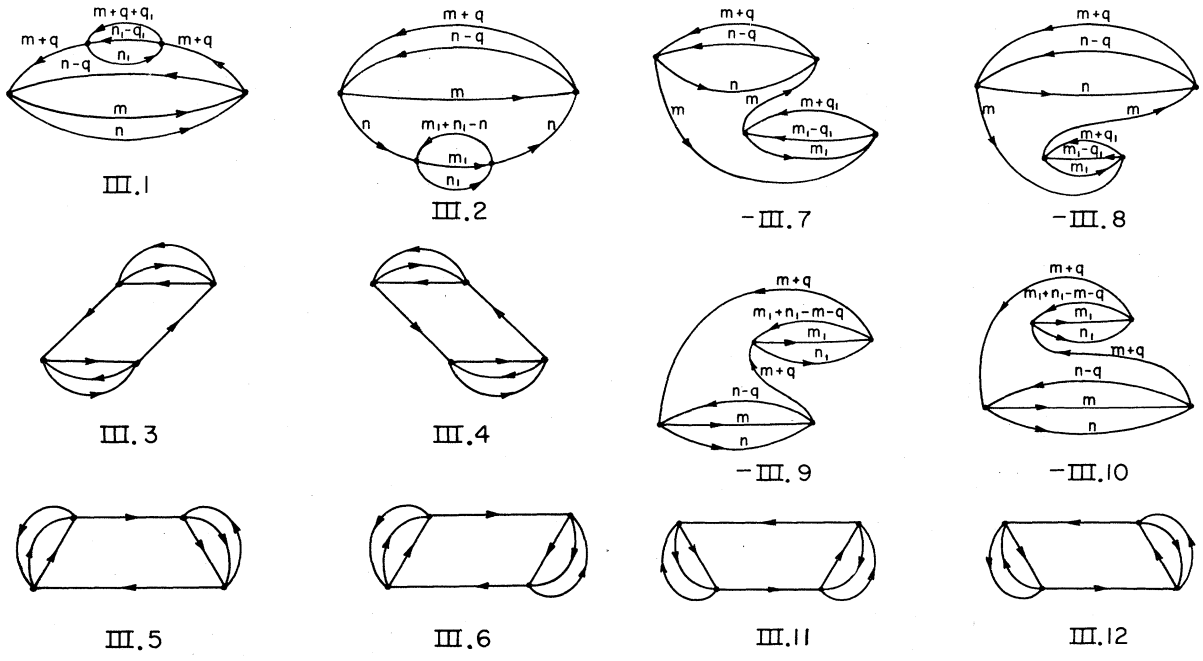

FIG. 33. Class III, fourth-order perturbation theory diagrams.

in the notation of Eq. (4.3). The function F is defined

$$F(\mathbf{p}, \mathbf{k}''') = 1, \quad |\mathbf{k}'''+\tfrac{1}{2}\mathbf{p}| > k_F, \text{ and } |\mathbf{k}'''-\tfrac{1}{2}\mathbf{p}| > k_F$$
$$= 0 \quad \text{otherwise.} \tag{4.34}$$

It is convenient to introduce the two-body scattering operator which has zero momentum in the Green's function. It satisfies the equation

$$\mathbf{t} = \mathbf{v} - \mathbf{v}\Gamma\mathbf{t}, \tag{4.35}$$

where $\Gamma = 1/(k''')^2$. We find this operator more convenient than the one of Amusia and Efimov (1968) as it avoids a principal part integral and is Hermitian, even off-the-energy shell. Then $\mathbf{K}$ can be shown to satisfy the equation (since V is purely repulsive, all the operations can be done without trouble)

$$\mathbf{K} = \mathbf{t} - \mathbf{t}\delta\mathbf{G}\,\mathbf{K}, \tag{4.36}$$

where the diagonal elements of δG are

$$\delta G(\mathbf{k}''') = -F(\mathbf{p}, \mathbf{k}''')\{1/[(k''')^2 - k_0^2] - 1/(k''')^2\}$$
$$+[1-F(\mathbf{p}, \mathbf{k}''')]/(k''')^2. \tag{4.37}$$

We can now iterate (4.36) to yield

$$\mathbf{K} = \mathbf{t} - \mathbf{t}\delta\mathbf{G}\,\mathbf{t} + \mathbf{t}\delta\mathbf{G}\,\mathbf{t}\delta\mathbf{G}\,\mathbf{t} - \cdots \tag{4.38}$$

To leading order in k_F each integration, characterized by the addition of another $\delta\mathbf{G}$, contributes, as explained above, another factor of k_F after substitution in (4.4). Hence if we set our goal as terms in the energy through order k_F^6, then we may break off (4.38) with the term involving $3\,\delta\mathbf{G}$'s.

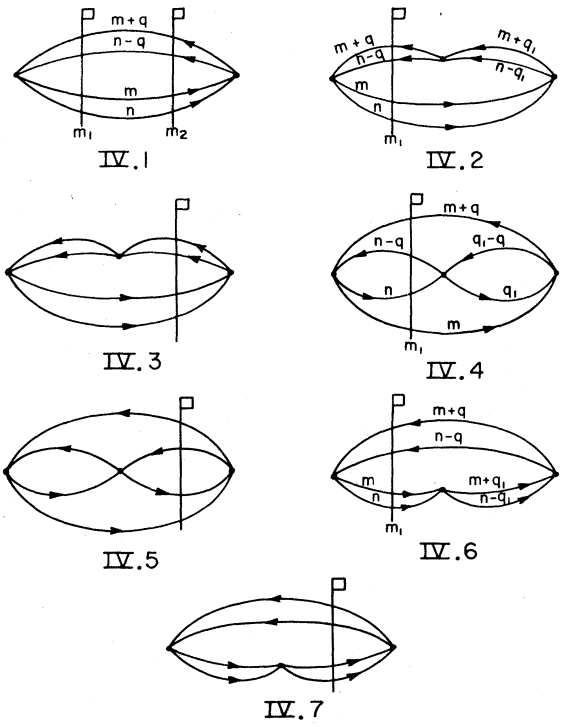

FIG. 34. Class IV, fourth-order perturbation theory diagrams.

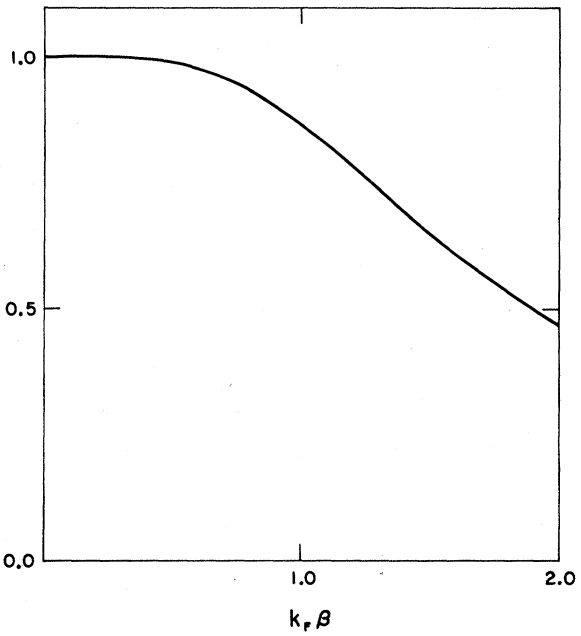

FIG. 35. Ratio of the hard-core simulating, velocity-dependent force energy shift to the hard-core force energy shift in the ladder approximation.

First let us evaluate the first term in (4.38) when substituted into (4.4). This evaluation can be done by noting that (4.35) is equivalent to the differential equation

$$[-\nabla^2 + v(r)]\Psi_p(\mathbf{r}) = p^2 \exp(i\mathbf{p}\cdot\mathbf{r}), \tag{4.39}$$

where

$$\langle \mathbf{q} \mid \mathbf{t} \mid \mathbf{p} \rangle = [1/(2\pi)^3]\int d\mathbf{r} \exp(-i\mathbf{q}\cdot\mathbf{r})v(r)\Psi_p(\mathbf{r}) \tag{4.40}$$

are the matrix elements of $\mathbf{t}$, and Ψ satisfies the boundary conditions that it be finite at $r=0$, and that $|\Psi_p(\mathbf{r}) - \exp(i\mathbf{p}\cdot\mathbf{r}|$ tend to zero like r^{-1} as r tends to infinity (Wu and Ohmura, 1962). We will need the well known (Wu and Ohmura, 1962) formula for the scattering length

$$\langle 0 \mid \mathbf{t} \mid 0 \rangle = a/2\pi^2. \tag{4.41}$$

If we make the usual partial wave decomposition of $\Psi_p(\mathbf{r})$ as

$$\Psi_p(\mathbf{r}) = \sum_{l=0}^{\infty} (2l+1) i^l \psi_l(p, r) P_l[\cos(\theta)], \tag{4.42}$$

where P_l are the Legendre polynomials, and θ is the angle between $\mathbf{p}$ and $\mathbf{r}$, then it follows that

$$\int d\mathbf{r} \exp(-i\mathbf{q}\cdot\mathbf{r})v(r)\Psi_p(\mathbf{r}) = 4\pi \sum_{l=0}^{\infty} (2l+1) P_l[\cos(\theta)] \times \int_0^{\infty} j_l(qr)v(r)\psi_l(p,r)r^2\, dr. \quad (4.43)$$

From Hermiticity of $\mathbf{t}$ and (4.43), it is now clear that the terms quadratic in the momenta come from $l=0$ and $l=1$ alone and that there are no cubic terms in the momenta. If we use the asymptotic form

$$\psi_l(p,r) = j_l(pr) - A_l(p)\, p^l/r^{l+1} \quad (4.44)$$

and the Hermiticity of the $l=0$ part, we can deduce in the same way that (4.41) is usually derived that

$$A_l''(0) = -\frac{1}{3}\int_0^{\infty} r^4 v(r)\psi_0(0,r)\, dr. \quad (4.45)$$

Thus, substituting the first term of (4.38) in (4.4), we obtain the contribution

$$E_1 = (3\pi)^{-1}\{(\nu-1)ak_F^3 + [\tfrac{3}{10}(\nu-1)A''(0) + \tfrac{9}{10}(\nu+1)A_1(0)]k_F^5\} + O(k_F^7). \quad (4.46)$$

The numerical factors arise from working out the momentum integrals in (4.4).

Next let us evaluate the second term of (4.38). By scaling the momenta by k_F we get a leading order contribution proportional to $k_F^4 a^2$. In addition, we will have terms both contributing in order k_F^5 and k_F^6. Let us break this term up as

---

$$(3/(8\pi k_F^3))\int d\mathbf{p}\, d\mathbf{k}_0\, d\mathbf{k}'''[\langle \mathbf{k}\mid \mathbf{t}\mid \mathbf{k}\rangle \delta G(\mathbf{k}''')(\nu\langle \mathbf{k}\mid \mathbf{t}\mid \mathbf{k}\rangle - \langle \mathbf{k}\mid \mathbf{t}\mid -\mathbf{k}\rangle)] + (3/8\pi k_F^3)\int d\mathbf{p}\, d\mathbf{k}_0\, d\mathbf{k}''' \times [\langle \mathbf{k}\mid \mathbf{t}\mid \mathbf{k}'''\rangle \delta G(\mathbf{k}''')(\nu\langle \mathbf{k}'''\mid \mathbf{t}\mid \mathbf{k}\rangle - \langle \mathbf{k}'''\mid \mathbf{t}\mid -\mathbf{k}\rangle) - \langle \mathbf{k}\mid \mathbf{t}\mid \mathbf{k}\rangle \delta G(\mathbf{k}''')(\nu\langle \mathbf{k}\mid \mathbf{t}\mid \mathbf{k}\rangle - \langle \mathbf{k}\mid \mathbf{t}\mid -\mathbf{k}\rangle)]. \quad (4.47)$$

The second integral in (4.47) can be broken into (by 4.37) F and $1-F$ parts of the $\mathbf{k}'''$ integration. By using (4.37) and (4.40), we can recast the F part as

$$-[3/(8\pi(2\pi)^6 k_F^3)]\int d\mathbf{p}\, d\mathbf{k}\, d\mathbf{k}'''\, d\mathbf{r}\, d\mathbf{r}'\Psi_k(\mathbf{r})v(r)(\{\exp[i\mathbf{k}'''\cdot(\mathbf{r}-\mathbf{r}')] - \exp[i\mathbf{k}\cdot(\mathbf{r}-\mathbf{r}')]\}/((k''')^2[(k''')^2-k^2])) \times F(\mathbf{p},\mathbf{k}''')k^2 v(r')[\nu\Psi_k(\mathbf{r}') - \Psi_{-k}(\mathbf{r}')]. \quad (4.48)$$

This quantity, as a function of $\mathbf{k}$ (before integration) regular and bounded, and the integration region is symmetrical in $\pm\mathbf{k}$. Thus, if we scale the momenta $\mathbf{p}$, $\mathbf{k}$ by k_F, the correction to the leading order will be k_F^2 smaller. As the leading order in (4.48) is k_F^5, we may discard the correction as we are only keeping terms through k_F^6. The necessary integral over $\mathbf{k}'''$ is readily done as

$$\int d\mathbf{k}'''\{1 - \exp[i\mathbf{k}'''\cdot(\mathbf{r}-\mathbf{r}')]\}/(k''')^4 = \pi^2 \mid \mathbf{r}-\mathbf{r}' \mid. \quad (4.49)$$

It is convenient to define the parameter

$$b_2 = (M/\hbar^2)^2(3/320\pi^2)\int d\mathbf{r}\, d\mathbf{r}'\Psi_0(\mathbf{r})v(r)\mid \mathbf{r}-\mathbf{r}' \mid v(r')\Psi_0(\mathbf{r}'). \quad (4.50)$$

Then (4.48) contributes $[(\nu-1)k_F^5 b_2/3\pi] + O(k_F^7)$ to the energy.

If we expand the $\mathbf{t}$ matrix elements in the $1-F$ part of the second integral of (4.47) to terms quadratic in the momentum, we obtain the contribution to the energy of

$$[3a/(2\pi)^5 k_F^3]\int d\mathbf{p}\, d\mathbf{k}\, d\mathbf{k}'''[1-F(\mathbf{p},\mathbf{k}''')](((\nu-1)A_0''(0) + 6\nu A_1(0)\{\mathbf{k}\cdot(\mathbf{k}'''-\mathbf{k})/[(k''')^2-k^2]\}) \quad (4.51)$$

which is of the order of k_F^6 as can be seen by scaling $\mathbf{p}$, $\mathbf{k}$, and $\mathbf{k}'''$. We can get the remainder of the contributions of the second term of (4.38) by expanding to order k^2 the $\mathbf{t}$ matrix elements in the first integral in (4.47). This expansion yields

$$[-3/(2\pi)^5 k_F^3]\int d\mathbf{p}\, d\mathbf{k}\,[\int d\mathbf{k}'''\delta G(\mathbf{k}''')]\{(\nu-1)a^2 + 2k^2a^2[(\nu-1)A_0''(0) + 6\nu A_1(0)]\}. \quad (4.52)$$

In order to summarize this contribution to the energy, and that from the third and fourth terms as well, it is convenient to introduce the notation

$$g_j = \frac{3}{2(2\pi)^3}\int_{|\frac{1}{2}\mathbf{p}+\mathbf{k}|\le 1;\ |\frac{1}{2}\mathbf{p}-\mathbf{k}|\le 1} d\mathbf{p}\, d\mathbf{k}\left((1/2\pi^2)\int d\mathbf{k}_1\{[(k_1^2-k^2)^{-1} - k_1^{-2}]F(k_F\mathbf{p}, k_F\mathbf{k}_1) - [1-F(k_F\mathbf{p}, k_F\mathbf{k}_1)]k_1^{-2}\}\right)^j \quad (4.53)$$

$$h_1 = [3/(2(2\pi)^3)]\int d\mathbf{p}\, d\mathbf{k}k^2((1/2\pi^2)\int d\mathbf{k}_1\{[(k_1^2-k^2)^{-1} - k_1^{-2}]F(k_F\mathbf{p}, k_F\mathbf{k}_1) - [1-F(k_F\mathbf{p}, k_F\mathbf{k}_1)]k_1^{-2}\}) \quad (4.54)$$

$$h_2 = [3/(2\pi)^5]\int d\mathbf{p}\, d\mathbf{k}\, d\mathbf{k}_1[1-F(k_F\mathbf{p}, k_F\mathbf{k}_1)]. \quad (4.55)$$

Then, we get

$$E_2=-g_1(\nu-1)k_F{}^4a^2+[(\nu-1)/3\pi]b_2k_F{}^5-(\nu-1)[2h_1-h_2]aA_0''(0)k_F{}^6+O(k_F{}^7), \tag{4.56}$$

where use has been made of the identity

$$[3/(2\pi)^5]\int d\mathbf{p}\,d\mathbf{k}\,d\mathbf{k}'''(1-F)\{[\mathbf{k}\cdot(\mathbf{k}'''-\mathbf{k})]/[(k''')^2-k^2]\}\equiv h_1 \tag{4.57}$$

to eliminate the terms involving $A_1(0)$. The third term in (4.38) can be broken up in a similar manner; however now there will occur integrals involving the product of two $\delta\mathbf{G}$'s. The contribution follows in the same manner as before and leads to

$$E_3=g_2(\nu-1)k_F{}^5a^3-(20/3)h_1(\nu-1)k_F{}^6ab_2+O(k_F{}^7). \tag{4.58}$$

The contribution from the fourth term is

$$E_4=-g_3(\nu-1)k_F{}^6a^4+O(k_F{}^7). \tag{4.59}$$

Thus, combining (4.46, 4.56, 4.58, and 4.59) we get for the ladder energy

$$\Delta E_LM/(Nh^2)=(3\pi)^{-1}(\nu-1)ak_F{}^3-g_1(\nu-1)k_F{}^4a^2+(3\pi)^{-1}\{(\nu-1)[\tfrac{3}{10}A_0''(0)+b_2]+(9/10)(\nu+1)A_1(0)\}k_F{}^5$$
$$+g_2(\nu-1)k_F{}^5a^3-2h_1(\nu-1)[A_0''(0)+(10/3)b_2]ak_F{}^6+h_2(\nu-1)aA_0''(0)k_F{}^6-g_3(\nu-1)k_F{}^6a^4+O(k_F{}^7). \tag{4.60}$$

Except for the term involving h_2, all the rest of this expression can be expressed in terms of the zero energy scattering phase shifts. Amusia and Efimov (1968) give the result

$$A_0''(0)+(10/3)b_2=\tfrac{1}{2}a^2r_0 \tag{4.61}$$

where r_0 is the effective range. This result can be obtained formally by iterating the integral equation for the normal (principal part) scattering operator (see Wu and Ohmura, 1962), using

$$\{\tfrac{1}{2}(\partial^2/\partial K^2)P\int d\mathbf{k}f(k^2)/[k^2-K^2]\}\,|_{K=0}=\int dk\{[f(k^2)-f(0)]/k^2\} \tag{4.62}$$

term-by-term to expand to order K^2 in the momentum, summing the coefficients of K^0 and K^2, and finally identifying the resulting terms with the effective range expansion.

$$K\cot(\delta_0)=-1/a+\tfrac{1}{2}r_0K^2 \qquad K^3\cot(\delta_1)=-1/A_1(0). \tag{4.63}$$

The quantity $A_0''(0)$ (or b_2) alone is not expressible in terms of phase shifts. This remark is in accord with Fig. 35 which shows that the ladder energy is not purely determined by the two-body phase shifts.

These results can also be shown to hold for velocity-dependent forces because the potential factors (except the first and last in each ladder term) do not depend on the hole state momenta, but only on the momentum transfer and the exchanged momentum transfer.

We can easily reduce the g's and h's to double integrals. The result is:

$$g_j=\frac{3}{\pi^{j+1}}\int_0^2 p\,dp\left(p\int_0^{1-\frac{1}{2}p}k^2\,dk(\tau_1-\tau_2)^j+\int_{1-\frac{1}{2}p}^{(1-\frac{1}{4}p^2)^{1/2}}k\,dk(1-\tfrac{1}{4}p^2-k^2)(\tau_1-\tau_2)^j\right), \tag{4.64}$$

$$h_1=\frac{3}{\pi^2}\int_0^2 p\,dp\left(p\int_0^{1-\frac{1}{2}p}k^4\,dk(\tau_1-\tau_2)+\int_{1-\frac{1}{2}p}^{(1-\frac{1}{4}p^2)^{1/2}}k^3\,dk(1-\tfrac{1}{4}p^2-k^2)(\tau_1-\tau_2)\right), \tag{4.65}$$

$$h_2=\frac{3}{\pi^2}\int_0^2 p\,dp\left(p\int_0^{1-\frac{1}{2}p}k^2\,dk\tau_3+\int_{1-\frac{1}{2}p}^{(1-\frac{1}{4}p^2)}k\,dk(1-\tfrac{1}{4}p^2-k^2)\tau_3\right), \tag{4.66}$$

where

$$\tau_1=p^{-1}\{(k^2+\tfrac{1}{4}p^2-1)\ln[(1+p+\tfrac{1}{4}p^2-k^2)/(1-\tfrac{1}{4}p^2-k^2)]+(1-\tfrac{1}{4}p^2)\ln[(1+\tfrac{1}{2}p)/(1-\tfrac{1}{2}p)]\}$$
$$+k\ln[(1+\tfrac{1}{2}p+k)/(1+\tfrac{1}{2}p-k)],$$
$$\tau_2=1+\tfrac{1}{2}p+[(1-\tfrac{1}{4}p^2)/p]\ln[(1+\tfrac{1}{2}p)/(1-\tfrac{1}{2}p)],$$
$$\tau_3=(\tfrac{2}{3}+\tfrac{1}{2}p-p^2)/24. \tag{4.66a}$$

Although these could have been carried further analytically [Lee and Yang (1957) have done g_1 analytically], we have preferred to evaluate (4.64–4.66) numerically. We obtain

$$g_1=-5.5661\times10^{-2} \qquad g_2=3.2031\times10^{-2}$$
$$g_3=-1.9156\times10^{-2} \qquad h_1=-1.3373\times10^{-2}$$
$$h_2=3.8196\times10^{-2}. \tag{4.67}$$

We now turn to those terms whose contributions start in fifth order in k_F. The sum of those diagrams which are elaborations of H3 contributes a term proportional to $k_F{}^5a^3\hbar^2/M$ in leading order; we may calculate the coefficient by evaluating Eq. (4.26) for the arguments of the potential set to zero. The coefficient (obtained by Monte Carlo integration) is $(5.74\times10^{-3}\pm1.0\times10^{-5})(\nu-1)$. By proceeding as we did above we may show that there are two terms contributed by the H3 sequence in sixth order in k_F. One term comes from expanding the contributions of the K matrices which now stand at each vertex of H3. This term contributes

$$3(5.74\times10^{-3})(\nu-1)(-3\pi g_1)a^4k_F{}^6\hbar^2/M$$
$$=9.03\times10^{-3}a^4(\nu-1)k_F{}^6\hbar^2/M.$$

The other contribution is of the form ab_2. It is

$$-[20/(27\pi^2)](\nu-1)k_F{}^6ab_2\hbar^2/M. \tag{4.68}$$

The other terms which start in fifth order are elaborations of R3. We obtain, proceeding as above, contributions of

$$(+2.863\times10^{-2}\pm1.7\times10^{-5})(\nu-1)(\nu-3)k_F{}^5a^3\hbar^2/M$$
$$+3(+2.863\times10^{-2})(\nu-1)(\nu-3)(-3\pi g_1)k_F{}^6a^4\hbar^2/M$$
$$+k_F{}^6c_1\hbar^2/M. \tag{4.69}$$

The term c_1 arises in a manner similar to the ab_2 term in H3; however, in the calculation of c_1 we must consider the effects of a hole–filled-state interaction in the presence of an excited Fermi sea. In this situation, the analysis of the low-density limit proceeds in a fashion similar to that of (4.39) *et seq.* except that (4.39) is modified to

$$[-\nabla^2+q^2+v(r)]\Psi_p(\mathbf{r})=(p^2+q^2)\exp(i\mathbf{p}\cdot\mathbf{r}), \tag{4.70}$$

where q^2 is the excitation energy of the Fermi sea. Equation (4.70) follows in the usual way (Wu and Ohmura, 1962) from (4.3), with the excitation energy included in the denominator. Let us define from (4.40)

$$K(k)=2\pi^2\langle\mathbf{k}\mid\mathbf{t}\mid0\rangle \tag{4.71}$$

and

$$\hat{K}_\pm(k)=(4\pi)^{-1}\int\exp(\mp\tfrac{1}{2}i\mathbf{k}\cdot\mathbf{r})v(r)\hat{\psi}_{1/2k}(\mathbf{r})\,d\mathbf{r}, \tag{4.72}$$

where $\hat{\psi}_{1/2k}$ is the solution of (4.70), with $\mathbf{p}=\frac{1}{2}\mathbf{k}$, and $q^2=\frac{3}{4}k^2$. If we expand

$$\hat{\psi}_{\frac{1}{2}k}(r)=\sum_{l=0}^{\infty}(2l+1)i^l\hat{\psi}_l(r)P_l[\cos(\theta)], \tag{4.73}$$

then we find

$$\hat{K}_\pm(k)=\sum_{l=0}^{\infty}(2l+1)(\pm1)^l\int_0^\infty j_l(\tfrac{1}{2}kr)v(r)\hat{\psi}_l(r)r^2\,dr. \tag{4.74}$$

We may now write down c_1. It is

$$c_1=[2(\nu-1)/9\pi^4]\int d\mathbf{k}$$
$$\times\{K^2(k)[(\nu-1)\hat{K}_-(k)-2\hat{K}_+(k)]-(\nu-3)K^3(0)\}/k^4. \tag{4.75}$$

We shall now turn to those sequences of terms whose contributions begin in sixth order in k_F. The self-energy corrections which are elaborations of the final third-order graph F3 are of this type. If we write this contribution as $k_F{}^6c_2$, then by application of the techniques used above we can show that

$$c_2=(2/9\pi^4)(\nu-1)\int dkK^2(k)$$
$$\times[\nu\hat{K}_+(k)-\hat{K}_-(k)-(\nu-1)K(0)]/k^4. \tag{4.76}$$

As $\hat{K}_+{}'(0)=\hat{K}_-{}'(0)\neq0$, the integrals (4.75–4.76) for c_1 and c_2 diverge logarithmically as k goes to zero. This behavior is symptomatic of the appearance of a $k_F{}^6\ln k_F$ term in the expansion. The sum c_1+c_2 can be reorganized as

$$c_1+c_2=[2(\nu-1)(\nu-2)/9\pi^4]\int d\mathbf{k}K^2(k)[\hat{K}_+(k)+\hat{K}_-(k)-2K(0)]/k^4$$
$$+[2(\nu-1)(\nu-3)K(0)/9\pi^4]\int d\mathbf{k}[K^2(k)-K^2(0)]/k^4. \tag{4.77}$$

The second line of (4.77) is $-40(\nu-1)(\nu-3)ab_2/(27\pi^2)$. We can isolate the log term by replacing the k_F dependence in the lower limit of the first integral and calculating the various contributions which arise. They are

$$c_a=\frac{(\nu-1)(\nu-2)}{4\pi^6k_F{}^6}\int_{|\frac{1}{2}p+k'|\le k_F,\ |\frac{1}{2}p+k|>k_F;\ |\frac{1}{2}p-k'|\le k_F,\ |\frac{1}{2}p-k|>k_F}d\mathbf{p}\,d\mathbf{k}\,d\mathbf{k}'\frac{[K(0)]^2\hat{K}_+{}'(0)}{k^3(1+\beta k)}, \tag{4.78}$$

$$c_b=\frac{(\nu-1)(\nu-2)}{4\pi^6}\int_{|\frac{1}{2}p+k'|\le1,\ |\frac{1}{2}p+k|>1;\ |\frac{1}{2}p-k'|\le1,\ |\frac{1}{2}p-k|>1}d\mathbf{p}\,d\mathbf{k}\,d\mathbf{k}'K^2(0)\hat{K}_+{}'(0)k[(k^2-k'^2)^{-2}-k^{-4}]$$
$$=(2.30\times10^{-2}\pm1.0\times10^{-4})K^2(0)\hat{K}_+{}'(0)(\nu-1)(\nu-2), \tag{4.79}$$

$$b_3=[2(\nu-1)(\nu-2)/9\pi^4]\int d\mathbf{k}\{K^2(k)[\hat{K}_+(k)+\hat{K}_-(k)-2K(0)]-2K^2(0)\hat{K}_+{}'(0)k/(1+\beta k)\}k^{-4}. \tag{4.80}$$

The quantities b_3 and c_b are now convergent, and the ln k_F part comes from c_a alone. Evaluating c_a analytically, we get

$$c_a=\frac{16}{9\pi^3}K^2(0)\hat{K}_+'(0)(\nu-1)(\nu-2)$$
$$\times\left\{-\ln(k_F\beta)+3\int_0^2 p(1-\tfrac{1}{2}p)^2(1+\tfrac{1}{4}p)[1+\tfrac{1}{2}p-(1-\tfrac{1}{4}p^2)^{1/2}]\left[1-\left(\frac{1-\frac{1}{2}p}{1+\frac{1}{2}p}\right)^{1/2}\right]dp\right\} \quad (4.81)$$

plus terms which vanish as k_F goes to zero. We have evaluated the integrals in Eq. (4.81) by Simpson's rule. It should be pointed out that the division between the $k_F^6\ln(k_F\beta)$ term and the k_F^6 term (c_a+b_3) is somewhat arbitrary because of the scale factor β.

One may easily show [since $\hat{K}_+'(0)$ comes from the $l=0$ terms alone], by considering the wave function in the region beyond the range of the potential as a linear combination of a solution (even in k) of Eq. (4.70) and a solution of the homogeneous part of Eq. (4.70) (even in k), that

$$\hat{K}_+'(0)=\tfrac{1}{2}\sqrt{3}a^2. \quad (4.82)$$

Thus we get

$$c_a=\{[8\sqrt{3}/(9\pi^3)]\ln(k_F\beta)+1.443\times10^{-2}\}$$
$$\times(\nu-1)(\nu-2)a^4. \quad (4.83)$$

If we combine all those non ladder terms which we have obtained thus far we get the contribution to the energy

$$(\nu-1)\{[5.74\times10^{-3}+2.863\times10^{-2}(\nu-3)]k_F^5a^3$$
$$+[9.03\times10^{-3}+3.44\times10^{-2}(\nu-2)+4.506\times10^{-2}(\nu-3)]$$
$$\times k_F^6a^4-[20(3\nu-7)/27\pi^2]k_f^6ab_2$$
$$-(\nu-2)[8\sqrt{3}/(9\pi^3)]k_F^6a^4\ln(k_F\beta)+b_3+\cdots\}. \quad (4.84)$$

It is to be noticed that the ln $(k_F\beta)$ term and b_3 vanish when $\nu=2$.

The contribution of the remainder of the sequences is of the form $k_F^6a^4$. Baker (1965a) calculated by Monte Carlo the values of the coefficients from the formulas given in Baker *et al.* (1963) for $\nu=2$. We list his values in Table IV. We remark that IIA.1 and II.5 separately are not of this form, but that their sum is, for $\nu=2$.

In order to generalize these results for $\nu\neq2$ we need only multiply the coefficients in Table IV by the factors in Table V.

In addition, II.5+IIA.1 contributes a $k_F^6\ln(k_F)$ term, when $\nu\neq2$. This term has been evaluated first by Efimov (1965) and then by Amusia and Efimov (1968) (called ϵ_6 by them) as

$$(32/27\pi^2)(\nu-1)(\nu-2)k_F^6a^4\ln(k_F\beta). \quad (4.85)$$

Hence the total contribution to leading order in logarithmic terms is

$$E_{\log}=(8/27\pi^3)(4\pi-3\sqrt{3})(\nu-1)(\nu-2)k_F^6a^4\ln(k_F\beta) \quad (4.86)$$

which vanishes for $\nu=1$ or 2. The ln terms come from states in which there are three simultaneous filled states. When $\nu\leq2$, at least two of the three such particles are identical. The Pauli principle prevents their close approach and therefore reduces the order in k_F of the contribution relative to what it would be for $\nu>2$.

We therefore will give two summaries of our results. The first, for general ν, includes only terms which stop at order $k_F^6\ln(k_F\beta)$ and does not include the terms $O(k_F^6)$. The second is for $\nu=2$ and will include in addition $O(k_F^6)$.

$$\Delta EM/(N\hbar^2)=(3\pi)^{-1}(\nu-1)ak_F^3+0.055661(\nu-1)k_F^4a^2$$
$$+[(\nu-1)/20\pi]a^2r_0k_F^5+[3(\nu+1)/10\pi]A_1(0)k_F^5$$
$$+(\nu-1)(0.02863\nu-0.04812)k_F^5a^3+(8/27\pi^3)$$
$$\times(4\pi-3\sqrt{3})(\nu-1)(\nu-2)k_F^6a^4\ln(k_F\beta)+O(k_F^6), \quad (4.87)$$

TABLE IV. Values of the coefficients.

Diagram	Coefficient	Standard deviation
I.6	-3.39×10^{-4}	4.2×10^{-6}
IA.1	-1.81×10^{-3}	1.4×10^{-5}
IA.2	-8.41×10^{-4}	3.6×10^{-6}
IA.3	-1.67×10^{-3}	9.0×10^{-6}
II.3	8.38×10^{-4}	6.4×10^{-6}
II.4[a]	8.38×10^{-4}	6.4×10^{-6}
II.5+IIA.1	2.9×10^{-4}	2.0×10^{-5}
II.7	-9.73×10^{-4}	4.6×10^{-6}
II.8	-1.900×10^{-3}	9.0×10^{-6}
II.9	4.96×10^{-4}	4.8×10^{-6}
II.10	1.74×10^{-4}	2.8×10^{-6}
II.11[a]	-1.900×10^{-3}	9.0×10^{-6}
II.12[a]	-9.73×10^{-4}	4.6×10^{-5}
IIA.2[b]	1.01×10^{-3}	4.7×10^{-5}
IIA.3	-2.29×10^{-4}	2.3×10^{-6}
IIA.4[a,b]	1.01×10^{-3}	4.7×10^{-5}
IIA.5	1.756×10^{-3}	6.2×10^{-6}
IIA.6	1.674×10^{-3}	8.7×10^{-6}
III.2	-1.589×10^{-3}	1.1×10^{-5}
III.9+10	2.404×10^{-3}	1.3×10^{-5}
Total	-1.73×10^{-3}	7.0×10^{-5}

[a] Identical with a previous diagram but must be included in the total.
[b] The error noted after Eq. (4.28) persisted in Baker (1965a), and we include what we believe to be a reliable estimate of these coefficients, based on the great stability of the ratio of the results of Baker *et al.* (1963) to those of Table III.

TABLE V. Diagram class factors.

Diagram class	Factor
I	$\nu-1$
IA	$\frac{1}{2}(\nu-1)(\nu^2-3\nu+4)$
II	$-(\nu-1)(\nu-3)$
IIA	$(\nu-1)(3\nu-5)$
III	$(\nu-1)^2$

where the expansion for the energy carried only this far is completely expressible in terms of the two-body scattering phase shifts. For $\nu=2$, we obtain

$$\Delta EM/(N\hbar^2)=(3\pi)^{-1}ak_F^3+0.055661k_F^4a^2+(20\pi)^{-1}a^2r_0k_F^5+(9/10\pi)A_1(0)k_F^5+0.00914k_F^5a^3+0.045899a^3r_0k_F^6+0.015680aA_0''(0)k_F^6-0.02216k_F^6a^4+O(k_F^7), \quad (4.88)$$

where a is the scattering length, r_0 the effective range, $A_1(0)$ is determined by the $l=1$, zero energy phase shift by (4.63), and $A_0''(0)$ is determined by (4.45). The quantity $A_0''(0)$ is not uniquely determined by the two-body phase shifts so far as we can tell.

E. The Soft, Repulsive Square-Well Potential

As an illustration of the calculation of the Fermi momentum expansion, we choose a soft, repulsive, square-well potential because most of the calculation can be done analytically, and because there are data available, (Sec. IV.C), with which we can compare our present results.

The first step is to solve for the $l=0$ wave function from (4.39), $p=0$. It is, for this case,

$$\psi_0(r)=\frac{\sinh\left[(MVr^2/\hbar^2)^{1/2}\right]}{(MVr^2/\hbar^2)^{1/2}\cosh\left[(MVc^2/\hbar)^{1/2}\right]}, \quad r\leq c,$$
$$=(1-a/r), \quad r>c, \quad (4.89)$$

where M is the mass, V the potential strength, c the width of the potential, and $\hbar$ is Planck's constant. The scattering length is, by (4.41), [or (4.89)],

$$a=c[1-\tanh(\rho)/\rho], \quad (4.90)$$

where

$$\rho=(MVc^2/\hbar^2)^{1/2}. \quad (4.91)$$

Next, using the asymptotic form (4.44) to compute $A_1(0)$, and (4.45) to compute $A_0''(0)$, we compute

$$\tfrac{1}{2}a^2r_0=\tfrac{1}{3}c^3\{1+\tfrac{3}{2}(1+\tanh^2\rho)/\rho^2-[(3/\rho)+(3/2\rho^3)]\tanh\rho\}, \quad (4.92)$$

$$A''(0)=\tfrac{1}{3}c^3\{[(3/\rho)+(6/\rho^3)]\tanh(\rho)-1-6/\rho^2\}, \quad (4.93)$$

$$A_1(0)=\tfrac{1}{3}c^3[1+3(1-\rho\coth\rho)/\rho^2]. \quad (4.94)$$

As the available data is for the special case $\nu=2$, we shall not need to calculate the other potential-dependent parameter b_3 of (4.80). The procedures necessary to calculate it are detailed in Baker (1965a), although that b_3 is different from the one in (4.80).

One can compute, as described in Sec. IV.A, the ladder energy by the solution of an integral equation. This calculation was done by Baker *et al.* (1963) although they did not publish the complete table. We will use their data for comparison. We can then compare this solution with the results of our expansion. Specializing (4.60) to $\nu=2$, we have

$$\Delta E_LM/(N\hbar^2)=(a/3\pi)k_F^3+(0.055661a^2)k_F^4+[(20\pi)^{-1}a^2r_0+(9/10\pi)A_1(0)+0.032031a^3]k_F^5+[0.013373a^3r_0+0.038196aA''(0)+0.019156a^4]k_F^6+\cdots \quad (4.95)$$

We give a short table (Table VI), based on Eqs. (4.90)–(4.95) of the ladder potential energy k_F expansion coefficients.

If we compute the ladder energy from a power series of four terms, the results are in excellent agreement with results calculated by the methods described in Sec. A. For the hard-core potential (actually $V=10^5$ for numerical reasons here) the error increases to about 8% at $k_Fc=1.5$, and decreases rapidly for smaller k_Fc. For weaker potentials, the range in k_Fc increases. For $V=1.0$, the error is about 4½% at $k_Fc=1.5$, and 11% at $k_Fc=2.0$. For $V=0.125$, the error is only 7% at $k_Fc=2.0$, and again decreases rapidly for smaller k_Fc.

We can conclude from these results that, in spite of the probable asymptotic nature of the k_F expansion, Eq. (4.95) forms a good summary of the ladder energy for low to moderate densities. If the ladder approximation energy in this density range is desired, it can be calculated by (4.95) with great resulting economy in effort compared to standard methods.

If we now form the difference between the complete energy and the ladder approximation as given by (4.88) and (4.95), we may compare it, for weak to moderate potentials, with the results found in Baker *et al.* (1963) and partially quoted in Sec. IV.C. When this comparison is made, the same general-error pattern emerges when due regard is taken for the fact that for weak potentials the difference is quite small. For very strong potentials tending towards the hard-core limit we have nothing with which to compare our results. However,

TABLE VI. Ladder-approximation coefficients.

V	A_1	A_2	A_3	A_4
0.125	4.2106×10^{-3}	8.7655×10^{-5}	5.6100×10^{-4}	-1.9594×10^{-5}
1.0	2.5296×10^{-2}	3.1636×10^{-3}	5.6428×10^{-3}	-5.0167×10^{-4}
5.0	5.9724×10^{-2}	1.7636×10^{-2}	2.8953×10^{-2}	3.6752×10^{-5}
∞	1.0610×10^{-1}	5.5661×10^{-2}	1.3813×10^{-1}	1.5339×10^{-2}

as long as the corrections calculated to the ladder approximation are small, we expect the results to be accurate.

V. THE INCLUSION OF ATTRACTIVE FORCES

The presence of attractive forces in the many-fermion problem is appreciably more difficult then the purely repulsive force problem dealt with in the previous section for several reasons. First of all, we will show that the presence of "Emery (1959) singularities" makes the K-matrix rearrangement invalid in the presences of any attractive force (of longer range than the repulsive forces) whatsoever. We do not believe that these are real singularities in the energy, as ordinary macroscopic sized systems do not appear to be a close enough approximation to an infinite system to possess them. Rather, they appear to represent an unfortunate choice of a method of summation of a series which is known to be divergent. We introduce an alternate procedure (R matrix) which is numerically very close to the Brueckner K-matrix method, but free from the "Emery singularities." Further, the location, or even the existence of singularities, which may occur at various points in the potential strength–density plane, must receive careful attention. The location of such singularities is of crucial importance to any program of series summation, as it is well known that the nearest singularity limits the radius of convergence of a Taylor series. No program which has as its goal the calculation of the ground-state energy of a many-fermion system can hope to be successful until it has taken account of at least the closest such singularities. In particular, it is widely recognized that in many ways nuclear matter, for example, is very much like a liquid drop and that the ground-state energy-vs-density curve should have a flat portion for low density corresponding to a condensed nucleus which does not fill the whole volume. The saturation minima obtained by approximate schemes have been represented as analytic continuations of the high-density portion of the curve. *However, the logical consequences of the liquid aspects of a many-fermion ground state must be taken into account.* From the theory of liquids and gases we expect, and indeed find, that there will be a potential strength for which the densities of the liquid and gaseous phases of the many-fermion system, interacting through an attractive potential with a strong repulsive core, will become equal, and a phase separation will cease to be. At this point, called the critical point, the theory of liquids and gases (and of cooperative phenomena in general) tells us there is *an analytic singularity.* This situation is in sharp contrast to the situation for a purely repulsive potential, where a low-density expansion proved in the previous section to be satisfactory because of the absence of a liquid–gas critical-point singularity. The presence of the critical singularity renders inadequate (as in classical statistical mechanics) approximation procedures based on the assumption of low density, since the ground state lies on the liquid side of the coexistence curve. A low-density expansion is blocked off from the liquid side of the coexistence curve by having to pass through the two-phase region, where the curves are flat. On the other hand, if one tries an expansion in terms of the number of interacting particles, which is accurate both for low density and weak interaction, one may again have trouble as the critical-point singularity lies directly between the origin in the density–potential strength plane and the liquid side of the coexistence curve. We propose a resummed potential strength expansion at fixed density which will avoid the critical point singularity.

A. The R-Matrix Rearrangements

We will now examine the solutions of the K-matrix equations (Sec. IV.A) for singularities in the presence of attractive forces outside a repulsive core. We have no need to consider purely attractive forces because it is well known (Blatt and Weiskopf, 1952) that, except when the forces are artificially limited, for example to $l=0$ only, a pure attraction causes the system to collapse to a volume of the order of the range of the force, irrespective of the number of particles.

In order to locate the values of the parameters which correspond to the nearest singularity, we start with the differential form of the K-matrix equation (Sec. IV.D) from which we have eliminated the center of mass coordinates. It is

$$[H_r+\lambda V]\omega=k^2\omega, \tag{5.1}$$

with H_r the relative coordinate kinetic energy, and V the potential energy when the wave function ω must be expanded in terms of

$$\exp(i\mathbf{k}\cdot\mathbf{r}), \qquad |\tfrac{1}{2}\mathbf{p}+\mathbf{k}|>k_F, \qquad |\tfrac{1}{2}\mathbf{p}-\mathbf{k}|>k_F. \tag{5.2}$$

The p and k are given in terms of the two hole momenta m and n as

$$\mathbf{k}=\tfrac{1}{2}(\mathbf{m}-\mathbf{n}), \qquad \mathbf{p}=\mathbf{m}+\mathbf{n}. \tag{5.3}$$

The condition for a singularity is the existence of a bound state solution to (5.1), subject to (5.2). Inspection reveals that the least attraction will be needed when

$$|\mathbf{m}| = |\mathbf{n}| = k_F. \tag{5.4}$$

Hence the usual K-matrix equation (in terms of a coordinate-space wave function) becomes

$$u_{kl}(r) = j_l(kr) - \frac{2}{\pi}\int_0^\infty G_{kl}(r,r')\,V(r')\,u_{kl}(r')\,(r')^2\,dr', \tag{5.5}$$

where, for condition (5.4),

$$G_{kl}(r,r') = \int_k^{k_F+(k_F^2-k^2)^{1/2}} \frac{k''\,dk''}{2(k_F^2-k^2)^{1/2}}[j_l(k''r)j_l(k''r')] + \int_{k_F+(k_F^2-k^2)^{1/2}}^\infty \frac{k''^2\,dk''}{k''^2-k^2}[j_l(k''r)j_l(k''r')]. \tag{5.6}$$

The limit as $k\to k_F$ requires special attention. In fact, it is on this account that we find it necessary to reorganize the summation of the energy series. There occur Emery singularities. Emery (1959, 1960) has shown that a singularity occurs when

$$\langle k_F | v | \psi\rangle = 0, \tag{5.7}$$

where ψ is the solution of an integral equation with $G_{kl}(r,r')$ replaced by [Eq. (42) of Emery, 1959]

$$\mathbf{F}=\mathbf{G}+\frac{\langle k_F|v\mathbf{G}v|k_F\rangle}{|\langle k_F|v|k_F\rangle|^2}|k_F\rangle\langle k_F| - \frac{\mathbf{G}v|k_F\rangle\langle k_F|}{\langle k_F|v|k_F\rangle} - \frac{|k_F\rangle\langle k_F|v\mathbf{G}}{\langle k_F|v|k_F\rangle},$$
$$|\psi\rangle = |k_F\rangle - \mathbf{F}v|\psi\rangle, \tag{5.8}$$

where

$$\langle r|\mathbf{G}|r'\rangle = \frac{2}{\pi}\int_{k_F}^\infty dk\,\frac{k^2 j_l(kr)j_l(kr') - k_F^2 j_l(k_Fr)j_l(k_Fr')}{k^2-k_F^2}, \tag{5.9}$$

and $|k_F\rangle = j_l(k_Fr)$. In the low-density limit, (5.7) corresponds to (Emery, 1960)

$$\tan\delta_l(k_F) = 0, \tag{5.10}$$

where δ_l is the phase shift of the corresponding Schrödinger equation. If we use a potential

$$\begin{aligned} v &= +\infty, && r<c,\\ &= -W, && c<r<d,\\ &= 0, && d<r, \end{aligned} \tag{5.11}$$

then it is easy to compute asymptotically for l large that

$$\tan\delta_l(k) \propto -[d^2Wm/((2l+3)\hbar^2)] + (c/d)^{2l+1}[2l+1+\tfrac{1}{2}(d^2Wm/\hbar^2)]. \tag{5.12}$$

(We use the sign convention on phase shifts that a simple repulsive core produces a positive phase shift.) For large l, the first term dominates as $c<d$, forcing $\tan\delta_l(k)$ negative no matter how weak W may be. Thus, at low density, the ladder series has an Emery singularity for l large enough with any attractive force at all. Baker and Kahane (1969) have followed these singularities numerically to higher density, and while they move to stronger potentials with increasing density, as we expect, there is always another for high enough l so that the entire attractive potential region of the k_F potential strength plane is filled with Emery singularities of the ladder series.

However, these results do not tell the whole story. If we examine the rate of approach of the potential $V_s(k)$ for which we have a singularity to $V_s(k_F)$, we find that

$$V_s(k)\sim V_s(k_F) - \omega/[\log(1-k/k_F)]. \tag{5.13}$$

As l increases, so does ω. The region in which $V_s(k)$ is lower than $V_s(0)$ is very tiny.

For example, from the relation between k_F and the volume per particle, we can compute that the average level spacing is

$$dN/dk_F = 3N/k_F, \tag{5.14}$$

and hence we expect, for a macroscopic sample, that the smallest that the argument of the log in (5.13) can be is about 10^{-24}. We have computed the singularity curve of the K matrix for a potential with a hard core and attractive square well [see Eq. (5.38) below] for $b=4a$. In that case for $l=0$, $k_F=1.0$, $V_s(0)\sim 4.3$, there is a maximum near $k/k_F=0.7$ of $V_s(0.7)\sim 10.2$, and $V_s(1)=3.2$. However, for a macroscopic sized system, we find $V_s(1-10^{-24})\sim 4.0$, *a long way* from the limit as $k\to k_F$! As l increases, the strength of potential needed to cause a singularity is generally more attractive, except for $k=k_F$, where, as we saw, it is less so. The region around $k=k_F$, where $V_s(k)$ is less than $V_s(0)$, decreases in size very rapidly. It is hard to ascribe much relevance in the physical world to a phenomenon which seems to require a much vaster than normal macroscopic sized system for its existence.

Brueckner and Gammel (1958a) made the simple approximation of adding a small excitation energy to the denominator of the Green's function [our Eq. (5.6), for example] as a numerical expedient to prevent an infinity in their numerical work. We have checked that this procedure has the effect of moving $V_s(k_F)$ well above (in most of the type of cases we are considering) $V_s(0)$.

We know very well that for certain potential shapes (potential of one sign) the energy is indeed singular

in the presence of any attraction at all—the well known nuclear collapse problem. This consideration suggests to us that the ladder series may be giving a "shape-independent" approximate description of the nuclear collapse phenomenon. For the potentials we are considering, we know that it is the "excluded-volume" effect of the hard cores in the many-body problem which prevents this collapse. (In any event, it does not seem relevant to the size of systems we are attempting to treat.) We therefore conclude that a different summation procedure than those based on the K matrix is required to make a valid singularity-free calculation of the many-body energy.

Baker and Kahane (1969) rearranged the energy series in powers, not of Brueckner's K matrix, but in powers of a closely related matrix which they called R. The reason that the ordinary potential strength expansion was rearranged into powers of K was to enable one to treat potentials with an infinite repulsive core. This feature must clearly be retained. The usual K matrix (in ladder approximation) is given by (4.6–4.18), except (4.13) is replaced by $\Delta(k)=E(k)=\frac{1}{2}k^2$. The low-density limit of the many-body energy is, as we have seen in the previous chapter

$$\Delta E=\frac{3}{(2\pi k_F)^3}\iint_{|\frac{1}{2}\mathbf{p}+\mathbf{k}|\leq k_F,\ |\frac{1}{2}\mathbf{p}-\mathbf{k}|\leq k_F} d\mathbf{k}\,d\mathbf{p} \times\sum_l (2l+1)\begin{pmatrix}\nu-1 & l & \text{even}\\ \nu+1 & l & \text{odd}\end{pmatrix}K_l(k), \quad (5.15)$$

and it is proportional to the scattering length

$$a=\tan\delta_0(0)=\int_0^\infty V(r)u_{00}(r)r^2\,dr. \quad (5.16)$$

This result corresponds to the standing wave normalization for the wave function (Brueckner, 1959; and Wu and Ohmura, 1962).

If we introduce the Green's function

$$\mathcal{G}_{kl}(r,r')=\int_0^\infty dk'' \times\frac{[k''^2 j_l(k''r)j_l(k''r')-k^2 j_l(kr)j_l(kr')]}{k''^2-k^2}, \quad (5.17)$$

then there is no singularity in the integrand at $k''=k$. We may, following usual procedures, (Wu and Ohmura, 1962) evaluate (5.17). It is

$$\mathcal{G}_{kl}(r,r')=-kj_l(kr_<)n_l(kr_>), \quad (5.18)$$

where $r_<$ and $r_>$ are the lesser and greater of r and r', respectively. This is exactly the standing wave (Wu and Ohmura, 1962) Green's function. The form (5.17) is well defined for all k's, and is also suitable for inclusion of the Pauli exclusion principle. Baker and Kahane (1969) therefore introduced

$$\tilde{G}_{kl}(r,r')=\int_0^\infty dk''\frac{[k''^2 j_l(k''r)j_l(k''r')-k^2 j_l(kr)j_l(kr')]}{k''^2-k^2} \times F(p,k'')+\tilde{a}(p,k)j_l(kr)j_l(kr'). \quad (5.19)$$

Form (5.19) of $\tilde{G}$ can now be well defined for all k and p, not just those in the Fermi sea as was the case for (4.12), by extending the definition of $F(p,k'')$ to be

$$\begin{aligned} F(p,k'')&=1, && \tfrac{1}{2}p-k_F>k'',\\ &=0, && (k''^2+\tfrac{1}{4}p^2)^{1/2}<k_F,\\ &=1, && k''-\tfrac{1}{2}p\geq k_F,\\ &=(k''^2+\tfrac{1}{4}p^2-k_F^2)/k''p, && \text{otherwise.} \end{aligned} \quad (5.20)$$

The second term $\tilde{a}(p,k)$ is arbitrary provided it vanishes when k_F does. They choose $\tilde{a}=k^2/k_F (k<k_F)$ as a simple function which minimizes the difference between $\tilde{G}$ and G.

The next step is to expand the solution of (4.14) in terms of the solution of

$$\tilde{u}_{kl}(r)=j_l(kr)-\frac{2}{\pi}\int_0^\infty \tilde{G}_{kl}(r,r')V(r')\tilde{u}_{kl}(r')r'^2\,dr'. \quad (5.21)$$

To do this, we observe that (4.14) can be rewritten as

$$u_{kl}(r)=Aj_l(kr)-\frac{2}{\pi}\int_0^\infty \tilde{G}_{kl}(r,r')V(r')u_{kl}(r')r'^2\,dr', \quad (5.22)$$

where

$$A=1+\frac{2}{\pi}\left(\int_0^\infty \frac{k^2\,dk''}{k''^2-k^2}F(p,k'')-\tilde{a}(p,k)\right) \times\left(\int_0^\infty j_l(kr')V(r')u_{kl}(r')r'^2\,dr'\right). \quad (5.23)$$

Thus, solving for A, we get

$$A=\left(1+\pi^{-1}(\tau_1-2\tilde{a})\int_0^\infty j_l(kr')V(r')\tilde{u}_{kl}(r')r'^2\,dr'\right)^{-1}, \quad (5.24)$$

where we use the notation (4.66a) of the previous chapter for τ_1. Hence, we have

$$u_{kl}(r)=A\tilde{u}_{kl}(r), \quad (5.25)$$

and

$$K_l(k)=R_l(k)/[1+(\tfrac{1}{2}\tau_1-\tilde{a})R_l(k)], \quad (5.26)$$

where we define the diagonal elements of the R matrix as

$$R_l(k)=\frac{2}{\pi}\int_0^\infty j_l(kr)V(r)\tilde{u}_{kl}(r)r^2\,dr. \quad (5.27)$$

The Emery singularity arises in (5.26) if $R_l<0$, as τ_1 can be arbitrarily large. From (5.26), the expansion of

$K_l(k)$ in powers of the R matrix is quite straightforward:

$$K_l(k)=R_l(k)-(\tfrac{1}{2}\tau_1-\tilde{a})R_l^2(k)+(\tfrac{1}{2}\tau_1-\tilde{a})^2R_l^3(k)+\cdots. \tag{5.28}$$

If we substitute (5.28) into (5.15), then as τ_1 diverges only logarithmically, the integral of every power is convergent; hence the expansion of ΔE (ladder) is well defined in powers of the R matrix, provided R itself is defined. The coefficients of the expansion, of course, are divergent like $(n!)$. This divergence is the same as that for K in powers of V. This similarity in divergence rates follows from the fact that, as $\tilde{G}(r,r')V(r')$ is bounded for $V(r)$ bounded, R must have a finite radius of convergence when expanded in powers of the potential strength. In the low-density limit we see that R has the standing wave singularity of $\tan\delta_l(k)$. These are well known to correspond to the occurrence of a two-body bound state.

In addition to resumming the series in terms of the R matrix, we must also prescribe how to resum the complete perturbation series in terms of R. This procedure is conceptually simplest (at least from the point of view of systematically giving all the terms) by expanding every K matrix in the K-matrix rearrangement in powers of R. Of course, as K is meaningless for the type of potentials considered, to establish the validity of the R-matrix rearrangement we must go directly from the V perturbation series to the R-matrix rearrangement.

Let us now consider the K matrices which result from the ladder-type insertions to convert all possible types of V vertices (see Fig. 15) into K vertices. They can be divided into two relevant categories. The first category comprises those in which the higher-order ladder insertions either begin or end with an E or F vertex (number of excited states changes by ±2). In this situation, we can apply the proof of the Hugenholtz Factorization Theorem (Sec. II.C) to show that the sum over all relative vertex orders between the different independent ends (as in Fig. 15) gives an effective denominator for the K matrix which has no contribution from the excitation of the Fermi sea. Here we only require those K matrices which either begin or end "on mass shell." They can be obtained as

$$\langle k'\mid K_l\mid k\rangle=\langle k'\mid R_l\mid k\rangle/[1+(\tfrac{1}{2}\tau_1-\tilde{a})R_l(k)], \tag{5.29}$$

where we define

$$\langle k'\mid R_l\mid k\rangle=\frac{2}{\pi}\int_0^\infty j_l(k'r)V(r)\tilde{u}_{kl}(r)r^2\,dr, \tag{5.30}$$

and the expansion of (5.29) is analogous to that of (5.28). The other category comprises all the others. For these the denominators include an excitation of the Fermi sea. The integral equation for the K-matrix wave function is now (4.14), but with

$$G_{kql}(r,r')=\int_0^\infty k''^2\,dk''\frac{j_l(k''r)j_l(k''r')}{k''^2-k^2+q^2}F(p,k'',k,q) \tag{5.31}$$

instead of (4.12). The Pauli principle function is such that the denominator is nonnegative definite where $F\neq0$; however, k^2-q^2 may be positive or negative. To handle these cases we introduce

---

$$\tilde{G}_{kql}(r,r')=\int_0^\infty dk''\,\frac{k''^2j_l(k''r)j_l(k''r')}{k''^2-k^2+q^2}F(p,k'',k,q)\quad\text{if}\quad q^2\geq k^2,$$

$$=\int_0^\infty dk''\,\frac{\{k''^2j_l(k''r)j_l(k''r')-(k^2-q^2)j_l[(k^2-q^2)^{1/2}r]\,j_l[(k^2-q^2)^{1/2}r']\}}{k''^2-k^2+q^2}F(p,k'',k,q)$$
$$+\tilde{a}(p,k,q)j_l[(k^2-q^2)^{1/2}r]\,j_l[(k^2-q^2)^{1/2}r']\quad\text{if}\quad k^2>q^2. \tag{5.32}$$

Then, if we define

$$\langle k'\mid R_1\mid k\rangle=\int_0^\infty j_l(k'r)V(r)\xi_{k,q,l}(r)r^2\,dr,$$

$$\langle k'\mid R_2\mid(k^2-q^2)^{1/2}\rangle=\int_0^\infty j_l(k'r)V(r)\eta_{k,q,l}(r)r^2\,dr, \tag{5.33}$$

where

$$\xi_{kql}(r)=j_l(kr)-\int_0^\infty\tilde{G}_{kql}(r,r')V(r')\xi_{kql}(r')r'^2\,dr',$$

$$\eta_{kql}(r)=j_l[(k^2-q^2)^{1/2}r]-\int_0^\infty\tilde{G}_{kql}(r,r')V(r')\eta_{kql}(r')r'^2\,dr', \tag{5.34}$$

for the wavefunction corresponding to (5.31) we can write

$$u_{kql}(r)=\xi_{kql}(r)-\frac{\eta_{kql}(r)\langle(k^2-q^2)^{1/2}\mid R_1\mid k\rangle L(p,k,q)}{1+L(p,k,q)\langle(k^2-q^2)^{1/2}\mid R_2\mid(k^2-q^2)^{1/2}\rangle}, \tag{5.35}$$

where

$$\begin{aligned} L(p,k,q)&=\int_0^\infty \frac{(k^2-q^2)}{(k''^2-k^2+q^2)}F(p,k'',k,q)\,dk''-\tilde{a}, && k^2>q^2\\ &=0, && k^2\leq q^2. \end{aligned} \tag{5.36}$$

Hence we find

$$\langle k'\mid K_q\mid k\rangle=\langle k'\mid R_1\mid k\rangle-\frac{\langle k'\mid R_2\mid(k^2-q^2)^{1/2}\rangle\langle(k^2-q^2)^{1/2}\mid R_1\mid k\rangle L(p,k,q)}{1+L(p,k,q)\langle(k^2-q^2)^{1/2}\mid R_2\mid(k^2-q^2)^{1/2}\rangle} \tag{5.37}$$

which leads directly to an expansion of K_q in powers of R_2. The Emery singularities are here seen to be associated with $\langle(k^2-q^2)^{1/2}\mid R_2\mid(k^2-q^2)^{1/2}\rangle=0$, which are analogous to those for an unexcited Fermi sea.

Baker and Kahane (1969) have investigated numerically the singularity structure of the R matrix for potentials of the form

$$\begin{aligned} V(r)&=10^5, && 0\leq r<a,\\ &=\tfrac{1}{2}[V(a^+)+V(a^-)], && r=a,\\ &=-\pi^2a^2/[2(b-a)]^2, && a<r\leq b, \end{aligned} \tag{5.38}$$

for $b=4a$, and $b=2a$. The structure that they find is complex; however, the singularities lie at considerably more attractive potentials than those required to produce saturation in the R-matrix approximation to the many-fermion energy. One is thus able to verify at least for sufficiently weak potentials of this type that the R-matrix resummation procedure satisfies the conditions we discussed in Sec. III.E, and so is a valid representation of the answer to the physical problem.

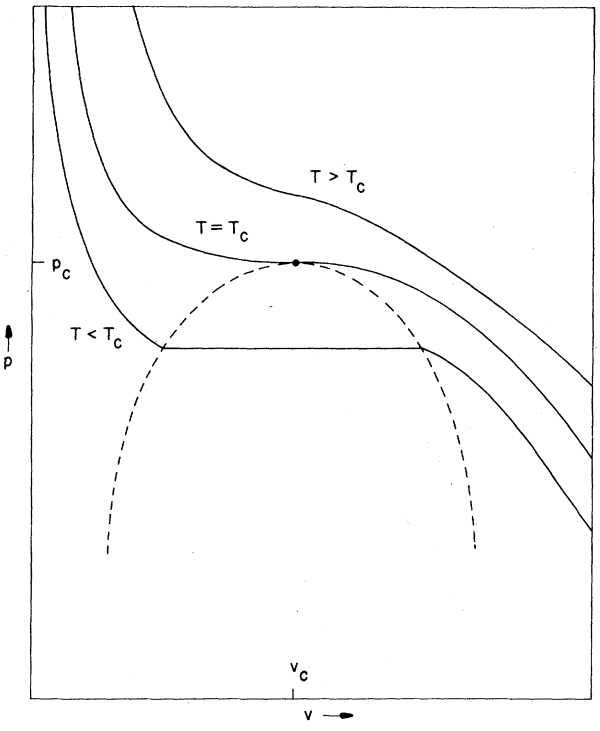

FIG. 36. Sketch of a typical pressure–volume diagram for a liquid–vapor system. The dashed line is the coexistence curve.

B. The Critical Point Singularity

In the previous section we have corrected the mathematical formalism for probably a more technical than physical singularity. In this section, we will be principally concerned with a physical effect. We will still consider forces with a strongly repulsive core surrounded by a pure attraction of finite depth and range. Although we are concerned in this article exclusively with the ground-state energy of a many-fermion system, it is sometimes helpful to understanding to consider a problem in the context of a larger one. This we shall do here by introducing a temperature. The ground state will be recovered in the limit as the temperature goes to zero, with the other relevant variables fixed.

Interacting systems with interparticle potentials of the general type we are discussing are quite common in nature and have been much studied. One of the most striking properties exhibited by an extremely wide variety of matter in bulk is that of change of phase—the boiling of water to form steam, for example. This phenomenon occurs at normal atmospheric pressure. As we increase the pressure, the temperature and density of the steam increases; finally, at a *critical point* (p_c, T_c, ρ_c) the density of water and steam become the same, and for a higher temperature (or pressure) there is no longer a change of phase.[2]

As one approaches the critical point from (for instance) higher temperature, various manifestations of the impending phase separation appear. A typical p–V diagram is shown in Fig. 36. The dashed line is the co-

[2] For a good recent review of the equilibrium theory of critical phenomena, clearly presented, the reader is referred to Fisher (1967).

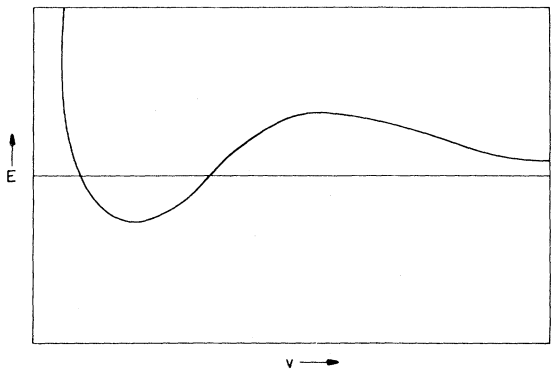

FIG. 37. Sketch of energy vs volume for the ground state of a many-fermion system with attractive forces present.

existence curve. For example, the density fluctuations become very large when a liquid and its vapor are in equilibrium with each other below the critical temperature at the same pressure. (They have different densities. In the absence of gravity, one expects to find various droplets of liquid dispersed throughout the volume.) This phenomenon is experimentally manifest as critical opalescence, i.e., the substance becomes cloudy.

Another type of system which displays an exactly analogous behavior is a ferromagnetic crystal near its Curie or critical point where spontaneous magnetization suddenly appears. Here the zero-field magnetic susceptibility becomes infinite at the critical point. One salient feature observed of critical points is that the singular physical behavior is represented by an analytic singularity in thermodynamic properties of these systems. A consequence is that a limit is set on the radius of convergence of ordinary perturbation theory by the existence of such a singularity. Any serious attempt to calculate the properties of many-fermion systems must consider the possibility of such a singularity and take account of it.

The argument that systems such as nuclear matter possess a two-phase region is quite straightforward. We start from the assumption that the many-fermion system is spatially homogeneous and that the energy is an analytic function of the density; then we show that this assumption leads to a contradiction. Consider a potential with a hard core plus an attractive part of strength, $\lambda=1-\epsilon$, $\epsilon>0$, where $\lambda=1$ is the strength required to produce a two-body bound state of zero energy. We will suppose that the pair-interaction volume is much larger than the hard-core volume. [In the nuclear case, the range of interaction is at least $2\frac{1}{2}$ times the hard-core diameter (Gammel and Thaler, 1957) or a ratio of more than 15:1 in volume.]

We can now imagine a configuration in which there are up to six interacting pairs per particle (face-centered cubic arrangement) without an appreciable increase in the kinetic energy per particle. Consequently, we expect to be able to obtain a negative many-body ground-state energy at a suitable density because of the relative many-body enhancement of potential energy over kinetic energy.[3] (This effect is evident in the nuclear case from an examination of the experimental binding energy per particle among the light elements [see, for example, Blatt and Weiskopf, 1952)]. However, as we showed in Sec. IV.D, for very low density, we have

$$(Em/N\hbar^2)=\tfrac{3}{5}k_F^2+(3\pi)^{-1}ak_F^3+\cdots, \quad (5.39)$$

where k_F is the Fermi momentum, and is proportional to the cube root of the density. Hence the energy is positive at very low density. By choosing $\lambda=1-\epsilon$, the scattering length a, is finite; although a is infinite for $\lambda=1$, which would vitiate this argument at that potential, a is finite and analytic for all $0\leq\lambda<1$. For high densities, the energy per particle becomes indefinitely great as the available amount of attraction per particle is bounded (because of the hard cores and finite range and depth), but the repulsive kinetic energy from restricting the available volume is not. The energy curve for a spatially homogeneous system must look like Fig. 37. We shall assume that the energy curve varies continuously with temperature as T goes to zero for fixed density (see the proof by Luttinger and Ward, 1960).

We now use the following rigorous result of statistical mechanics. The Helmholtz free energy (per particle) is convex (Ruelle, 1963; Fisher, 1964)

$$\Psi[T,\tfrac{1}{2}(v_1+v_2)]\leq\tfrac{1}{2}\Psi(T,v_1)+\tfrac{1}{2}\Psi(T,v_2), \quad (5.40)$$

with continuous derivative for all (nonzero) temperatures. The Helmholtz free energy (see, for example, Epstein, 1937) is defined as

$$\Psi=E-TS, \quad (5.41)$$

where E is the internal energy (per particle), T the absolute temperature, and S the entropy (per particle). Now the entropy per particle (Hill, 1956) diverges to plus infinity like the logarithm of the volume in the limit of large volumes. We may now pick a temperature small enough so that, for all volumes in any given range between a lower limit greater than the jamming volume and less than some finite upper limit, Ψ is within any preassigned distance of E as the entropy is bounded in

[3] A more nearly rigorous proof can be given by dividing space up into equal cubes, each containing, say, three or more particles. If we then impose zero boundary conditions along the cube boundaries, we have restricted the class of wave functions allowed, and hence possibly raised the ground-state energy. If we now drop the attractive intercube interactions and thicken the walls to take account of the intercube repulsive interactions, we reduce our problem to a set of finite problems which give an upper bound to the energy of the complete problem. The application of variational techniques [see, for example, Austern and Iano (1960)], now suffice to establish a negative eigenvalue for some intermediate density.

that range. In the low-density (large-volume) limit for any $T>0$, however, Ψ tends $-\infty$ because E is bounded, and $S\to+\infty$. This argument establishes a region where Ψ is positive. Therefore, the Helmholtz free energy under these assumptions fails to be convex, which is a contradiction. We conclude that the ground state is not one spatially homogeneous phase. We may, however, construct a convex Ψ by taking the convex hull of the spatially homogeneous Ψ, i.e., by drawing the tangent line across the reentrant portions, as in Fig. 38. This tangent line is realized by a two-phase system of suitable proportions of spatially homogeneous systems at densities A and B to construct the required intermediate density.

Let us now consider our system at very high temperature. By the correspondence principle (Wigner, 1932), quantum effects become negligible and we may consider classical behavior. The attractive interaction energies, having a finite maximum, become inconsequential compared to the kinetic energies, and hence the possibility of a liquid–vapor-type phase change ceases to exist[4]: if we imagine a liquid droplet formed, the attraction would be too weak to bind a particle having even the average kinetic energy, and hence the droplet would immediately evaporate. We concluded, therefore, that, as there is a two-phase region for very low temperature and no two-phase region for very high temperature, there must be a positive least upper bound to temperatures for which two phases are possible. This temperature we call the critical temperature. Although we recognize that the boundary of the two-phase region could have a flat top (up as in Fig. 36), we will continue to treat the simpler case where the top is a single point, which seems to be the usual circumstance observed in many analogous cases.

Having established the existence of a critical temperature, we may ask how its location varies as a function of the strength of the attractive part of the potential λ. For weaker λ, there is less binding energy available and a stronger tendency for droplets to evaporate. Hence the critical temperature decreases as λ decreases. When λ is zero (hard cores only), there is no possibility of a liquid, as a droplet would have no binding energy at all.

This argument implies the convexity of E at $T=0$ (except for a possible order–disorder transition at higher density). Hence, interpolating between $\lambda=0$ and Fig. 37, there must be a greatest lower bound to λ's which have nonconvex E-vs-v curves under the spatially homogeneous constraint. Consequently, there exists a critical potential $0<\lambda_0<1$ for which the critical temperature is exactly zero. There is a corresponding critical density ρ_c (or perhaps a range of densities). The significance of this critical point (λ_c, ρ_c) in the (potential strength–density) plane for fixed temperature (zero) is, as explained above, the reasonable expectation that it must be an analytic singularity, as is every other known critical point.

[4] There may still be a solid–fluid phase change at high density on account of the hard cores, but we are not presently concerned with this. See Gaunt and Fisher (1965).

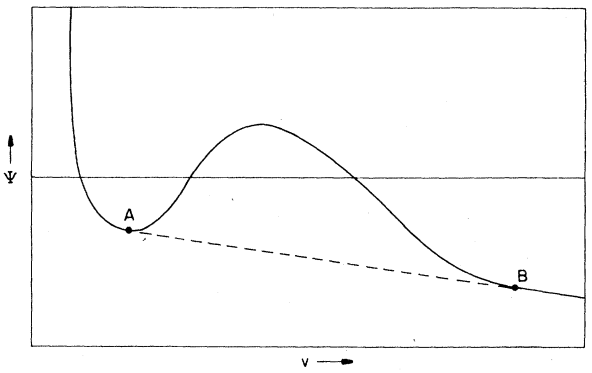

FIG. 38. Free energy vs volume for a low-temperature many-fermion system with attractive forces present. The dashed line is the convex hull or two-phase portion.

From the foregoing discussion it is plain that the ground state of such a many-fermion system is a cooperative state which can rightly be considered as a liquid.[5] Approximation procedures based solely on the assumption of a dilute gaslike system are not adequate as the density, rather than being low, is higher than critical density, which is the relevant density for the importance of higher-order cluster interactions.

C. The Coexistence Curve

By the coexistence curve, we mean here that curve in the k_F potential strength plane passing through the critical point, which forms the boundary of a stable one-phase region, i.e., the curve where the coexistence of two phases just becomes possible. In this section, we will examine whether one may expect the coexistence curve to be a locus of singularities or not. This question is important as it is precisely on the coexistence curve (liquid side) that we seek to evaluate the energy of, for example, infinite nuclear matter.

Baker and Kahane (1969) have investigated the nearest singularity in the R matrix for several potential shapes. It starts, in the limit of zero density, at the strength needed to form a two-body bound state, and as the Fermi momentum increases the strength of the interaction at the singularity generally increases. This increase is in accord with the idea that as the density increases the low-frequency states are excluded by the Pauli principle, and a stronger interaction is required to form a bound state. That such singularities should

[5] For a description of the Bohr liquid drop model of the nucleus, see, for example, Evans (1955). The successful aspects have long been recognized to be the bulk properties, surface energies, separation energies, etc., which one would expect from either a classical or quantal liquid, which are, of course, just the aspects relevant to the present discussion.

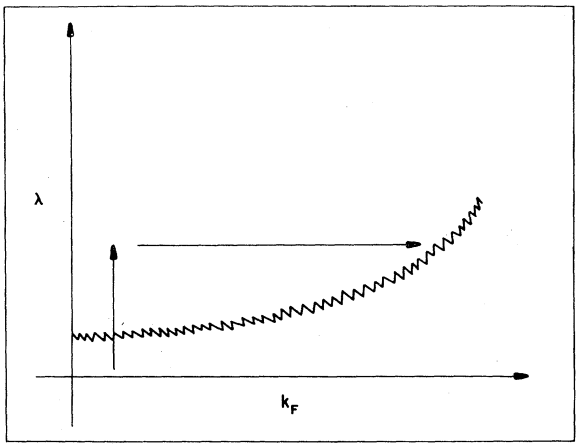

FIG. 39. Path in the $\lambda-k_F$ plane which leads to the occurrence of a spatially inhomogeneous (two-body) portion of the many-body wavefunction. The jagged line is a line of singularities (fixed l).

exist has long been recognized (Emery, 1959; Balian, 1962). The relevant question, insofar as a study of the ground-state energy of a many-fermion system is concerned, is their location (in the $k_F-\lambda$ plane) relative to the coexistence curve. If none of these singularities lie in the one-phase region, then they are, in principal, no impediment to the calculation of the ground-state energy. If, on the other hand, they intrude into the one-phase region, then they proscribe the calculation of the ground-state energy there. We have argued in the previous section that, for the type of potentials we are considering (see Sec. B), the many-body effects which enhance the potential relative to the kinetic energy contributions cause the many-body binding energy per particle to increase when the number of particles in the system does. Consequently, a weaker potential is required to cause a given binding energy per particle for a larger system than for a smaller one. Therefore we expect the two-body bound states which cause singularities in the ladder approximation to occur for stronger potentials than saturation.

We can give significance to the low-density terminology of bound states in the presence of a Fermi sea by a discussion in terms of spatial homogeneity. In the low-density case, the normalization of the wave function when two particles are close together (in a "bound" state) is proportional to $v^{-1/2}$ (v is volume), instead of $1/v$, as it would be if they were uncorrelated. This region will persist as we increase the density of the surrounding Fermi sea. The effect of the presence of the Fermi sea (Gomez *et al.*, 1958) is to prevent the occurrence of most of the low frequencies in the wave function. They (Gomez *et al.*, 1958) say that it "heals" quickly; however, the amplitude of the "healed" (undisturbed frequency) portion of the wavefunction will differ from that of the unperturbed wavefunction when there is a spatially inhomogeneous portion present, as there will be a nonzero fraction of the total normalization in the correlated portion. As the density of the Fermi sea is increased, finally one must use such high frequencies (high kinetic energies) to construct the wavefunction that it becomes energetically unfavorable as compared to the spatially homogeneous state. (See Fig. 39 for the path followed in this argument in the $\lambda-k_F$ plane.) Since the three-, four-, etc. body scattering matrices appear, as has been emphasized by Bethe (1965), as part of the energy expansion, one finds the same phenomena there as in the two-body case. An analytic singularity will occur in the n-body scattering matrix, where the spatially inhomogeneous case (normalization of the wavefunction when all particles are remote from each other decreases) becomes more favorable than the spatially homogeneous case. If we consider the limit as n becomes infinite for the n-body scattering matrix in a sea of fixed density, the location of the singularity will be the coexistence curve—as the breakdown of spatial homogeneity (one phase) is the *definition* of a liquid–vapor coexistence curve. Consequently, we conclude that the coexistence curve is a limit point of singularities of subsequences which occur in the complete energy. Fortunately, as we have discussed above, the limit, for potentials of the sort we are treating, is approached from the more strongly attractive side, and we are not barred, in principle, from computing the energy on the coexistence curve from the less strongly attractive side.

As the coexistence curve is a little bit complex we have included a sketch of it in Fig. 40. There are three distinct horizontal bands. Below the critical point ($\lambda<\lambda_C$) liquid and gas merge indistinguishably into one another. The next band has a real gas and a real liquid. It lies in the range $\lambda_C\leq\lambda\leq\lambda_B$, with λ_B the strength of potential interaction required to bind the liquid phase with zero binding. In this band, the system exerts positive pressure on the walls of the vessel (as it did in the lowest horizontal band). In the top band ($\lambda>\lambda_B$) the density of the gas phase is zero, and the liquid therefore does not fill the container in the two phase region. It is in this self-bound region that the saturation point of nuclear matter lies. The liquid coexistence curve in this band can be obtained in the usual way by looking for the minimum (approached from high density) in the energy per particle vs k_F for fixed interaction strength. In the second band, the more complex Gibbs double-tangent construction (Fig. 38) must be used to locate the coexistence curve.

Whether or not the coexistence curve is a line of singularities of the analytic function

$$\hat{E}(k_F,\lambda)=\sum_{n=0}^{\infty}\lim_{N\to\infty}{}_Ne_n\lambda^n, \tag{5.42}$$

as well as

$$E_\infty(k_F,\lambda)=\lim_{N\to\infty}\sum_{n=0}^{\infty}{}_Ne_n\lambda^n, \tag{5.43}$$

is clearly of crucial importance to any attempt to compute the energy on the coexistence curve. Katsura (1954, 1960) has examined a classical model and shown that, in spite of Yang and Lee's (1952) results on (5.43), it is doubtful whether the singularity of (5.42) coincides with the irregular point of (5.43).

That (5.42) and (5.43) are not necessarily the same can be seen from the example where $_Ne_n$ are the series expansion coefficient of the function

$$\{1+\exp[N(1-\lambda)]\}^{-1}.$$

In this case, (5.42) yields $\hat{E}(\lambda)\equiv 0$, while $E_\infty(\lambda)=U(\lambda-1)$, the unit step at $\lambda=1$. While $\hat{E}$ is analytic (and trivial) everywhere, E_∞ has a line of singularities on Re $(\lambda)=1$.

There is some numerical evidence (Baker, 1967) to indicate that for the nearest-neighbor lattice gas the coexistence curve does not contain singularities of (5.42) except for the critical point itself. Katsura (1955, 1963) and Saito (1961) have proved for the long-range, Huisimi–Temperley model that the coexistence curve is not a line of singularities of (5.42). Of course, in both the above cases (5.43) has a line of singularities on the coexistence curve.

Thus the fundamental question of whether (5.42) has a line of singularities along the coexistence curve is as yet unanswered—thereby making any calculation of the saturation properties of such a many-fermion system extremely difficult. It is reasonably clear from the arguments we have advanced that (5.43) does possess a line of singularities along the coexistence curve. There is, as we indicated above, some indirect evidence that (5.42) may not have these singularities, except at the critical point, or that if they are there they are of such a nature as to be numerically inconsequential. We will proceed on the optimistic assumption that we need take account only of the critical point itself out of this class of singularities.

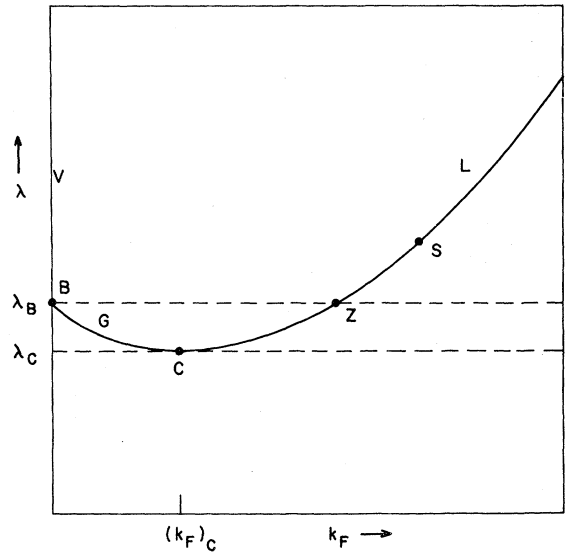

FIG. 40. The solid curve is the coexistence curve for a many-fermion system at zero temperature. It consists of three parts. Part L which runs right from point C is the liquid coexistence curve. Part G which runs from B to C is the gas coexistence curve, and part V which runs vertically up from B is the gas coexistence curve when the gas phase is a vacuum. Point C is the critical point. Point Z is where the energy per particle in the liquid phase on the coexistence curve crosses zero. Point S is a typical saturation point corresponding to a zero slope in the energy per particle vs k_F curve. The region above the coexistence curve is the two phase region and that below is the one phase region.

D. Evaluation of the R-Matrix Expansion Through Fourth Order

From the discussion in the preceding two sections, it is plain that any sequence of successive approximations to the energy of the ground state of a many-fermion system with attractive forces must take into account the critical singularity, and must be designed in such a way as to avoid its adverse effect on the convergence. One such procedure is very close to the original program of Brueckner. It is to fix the density (k_F), and then calculate an expansion in successively higher powers of the R matrix. In this way we will pass from the non-interacting system at fixed density (whose solution is known exactly), through the one-phase region, to the liquid coexistence curve where the infinite system of fermions is saturated, i.e., in equilibrium with the vacuum. This path should be one along which the energy is an analytic function of the potential strength, and so this procedure, leaving aside the problem raised in Sec. C, gives a well-defined method for determining the energy of such a system.

The actual execution of such a program requires only technique and persistence, and does not present any difficulties in principle. We will review one such calculation by Baker *et al.* (1970). If one sums out all the ladder insertions, then the series of diagrams which remain, with a $K(R)$ at each vertex is, through fourth order: B1, R3, H3, F3, I.6, IA.1, IA.2, IA.3, II.3, II.4, II.5, II.7, II.8, II.9, II.10, II.11, II.12, IIA.1, IIA.2, IIA.3, IIA.4, IIA.5, IIA.6, III.2, III.9+10, IV.1, IV.4, IV.5, IV.6, and IV.7. These are pictured in Fig. 27–34. There are two types of R matrices which occur in these diagrams. Those in which the Fermi sea is excited, and those in which it is not excited. The elimination of the excitation of the Fermi sea is a result of the Hugenholtz Factorization Theorem, as was explained in Sec. A. We now catalogue the vertex types which fall in each category. They are illustrated in Fig. 15. The vertices E, F, G, H, and I have no excitation of the Fermi sea, but in the vertices A, B, C, and D we must include the effects of such excitation. The vertex J, which is the sum of self-energy bubbles on all hole and filled-state lines at a given vertex position, is a special case. The R matrix corresponding to a bubble on a filled-state

line must be corrected for the excitation of the Fermi sea, while that corresponding to a bubble on a hole line need not be. We point out that because of the sums involved in the Hugenholtz Factorization Theorem, considerable care must be exercised in writing out the high-order perturbation terms to avoid over counting. We also mention that, although the K-matrix procedure sums out all A vertex insertions, there can nevertheless occur A vertices in the K diagram expansion, when, for example, there are three or more filled states present at the same time in a diagram. However, this effect does not occur until fifth-order in the expansion.

Through fourth order in K, we may use the following special feature to restrict the number of parameters on which the R matrix in the presence of an excited Fermi sea depends. To this order, every excitation consists of a single filled-state, hole pair which combines with a filled state at the previous or next vertex to form an unexcited fermi sea. Therefore, except for a hole momentum, over which we must integrate in any case, the excitation energy is directly related, by momentum conservation, to either the initial or final relative momentum at that vertex. Hence, by averaging over the allowed values of the hole momentum in a manner similar to (4.11), we may again reduce the R matrix to a dependence only on k, k', and l. If one wishes to proceed to higher order than four, one must then know R as a general function of the excitation energy. One further special simplification is available on this account. One finds (we will see this result below) that the averaged excitation energy always exceeds the energy of the incident state, so that R and K are equal in this case. The calculational formulae are now (5.32), case $q^2 \geq k^2$. The definition of the average value of p changes, because we now have a vertex with one incident filled-state line instead of an unexcited Fermi sea as in (4.11). It is

$$\tfrac{1}{4}\bar{p}^2 = \frac{k_F{}^4 + k^4/15^2}{k_F{}^2 - \frac{1}{3}k^2}, \qquad k < k_F$$
$$= k^2 + \tfrac{3}{5}k_F{}^2. \qquad k \geq k_F \qquad (5.44)$$

As $\bar{p} > k_F$ always, it follows from (5.20) that F is never zero. The value of $(q^2 - k^2)$ is, basically, $(2k)^2 - (k)^2 +$ mean square average of a hole momentum. The average is restricted by the given value of k. This quantity works out to be

$$q^2(k) - k^2 = 3k^2 + \frac{k_F{}^4 - \frac{4}{3}k_F{}^3 k + k_F{}^2 k^2 - 4k^4/15}{k_F{}^2 - \frac{1}{3}k^2}, \qquad k < k_F$$
$$= 3k^2 + \tfrac{3}{5}k_F{}^2. \qquad k \geq k_F{}^2 \qquad (5.45)$$

The wave function and R matrix follow in the same manner as described in Sec. A.

Baker *et al.* (1970) have used these formulas to produce the desired matrix elements numerically by means of a high speed digital computer. For the details of this aspect one should consult their paper. They selected the following potential for consideration in their paper. First, for states of even relative angular momentum, we have

$$V_T(r) = V_1, \qquad V_S(r) = V_2 \qquad 0 < r < c,$$
$$V_T(r) = V_3, \qquad V_S(r) = V_4 \qquad c < r < d$$
$$V_T(r) = V_S(r) = 0 \qquad d < r \qquad (5.46)$$

where V_S is the singlet potential and V_T is the triplet potential. For states of odd relative angular momentum, they chose

$$V_T(r) = V_5, \qquad V_S(r) = V_6 \qquad 0 < r < c$$
$$V_T(r) = V_S(r) = 0 \qquad c < r. \qquad (5.47)$$

The parameters in this potential were chosen as follows:

$$c = 0.4f, \qquad d = 29c/7$$
$$V_1 = V_2 = V_5 = V_6 = 10^5 \hbar^2/Mc^2$$
$$V_3 = 1.25(7\pi/44)^2 \hbar^2/Mc^2, \qquad V_4 = 0.96(7\pi/44)^2 \hbar^2/Mc^2. \qquad (5.48)$$

They have fitted the two-body data $a_T = 5.39f$, $r_{0T} = 1.71f$, and $a_S = -23.7f$ to determine these parameters. In addition, they computed $E_T = -2.20$ MeV, and $r_{0S} = 2.14f$ instead $2.6f$. Here f is fermis, a is scattering length, r_0 is effective range, and E_T is the triplet ground-state energy. The singlet phase shift, δ_0 equals 0 for k around 150 MeV instead of 200 MeV as it should.

In the evaluation of the contributions to the R-matrix expansions one must sum over the various spin and isotopic spin states, in addition to the integrals over the intermediate momenta. Through fourth order in R, up to four independent spins and isospins can occur, a total of 256 different states for this type of potential. Although this sum needs to be performed only once for each diagram, the formulas that result are rather awkward and may indeed contain as many as 256 terms. Baker *et al.* (1970) give a group theory procedure, valid through fourth order, which reduces these sums to the evaluation of at worst the trace of 3×3 matrices instead of 256×256.

As it is necessary to evaluate many multidimensional integrals [Eq. (2.41)] in which the R-matrix elements appear in the integrand, Baker *et al.* (1970) used an empirical representation to make their calculations feasible. The integrals were evaluated by Monte-Carlo integration procedures.

As a partial guide to the accuracy to be expected, Baker and Kahane (1969) have performed an analogous calculation on a model taken from classical statistical mechanics, which however retains many of the essential

features. It is the "lattice gas." For this system (Rushbrooke and Scoins, 1962, 1963) there is extensive perturbation series data available, equivalent to terms of the order of V^9. They summed the series through the highly effective Padé approximant method,[6] (Baker, 1965b; Baker and Gammel, 1970). They found that while the very earliest approximations are rather wide of the mark, the improvement is quite rapid and that, except near the critical point, the location of the coexistence curve is determined to within about 0.02%. Even the [2, 2] Padé approximant, which uses only four terms in these series, gives about 2% in accuracy, except near the critical point where it is only 10% off. They evaluated the energy (actually the free energy) at the corresponding approximate locations determined for the coexistence curve. Using all terms avail-

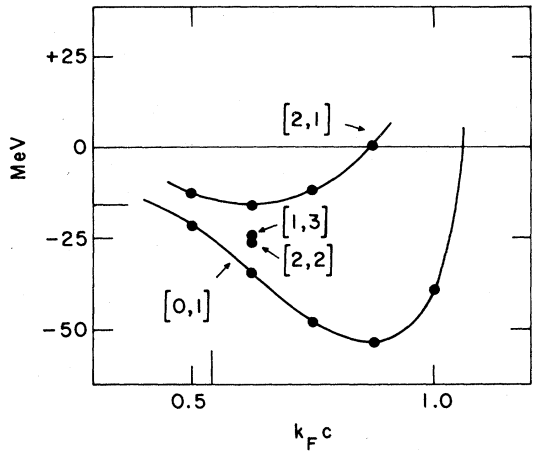

FIG. 41. Padé approximants to the binding energy of the many-fermion system using a model force. The large tic marks are the experimental "nuclear matter" density and energy.

able, they obtained (except near the critical point) at least four figure agreement with the known answers, and even better results on the gas side of the coexistence curve. Using only four terms (the [2, 2] Padé approximant), they obtained an accuracy of about 1%, except near the critical point. The results for the problem of Baker *et al.* (1970) may not be quite so rapidly convergant, as the second term in the R-matrix expansion is anomalously small, and their potential is more complex than the model one.

In Tables VII and VIII we list the numerical results of Baker *et al.* (1970) for the various diagrams. The density $k_F=0.625$ was chosen at which to evaluate the

TABLE VII. R-matrix expansion data (units $1=259.2$ MeV).

Diagram	$k_FC=0.5$ Value	$k_FC=0.5$ Deviation	$k_FC=0.625$ Value	$k_FC=0.625$ Deviation	$k_FC=0.75$ Value	$k_FC=0.75$ Deviation	$k_FC=0.875$ Value	$k_FC=0.875$ Deviation
Zero order ($0.3k_F^2c^2$)	0.075		0.11719		0.16875		0.22969	
First order								
B1	-0.1560		-0.2492		-0.3537		-0.4366	
Second order								
B1	1.1379×10^{-3}		5.098×10^{-4}		-1.507×10^{-5}		1.194×10^{-3}	
Third order								
B1	-1.666×10^{-4}		-1.102×10^{-4}		-1.084×10^{-4}		-1.602×10^{-4}	
H3	-3.370×10^{-3}	$\pm6\times10^{-5}$	-4.472×10^{-3}	$\pm9.0\times10^{-5}$	-7.92×10^{-3}	$\pm1.3\times10^{-4}$	-1.191×10^{-2}	$\pm2.5\times10^{-4}$
R3	-1.22×10^{-3}	$\pm6\times10^{-5}$	6.09×10^{-4}	$\pm1.7\times10^{-4}$	1.53×10^{-2}	$\pm6\times10^{-4}$	7.88×10^{-2}	$\pm1.7\times10^{-3}$
F3	5.33×10^{-2}	$\pm3.6\times10^{-4}$	1.29×10^{-1}	$\pm1.3\times10^{-3}$	3.26×10^{-1}	$\pm2.6\times10^{-3}$	7.44×10^{-1}	$\pm7.7\times10^{-3}$
Total	4.85×10^{-2}	$\pm3.7\times10^{-4}$	1.25×10^{-1}	$\pm1.3\times10^{-3}$	3.33×10^{-1}	$\pm2.6\times10^{-3}$	8.11×10^{-1}	$\pm7.9\times10^{-3}$

[6] The Padé approximant method is an approximate method of analytic continuation where a ratio of polynomials is used to extend the knowledge of the function value further from the origin than one might naively suppose possible. It has been used to good effect in many problems of physics involving both convergent and asymptotic series.

TABLE VIII. Four-order R-matrix expansion data for $k_F c = 0.625$ (units $1 = 259.2$ MeV).

Diagram	Value	Deviation
B1	5.084×10^{-6}	
I6	-2.66×10^{-4}	$\pm8\times10^{-6}$
IA.1	-2.52×10^{-3}	$\pm9.5\times10^{-5}$
IA.2	-1.56×10^{-3}	$\pm5.5\times10^{-5}$
IA.3	-2.37×10^{-3}	$\pm1.2\times10^{-4}$
II.3	6.1×10^{-5}	$\pm9\times10^{-6}$
II.4[a]	6.1×10^{-5}	$\pm9\times10^{-6}$
II.5	-9.1×10^{-3}	$\pm5\times10^{-4}$
II.7	-1.40×10^{-4}	$\pm7\times10^{-6}$
II.8	-2.29×10^{-4}	$\pm2.8\times10^{-5}$
II.9	-7.7×10^{-5}	$\pm6\times10^{-6}$
II.10	2.0×10^{-5}	$\pm5\times10^{-6}$
II.11[a]	-2.29×10^{-4}	$\pm2.8\times10^{-5}$
II.12[a]	-1.40×10^{-4}	$\pm7\times10^{-6}$
IIA.1	-0.1516	$\pm9.5\times10^{-4}$
IIA.2	-5.3×10^{-4}	$\pm4\times10^{-5}$
IIA.3	-6.4×10^{-4}	$\pm5\times10^{-5}$
IIA.4[a]	-5.3×10^{-4}	$\pm4\times10^{-5}$
IIA.5	4.45×10^{-3}	$\pm8.5\times10^{-5}$
IIA.6	4.32×10^{-3}	$\pm1.0\times10^{-4}$
III.2	-3.23×10^{-3}	$\pm9\times10^{-5}$
III.9+10	3.68×10^{-3}	$\pm7.5\times10^{-5}$
IV.1	-0.1117	$\pm8.5\times10^{-4}$
IV.4	8.6×10^{-3}	$\pm2.5\times10^{-4}$
IV.5[a]	8.6×10^{-3}	$\pm2.5\times10^{-4}$
IV.6	-1.637×10^{-2}	$\pm3.5\times10^{-4}$
II.7[a]	-1.637×10^{-2}	$\pm3.5\times10^{-4}$
Total	-0.2878	$\pm1.6\times10^{-3}$

[a] Identical to a previous diagram (but must be added to find the total fourth-order coefficient).

fourth-order terms since it seems close to saturation for their potential.

In order to analyze what this data implies about the ground-state energy of a many-fermion system interacting with this potential, Baker *et al.* (1970) used the Padé approximant method. We show in Fig. 41 a plot of their results for successively more accurate Padé approximants. The most accurate Padé approximants are

$$[2,2] = -25.6 \text{ MeV},$$
$$[1,3] = -24.3 \text{ MeV} \qquad (5.49)$$

for $k_F c = 0.625$.

They also summed the available terms by the Borel method, and obtained closely similar results.

It is to be noted that the fourth-order term is substantial (larger than the first-order term in this example), and that many diagrams make important contributions to it. Numerically the largest contributions in fourth order come from the three-body cluster terms (IIA.1 and II.5) and the self-energy insertions (Class IV).

These results are in accord with experience with the coexistence curve in classical liquid systems. An accurate result cannot be obtained by considering only the result of pair interactions, even in the presence of a medium, taken account of in an averaged manner. The higher clusters behavior is essential. Indeed this aspect is the essence of the name given to the field, i.e., cooperative phenomena. By use of sophisticated summation procedures such as the Padé method, one can sensitively extrapolate the trends apparent in the low-order clusters and thus obtain accurate estimates sooner than would otherwise be possible.

In classical systems, procedures based on the summation of terms corresponding to two-particle clusters or special classes of diagrams have not been very successful when applied to the liquid coexistence curve (Levesque, 1966), even though some of them do well on the gas side. We know of no reason to suppose that the quantum problem of a many-fermion system with its more complex interaction and quantum complexities should yield to such methods. We do feel, however, that the methods, as outlined in this section, which have proved successful (Baker and Kahane, 1969; Gaunt and Baker, 1970; Baker and Rushbrooke, 1970) in other analogous systems will be powerful enough to solve the many-fermion problem, although one may need to go to higher than fourth-order perturbation theory to do justice to the complex nucleon–nucleon interaction.

Amusia, M. Ya. and V. N. Efimov, 1968, Ann. Phys. (New York) **47,** 377.
Austern, N. and Iano, P., 1960, Nucl. Phys. **18,** 672.
Baker, G. A. Jr., 1962, Phys. Rev. **128,** 1485.
——, 1963, Phys. Rev. **131,** 1869.
——, 1965a, Phys. Rev. **140,** B9.
——, 1965b, Advan. Theoret. Phys. **1,** 1.
——, 1967, Phys. Rev. **161,** 434.
——, 1970, J. Math. Phys. **11,** 2302.
——, and J. L. Gammel, 1970, editors, *The Padé Approximant in Theoretical Physics* (Academic, New York).
——, J. L. Gammel, and B. J. Hill, 1963, Phys. Rev. **132,** 1373.
——, B. J. Hill, and R. J. McKee, Jr., 1964, Phys. Rev. **135,** A922.
——, M. F. Hind, and J. Kahane, 1970, Phys. Rev. C **2,** 841.
——, and J. Kahane, 1969, J. Math. Phys. **10,** 1647.
——, and G. S. Rushbrooke, 1970, Phys. Rev. B **2,** 706.
Balian, R., 1962, in *The Many-Body Problem* edited by C. Fronsdal (Benjamin, New York), p. 286.
Blatt, J. M. and V. F. Weisskopf, 1952, *Theoretical Nuclear Physics* (Wiley, New York).
Bethe, H. A., 1965, Phys. Rev. **138,** B804.
——, B. A. Brandow, and A. G. Petschek, 1963, Phys. Rev. **129,** 225.
Brandow, B. H., 1966, Phys. Rev. **152,** 863.
——, 1967, Rev. Mod. Phys. **39,** 771.
Brueckner, K. A., 1955, Phys. Rev. **100,** 36.

——, 1959, in *The Many-Body Problem*, edited by C. de Witt (Wiley, New York), pp. 47–154.
——, and J. L. Gammel, 1958a, Phys. Rev. **109,** 1023.
——, and J. L. Gammel, 1958b, Phys. Rev. **109,** 1040.
——, and K. S. Masterson, 1962, Phys. Rev. **128,** 2267.
Crichton, J. H. and R. H. Anderson, 1967, private communication.
Day, B. D., 1967, Rev. Mod. Phys. **39,** 719.
——, 1969, Phys. Rev. **187,** 1269.
Dyson, F. J., 1952, Phys. Rev. **85,** 631.
Efimov, V. N., 1965, Phys. Letters **15,** 49; **17,** 80.
——, and M. Ya. Amusia, 1964, Zh. Eksp. Teor. Fiz., **47,** 581 [Sov. Phys—JETP **20,** 388 (1965)].
Emery, V. J., 1959, Nucl. Phys. **12,** 69.
——, 1960, Nucl. Phys. **19,** 154.
Epstein, P. S., 1937, *Textbook of Thermodynamics* (Wiley, New York).
Evans, R. D., 1955, *The Atomic Nucleus* (McGraw-Hill, New York).
Fisher, M. E., 1964, Arch. Ratl. Mech. Anal. **17,** 377.
——, 1967, Rept. Progr. Phys. **30,** 615.
Franz, L. M., and R. L. Mills, 1960, Nucl. Phys. **15,** 16.
Gammel, J., and J. Nuttall, 1965, Phys. Rev. **138,** B1382.
——, and R. M. Thaler, 1957, Phys. Rev. **107,** 291, 1337.
Gaunt, D. S., and G. A. Baker, Jr., 1970, Phys. Rev. B **1,** 1184.
——, and M. E. Fisher, 1965, J. Chem. Phys. **43,** 2840.
Goldstone, J., 1957, Proc. Roy. Soc. (London) **A239,** 267.
Gomez, L. C., J. D. Walecka, and V. F. Weisskopf, 1958, Ann. Phys. (New York) **3,** 241.
Gröbner, W. and N. Hofreiter, 1958, *Integraltafel, Zweiter Teil, Bestimmte Integral* (Springer-Verlag, Berlin).
Haftel, M. I., and F. Tabakin, 1970, Nucl. Phys. **A158,** 1.
Hardy, G. H., 1956, *Divergent Series* (Oxford U. P., New York) Chapt. VIII.
Hill, T. L., 1956, *Statistical Mechanics* (McGraw-Hill, New York).
Huang, K., and C. N. Yang, 1957, Phys. Rev. **105,** 767.
Hugenholtz, M. N., 1957, Physica **23,** 481.
Irwin, E. J., 1963, Ph.D. thesis, Cornell University.
Jeffreys, H., and B. S. Jeffreys, 1950, *Methods of Mathematical Physics* (Cambridge U. P., New York) Chapt. 17.
Kallio, A. and B. D. Day, 1969, Nucl. Phys. **A124,** 177.
Katsura, S., 1954, Progr. Theoret. Phys. (Kyoto) **11,** 476.
——, 1955, Progr. Theoret. Phys. (Kyoto) **13,** 571.
——, 1960, Prog. Theoret. Phys. (Kyoto) **23,** 390, and references therein.
——, 1963, Advan. Phys. **12,** 391 (review article).
Katz, A., 1962, Nucl. Phys. **29,** 353.
Kober, H., 1957, *Dictionary of Conformal Representations* (Dover, New York) pp. xiii and 103.
Köhler, H. S., 1969, Nucl. Phys. **A128,** 273.
Lee, T. D., and C. N. Yang, 1957, Phys. Rev. **105,** 1119.
Levesque, D., 1966, Physica **32,** 1985.
Luttinger, J. M. and J. C. Ward, 1960, Phys. Rev. **118,** 1417.
Montroll, E., 1960, in *The Theory of Neutral and Ionized Gas*, edited by C. de Witt (Wiley, New York), p. 110.
Muir, T., 1960, (revised and enlarged by W. H. Metzler) *A Treatise on the Theory of Determinants* (Dover, New York).
Pauling, L. and E. B. Wilson, 1935, *Introduction to Quantum Mechanics*, (McGraw-Hill, New York).
Rajaraman, R., and H. A. Bethe, 1967, Rev. Mod. Phys. **39,** 745.
Ruelle, D., 1963, Helv. Phys. Acta **36,** 183, 789.
Rushbrooke, G. S. and H. I. Scoins, 1962, J. Math. Phys. **3,** 176.
——, 1963, J. Math. Phys. **4,** 998.
Saito, N., 1961, J. Chem. Phys. **35,** 232.
Schiff, L. I., 1949, *Quantum Mechanics* (McGraw-Hill, New York) Sec. 15.
Tolmachev, V. V., 1961, Dokl. Akad. Nauk. S.S.S.R. **141,** 582 [Sov. Phys.-Dokl. **6,** 976 (1962)]. This reference gives a more general discussion of the cancellation of divergences for finite internal momenta.
Wigner, E., 1932, Phys. Rev. **40,** 749.
Wu, T. Y. and T. Ohmura, 1962, *Quantum Theory of Scattering* (Prentice-Hall, Englewood Cliffs, New Jersey).
Yang, C. N., and T. D. Lee, 1952, Phys. Rev. **87,** 404, 410.